INSTITUT **F**ÜR **H**YDROLOGIE
ALBERT-**L**UDWIGS-**U**NIVERSITÄT **F**REIBURG IM **B**REISGAU

Elisabeth Helen Krüger

The Behaviour of Fluorescent Dye Tracers in Hypersaline Saturated Media and Environmental Tracers Marking the Fresh-Saline Water Interface in the Western Dead Sea Margin

Diplomarbeit unter der Leitung von Prof. Dr. Ch. Leibundgut
Freiburg im Breisgau, Dezember 2006

INSTITUT **F**ÜR **H**YDROLOGIE
ALBERT-**L**UDWIGS-**U**NIVERSITÄT **F**REIBURG IM **B**REISGAU

Elisabeth Helen Krüger

The Behaviour of Fluorescent Dye Tracers in Hypersaline Saturated Media and Environmental Tracers Marking the Fresh-Saline Water Interface in the Western Dead Sea Margin

Referent: Prof. Dr. Christian Leibundgut
Koreferent: Dr. Christoph Külls

Diplomarbeit unter der Leitung von Prof. Dr. Ch. Leibundgut
Freiburg im Breisgau, Dezember 2006

Acknowledgements

I would like to thank Prof. Dr. Christian Leibundgut for the patronage of this work.

Cordial thanks to my supervisor, Dr. Christoph Külls, for initiating this work, for being co-referent, and for being full of inspiring ideas and good advice. Special thanks to Dr. Noam Weisbrod for being a most helpful advisor in Israel and for his patience and care.

I would like to express my gratitude to the people in Israel, without whom my work there would have been impossible:

Einat Magal for the wonderful cooperation and for her warm hospitality; Yossi Yechieli for his advice and support in the field work; Haim Hemo for his help in all technical issues in the field.

I want to thank Amir Sandler for the XRD analysis and Dina Stiber, Olga Yoffee and Sara Erlich for the chemical analysis; Ludmilla Katz for her help in the laboratory and for the chemical analyses; Amit Gross for giving me a space to work in the laboratory; Mihail Kugel for the construction of the columns. Many thanks to the members and students at the Department for Environmental Hydrology and Microbiology, BIDR for their help and support.

The funding of this project by the BMBF (Bundesministerium für Bildung und Forschung) is gratefully recognized. Thanks to Hydroisotop GmbH for the analysis of the radium isotopes and ^{34}S, and to Harald Oster for the analysis of the CFCs; Jochen Wenninger for the analysis of ^{2}H and ^{18}O and Emil Blattmann for the supply with field instruments. Most cordial thanks to Hannes Leistert for supporting my work with the modelling of CFCs and radium isotopes, even though I could not make this part of my thesis.

My personal thanks go to Hanan Meron for his help with everything and to Jenia Gutmann for taking care of me. Thanks to the students in the Midrasha for making me feel at home. Thank you, Andrea Wachtler, for being a ceaseless motivator and for your advice and proof-reading. And last but not least my special thanks to my mother for proof-reading and to her and the rest of my family for their never-ending support and care.

Contents

List of Figures

List of Tables

List of Figures in the Annex

Abbreviations

a.s.l.	above sea level
BMBF	Bundesministerium für Bildung und Forschung
BP	before present
b.s.l.	below sea level
BTC	breakthrough curve
b.w.h.	below well head
C	concentration
C_0	initial concentration
CDT	Canyon Diablo Troilite
CDE	convection – dispersion model (advection – dispersion model)
D	dispersion coefficient
dpm	disintegrations per minute per kilogram of water
DSW	Dead Sea water
EC	electric conductivity
GMWL	Global Meteoric Water Line
GW	groundwater
^{2}H	deuterium
IAEA	International Atomic Energy Association
IHF	Institute for Hydrology Freiburg
ISOHIS	Isotope Hydrology Information System
K_d	distribution coefficient
M	tracer mass
M_0	initial (injected) tracer mass
MMWL	Mediterranean and Middle Eastern Meteoric Water Line
MWL	Meteoric Water Line
^{18}O	oxygen-18
PDM	Peedee Belemnite
ppm	parts per million
R	retardation factor
rpm	rotations per minute
SI	saturation indices
SLAP	Standard Light Antarctic Precipitation
TDS	total dissolved solids
v	pore velocity
VSMOW	Vienna Standard Mean Ocean Water

Summary

The aim of this study is to test the feasibility of the application of tracers in hypersaline media and to investigate the fresh-saline water interface along the western Dead Sea shore. A comprehensive literature research is presented as part of this study, which supplies a basis of knowledge for the investigation of the processes in highly saline environments using tracer methods.

The study was conducted in cooperation of the Geological Survey of Israel and the Department for Environmental Hydrology and Microbiology, Blaustein Intitutes for Desert Research (BIDR) at the Ben-Gurion University of the Negev, Israel with the Institute for Hydrology at Albert-Ludwigs-University, Freiburg.

The Dead Sea Basin is part of the Syrian-African Rift system and lies approximately 410 meters below sea level. As the area lies in the lee of the Judean Mountains it forms a hot, dry desert with an average annual rainfall of less than 80 mm. The study area is located in the Quarternary Aquifer which consists of gravel, clay and sands intercalated by lacustrine sediments (salt and clay layers). Recharge of the aquifer is supplied through leakage from the Mountain Aquifer and possibly also by flash floods that occur within the nahals during the winter. This fresh water meets the saline groundwater in the surroundings of the Dead Sea, forming the fresh-saline water interface under investigation. The water of the Dead Sea has a salinity (TDS) of approximately 340 g/l and therefore it has a high density, high viscosity and great ionic strength, making it a complex liquid to work with.

The system was explored by analysing samples collected along a profile of the fresh-saline water interface for the following environmental tracers: major ions, stable isotopes of H, O and S as well as radium isotopes.

The major ions indicated mixing of two end-member waters, while sulfate and bicarbonate were reduced with increasing salinity, indicating that the waters are supersaturated with respect to these ions. This theory was supported by saturation indices calculated using the Pitzer equations.

The stable isotopes of the water molecule plotted in a straight line connecting the fresh water sample, which plotted amongst the rainfall isotopic data of Israel and western Jordan, and the most saline sample being close to the isotopic signature of the Dead Sea. The question arose as to whether the connecting line on which the samples plot is a definite indicator of the mixing of two end-member waters, and whether this process could be distinguished from a single water type dissolving evaporitic salt, which is embedded beneath the groundwater table and therefore it would not be dry salt. A salt 'containing' a significant amount of water would contribute an isotopic signature to the mixed sample, while a water sample of a single source, which has dissolved dry salt would retain the isotopic signature of that one water. This question was come by, by checking the ionic ratios of Na/Cl, Br/Cl and Ca/SO_4. These ratios supported the assumption of the waters having different salinities to be the result of mixing and negated the theory of salt dissolution in this specific location.

Increasing δ^{34}S-values in the SO_4^--ion, as found in the samples with increasing salinity are a sign of bacterial sulfate reduction. This trend did not continue in the most saline sample, even though the stable isotope composition of H and O, as well as the water chemistry

indicated that a continuous process of mixing was taking place and therefore the abrupt termination of sulfate reduction seemed surprising. This observation could be explained by a near-shore circulation of Dead Sea water (being depleted in $\delta^{34}S$), which penetrates the sub-surface and then ascends and mixes with the water in the sampling location. The assumptions comply with findings of Mazor (1997) and Zak (1997).

$^{228}Ra/^{226}Ra$ ratios approve with the theory of two end-member waters mixing, as found by the analysis of the other natural tracers, without any dissolution processes.

In order to get an understanding of the behaviour of fluorescent dye tracers in hypersaline media, batch and column experiments were conducted in varying salinity levels up to the concentration of Dead Sea water with the following tracers: Uranine, Pyranine and Naphtionate; batch experiments only were realised with Eosin, as this tracer proved to be unsuitable for the use in high salinities. The sediments used were collected from the Dead Sea Basin and comprised grain sizes of coarse sands to silt, which consisted mainly of calcite and quartz.The response of the tracers to increasing salinity in combination with pH and electric conductivity measurements was observed prior to and after the batch and column experiments.

The results of the batch experiments showed that Uranine fluorescence extinction becomes rather high with increasing salinity, especially at salinities above a TDS concentration of 200 g/l. Pyranine showed a more steady performance than Uranine, while the overall trend of decreasing fluorescence with increasing salinity was similar to that of Uranine. Eosin fluorescence showed a steep decrease with the increase in salinity. However, Naphtionate fluorescence was quenched to a certain decree in low salinities and this extinction remained constant, showing no effect towards higher salt contents.

The results of the column experiments in which coarse sands constituted the matrix, were roughly consistent with the results of the batch experiments. The Uranine breakthrough curves showed great retardation with the increase in salinity, Pyranine breakthrough curves peaked at a salt concentration of approximately 65 g/l and were attenuated at higher salinities, but they remained steady, even when salt concentrations reached the level of Dead Sea water. Naphtionate breakthrough curves were more or less constant throughout all salinity levels and the constant quenching rate found in the batch experiments could not be identified in the column experiments, presumably because of the shorter contact time of matrix and solution.

In order to determine characteristic parameters describing the behaviour of the tracers in column experiments with saline water, two different models were applied for fitting calculated curves to the measured breakthroughs. One was the equilibrium convection dispersion model developed by Zuber & Maloszewski (1982) and the other one was the CXTFIT-code written by Toride et al. (1999), a non-equilibrium model taking into account reversible and irreversible adsorption and degradation. The more complex CXTFIT-code delivered the better fitting curves.

Finally, a field experiment was carried out within the study area to assess the applicability of an online-fluorimeter (GGUN-FL by Geomagnetism Group, Neuchâtel) in hypersaline groundwater. The tracers Naphtionate and Pyranine were applied in this field experiment and all three elements, the online-fluorimeter as well as both tracers delivered satisfying results, proving their suitability for the use in highly saline environments.

Keywords: *brine, fluorescent tracers, stable isotopes, radium, fresh-saline water interface, Dead Sea, groundwater.*

Zusammenfassung

Ziel dieser Arbeit ist, die Anwendbarkeit verschiedener Markierstoffe in hypersalinen Medien zu testen sowie den Grenzbereich zwischen Frisch- und Salzwasser entlang des westlichen Ufers des Toten Meeres zu untersuchen. Eine umfassende Literaturvorstellung, die als Basis für Forschungen zum Thema der Anwendung von Tracern in salzhaltigem Wasser dienen kann, steht zu Beginn der Arbeit.

Die Studie ist im Rahmen des „Young Scientist Exchange Programme“ durchgeführt worden, finanziert durch das Bundesministerium für Bildung und Forschung (BMBF), in Zusammenarbeit zwischen dem Department for Environmental Hydrology and Microbiology, Blaustein Institutes for Desert Research der Ben-Gurion Universität des Negev sowie dem Geological Survey of Israel und dem Insitut für Hydrologie der Albert-Ludwigs-Universität, Freiburg.

Das Tote Meer ist Teil der syrisch-afrikanischen Riftzone und liegt auf etwa 410 Metern unter dem Meeresspiegel. Diese Gegend ist durch ihr heißes, trockenes Klima mit einem mittleren Jahresniederschlag von unter 80 mm ausgezeichnet, was dadurch hervorgerufen wird, dass sie sich im Lee der Judäischen Berge befindet. Das Forschungsgebiet liegt im mittleren Teil des westlichen Toten Meergrabens, im Quartären Aquifer, der aus Kiesen, Ton und Sand sowie darin eingebetteten lakustrischen Ablagerungen aus Ton- und Salzschichten besteht. Grundwasserneubildung entsteht hauptsächlich durch das Einströmen von Grundwasser aus dem Mountain Aquifer in den Quartären Aquifer und lokal auch durch die Sturmfluten in den Nahals (trockene Flussbetten) im Winter. Dieses frische Wasser trifft an der Frisch-Salzwasser-Grenze auf das hochsalinare Grundwasser in der Umgebung des Toten Meeres. Das Wasser des Toten Meeres hat einen Salzgehalt von etwa 340 g/l und hat somit eine sehr hohe Dichte, Viskosität und Ionenkonzentration, wodurch Effekte auftreten, die die Arbeit mit diesem Wasser erschweren können.

Die Grenzschicht von frischem und salzhaltigem Wasser wurde untersucht, indem Proben entlang eines Profils der Frisch-Salzwasser-Grenzschicht gezogen und auf die Zusammensetzung von natürlichen Tracern analysiert wurden. Diese sind: Hauptionen, stabile Isotope von H, O und S sowie Radiumisotope.

Die Hauptionenanalyse deutet durch die lineare Zunahme der einzelnen Ionen mit zunehmender Salinität, auf die Mischung zweier „end-member“ - Wassertypen hin, während abnehmende Sulfat- und Bicarbonat-Gehalte mit zunehmender Salinität darauf hinweisen, dass die Wässer an sulfatischen und carbonatischen Phasen übersättigt sind. Diese These wird durch Sättigungsindizes, die mithilfe der Pitzer-Gleichungen berechnet wurden, bestätigt.

Auch die stabilen Wasserisotope weisen durch die sich in der graphischen Darstellung ergebende Mischungsgerade, auf die lineare Mischung zweier Wassertypen hin. Es stellte sich die Frage, ob diese Mischungsgerade ein eindeutiges Indiz für die Mischung zweier „end-member“ – Wässer sei, und ob dieser Mischprozess unterschieden werden könne von der Lösung von Salzschichten durch einen einzigen Wassertyp. Eine solche Salzschicht wäre, wenn sie unterhalb des Grundwasserspiegels läge, kein trockenes Salz, sondern wäre mit einer gewissen Menge Wasser versetzt. Dieses Wasser würde zum Mischwasser eine signifikante isotopische Signatur beitragen, während eine Wasserprobe, die einer einzigen Quelle entspringt und trockenes Salz löst, die Signatur dieses einen

Wassertyps beibehielte. Diese Frage wird durch die Überprüfung der Ionenverhältnisse von Na/Cl, Br/Cl and Ca/SO_4 beantwortet, die die These der Mischung zweier Wassertypen unterstützt und die Vermutung, dass Lösungsprozesse Teil dieses lokalen Systems seien, negiert.

Der Anstieg der $\delta^{34}S$-Werte im Sulfat-Ion mit zunehmender Salinität, deutet auf bakterielle Sulfatreduktion hin. Dieser ansteigende Trend trifft für die salzigste Probe allerdings nicht zu, da die $\delta^{34}S$-Werte in den zwei salzhaltigsten Proben konstant bleiben, obwohl die Isotopensignatur von H und O sowie die Wasserchemie auf einen kontinuierlichen Mischungsprozess hinweisen und somit auch einen kontinuierlichen Prozess der Sulfatreduktion erwarten ließen. Diese Beobachtung könnte durch eine ufernahe Zirkulation von Totem Meerwasser (welches bezüglich $\delta^{34}S$ abgereichert ist) erklärt werden, welches in die ufernahen Bodenschichten infiltriert und sich als aufsteigendes Wasser mit dem Mischwasser am Beprobungsort vermischt. Diese Annahme stimmt mit Analysen von Mazor (1997) und Zak (1997) überein.

$^{228}Ra/^{226}Ra$ – Verhältnisse stimmen mit der Theorie der Mischung zweier Wassertypen ohne Lösungsvorgänge überein, wie es die Ergebnisse der anderen natürlichen Tracer andeuten.

Um das Verhalten von Fluorezenztracern in hypersalinen Medien zu verstehen, wurden im Rahmen dieser Arbeit Batch- und Säulenversuche in variierenden Salinitätsstufen, bis hin zur Salzkonzentration des Toten Meerwassers, durchgeführt. Dabei wurden folgende Tracer untersucht: Uranin, Pyranin und Naphtionat; mit Eosin wurden nur Batch-Versuche durchgeführt, da diese die Untauglichkeit dieses Tracers zur Anwendung in hochsalinaren Wässern erwiesen. Die verwendeten Sedimente stammen aus dem Toten Meergraben und fügen sich zusammen aus einem Korngrößengemisch von grobem Sand bis feinem Schluff und bestehen hauptsächlich aus Calcit und Quartz. Das Verhalten der Tracer mit zunehmender Salinität wurde im Zusammenhang mit dem pH-Wert und der Leitfähigkeit, sowohl vor als auch nach den Batch- und Säulenversuchen beobachtet.

Die Ergebnisse der Batch-Versuche deuten an, dass Uranin mit zunehmender Salinität recht stark absorbiert wird, vor allem ab Salzkonzentrationen über 200 g/l. Pyranin erweist sich in hohen Salinitäten als etwas stabiler, wobei der Gesamtverlauf ähnlich dem des Uranins ist. Die Fluoreszenz bei Eosin nimmt mit zunehmendem Salzgehalt stark ab. Beim Naphtionat dagegen ergibt sich eine gewisse Fluoreszenzlöschung schon bei geringem Salzgehalt, die sich dann mit zunehmender Salinität nicht mehr ändert.

Aus den Säulenversuchen, in denen grobe Sande die Matrix stellten, ergeben sich grob ähnliche Ergebnisse wie aus den Batchversuchen. Die Durchgangskurven des Uranin weisen kontinuierlich stärker werdende Retardation des Tracers mit zunehmender Salinität auf. Die Amplitude der Durchgangskurven des Pyranin erreicht bei einem Salzgehalt von 65 g/l ein Maximum und wird in höheren Salinitäten gedämpft, allerdings bleibt diese Dämpfung konstant, auch bei einem Salzgehalt im Niveau des Toten Meerwassers. Naphtionat weist relativ konstante Durchgangskurven durch alle Salinitäten hindurch auf, wobei die in den Batchversuchen beobachtete, konstante Fluoreszenzlöschung hier nicht auftritt, was vermutlich durch die geringere Kontaktzeit zwischen Matrix und Tracerlösung bedingt ist.

Die Bestimmung von characteristischen Parametern mittels Modellanpassung erfolgte mit zwei Modellen: Dem einfachen Dispersionsmodell nach Zuber & Maloszewski (1982),

das eine reine Gleichgewichtsreaktion des Tracers mit der immobilen Phase darstellt und dem CXTFIT-Code, ein Ungleichgewichtsmodell nach Toride et al. (1999), welches kinetische Reaktionen erster Ordnung beschreiben kann, also gute Anpassungen für Tracerdurchgangskurven mit Tailings liefert. Dementsprechend wurde letzteres Modell als das für die gemessenen Durchgangskurven angemessenere Modell bewertet.

Als letzter Schritt wurde ein Feldversuch im Untersuchungsgebiet durchgeführt, um die Anwendbarkeit eines In-situ-Fluorimeters (GGUN-FL der Geomagnetism Group, Neuchâtel) in hypersalinem Grundwasser zu erproben. Hierbei wurden Naphtionat und Pyranin eingesetzt und für alle drei getesteten Elemente, das in-situ-Fluorimeter sowie die beiden Tracer, wurde die Anwendbarkeit im hypersalinen Grundwasser bestätigt.

Schlüsselworte: *Salzwasser, Fluoreszenztracer, stabile Isotope, Radium, Frisch-Salwassergrenze, Totes Meer, Grundwasser.*

1. Introduction

This study was conducted under the Young Scientist Exchange Programme, which is financed by the BMBF (Bundesministerium für Bildung und Forschung), between the Department of Environmental Hydrology and Microbiology, Blaustein Institutes for Desert Studies (BIDR) at the Ben-Gurion University of the Negev and the Geological Survey of Israel together with the Institute for Hydrology at Albert-Ludwigs-University, Freiburg.

The project was initiated because the understanding of the processes dominating the fresh-saline water interface along a rapidly changing shoreline, such as that of the Dead Sea, need to be consolidated. The level of the Dead Sea is receding at the rate of approximately one meter each year, triggering massive changes in the groundwater environment. Why this is so important is because it has taken only a few decades for the changes in lake level and the changes taking place underground to cause the ground in the vicinity to become unstable. This has a major effect on the people living in this area.

In the case of the Dead Sea it is the formation of sinkholes, which develop through the dissolution of underground salt layers, reaching a diameter of several meters or more, which form when the ground suddenly collapses without warning.

Salt and hypersaline water is ubiquitous in this complex system and the knowledge of what is the source of the salinity is essential for understanding the processes that occur underground and are invisible for the eye.

1.1 Objectives

The aim of this study is to test the feasibility of various tracers in identifying the dominating processes of a hypersaline groundwater environment. The quest for these tracers has two parts: 1) system investigations of the study area comprising the analysis of environmental tracers and, 2) an empirical study of fluorescent dye tracers.

Environmental tracers are mostly well studied within the Dead Sea area and existing data served as a good reference for the interpretation of the analytical data. With the help of these tracers it was possible to create a comprehensive picture of the local surroundings.

The application of fluorescent dye tracers has so far been restricted to fresh water systems and has seldom been used in seawater environments. Within hypersaline conditions investigations on the behaviour of fluorescent dye tracers to date have not been researched. Expectations on their behaviour based on the knowledge about the latter in fresh water environments may be invalidated when these tracers are applied to waters of increased density, viscosity and ionic strength. Therefore, the results of these investigations can be regarded as a beneficial contribution to the state of research in the applicability of dye tracers in hypersaline environments.

1.3 State of the Art

1.3.1 Use of Fluorescent Dye Tracers (in Brines)

The use of fluorescent dye tracers in geohydrology has been described by numerous authors. A broad compilation is given by Kaess (1998) giving a brief overview over a majority of the different dye tracers and their characteristics. A detailed description of a range of dye tracers has been compiled by Flury & Wai (2003), throwing a light on advantages and disadvantages in the use of the different dyes and their application with an emphasis on vadose zone hydrology. Adsorptive characteristics of dye tracers in different media with a strain on dye and media properties, has been written by Kasnavia et al. (1999). Earlier findings with important basics about these tracers have been put forward by Smart & Laidlaw (1977).

Leibundgut (1974) analysed Uranine and Sulforhodamine G with respect to their adsorptive behaviour, sensitivity to the radiation of light, temperature and quenching, and the applicability of these tracers in ground- and surface waters. In (1981) Leibundgut published an article about the adsorptive behaviour of Uranine and two optical brighteners (Tinopal and Uvitex) in laboratory experiments with sand and brown soil.

Behrens (1986) investigated water tracer chemistry as a factor determining the performance in analytics of fluorescent dye tracers as well as salts. Special recognition to background characterisation in dye tracing has been given by Smart & Karunaratne (2002). Most of these publications do not consider Sodium-Naphtionate (in the following simply referred to as Naphtionate) as a hydrologic dye tracer. This tracer has been paid attention to by Leibundgut & Wernli (1986), pointing out its favorable sorption behaviour being in the same range as that of Uranine and Eosine, and its suitability for short-distances tracer tests in porous media.

With respect to the use of dye tracers in saline groundwater, studies to this point have been very scarce. Rhodamine Water Tracer was studied in a marshland upwelling system by Richardson et al. (2004). E. Magal, who was my exchange partner in this project, was working on the use of dye tracers in brines at the same time that this study was carried out and our personal communication led to fruitful cooperation.

Chemical characterisation, batch, column and modelling studies with a fluorescent dye tracer, namely Rhodamine WT, have been conducted by Sutton et al. (2001).

1.3.2 Stable Isotopes (^{2}H, ^{18}O, ^{34}S) and Radium in Saline Environments

Explanations on the use of the stable isotopes ^{18}O and ^{2}H in this study are based on the syntheses of Kendall & McDonnell (1998), Kaess (1998), as well as findings of Gat & Gonfiantini (1981). Sulfur stable isotope background is referred to Hoefs (1997), and data of the area was acquired from Nissenbaum (1975) and Nissenbaum et al. (1990). Geochemical evaluation is based on the explanations of Mazor (2004) and local hydrogeological data is extracted from Lewenberg (2005).

Stable isotope and geochemistry methods in the study of salinisation processes in groundwater have been investigated, amongst others, by Bennetts et al. (2005), referring to age-

related salinity contents of groundwater in combination with ion-ratios, where the age and recharge pattern is determined by stable isotope and ion composition.

Kim et al. (2002) used isotopic data of oxygen, hydrogen, sulfur and strontium, as well as hydrochemical data to prove salinisation by seawater intrusion and its distribution on a volcanic island.

Ghabayen et al. (2005) investigated sources of salinisation in the Gaza aquifer with different ionic ratios and used $\delta^{11}B$ and $^{87}Sr/^{86}Sr$ isotopic compositions to study their importance as monitoring tools.

In order to investigate the evolution of saline to fresh ground waters of a Permian to Triassic section of the sedimentary cover in northern Switzerland / south-western Germany, Barth (2000) utilized boron isotopic composition in combination with oxygen, hydrogen and sulfur isotopes and hydrochemical tracers for distinguishing the different saline water types.

Kloppmann et al. (2001) studied mixing behaviour of two end-member ground waters in the vicinity of a Permian salt dome in the northern German Basin evidenced by boron, strontium, oxygen and hydrogen isotopes. Groundwater salinisation influenced by potash mining in north-eastern Spain traced by sulfur isotopes has been described by Otero & Soler (2002). In the same research field Ayora et al. (1995) published an article on the modelling of sulfur and oxygen isotopic composition of sulfates throughout a complete evaporite sequence (halite-potash), contributing to the understanding of the evolution of the Upper Eocene South Pyrenean basin.

Analysis of the stable isotope composition of the water molecule of the Dead Sea has been carried out by Gat (1984) and isotopes and water stratification of the Judea Group aquifer as indicated by the isotopes has been described by Kronfeld et al. (1992). Nissenbaum (1975) explained the microbiology and biogeochemistry of the Dead Sea with respect to the ion composition and changes in the latter resulting from biologic activity, dwelling on the sulfur cycle in the lake. In (1990) Nissenbaum et al. published an article on nutrients found in pore waters from Dead Sea sediments, namely carbonate, phosphate, ammonia and sulfate, taken from different depths and analysed their possible origin and evolution. Gavrieli et al. (2001) stress the implications of the sulfur system in anoxic subsurface brines in brine evolution pathways.

Radium background given in this study is based on the chapter written by Kraemer & Genereux (1998).

Radium is frequently used as a tracer in fresh-saline water systems, especially in determining submarine groundwater discharge (SGD) and the mixing of fresh and seawater in estuaries. Authors who have dealt with this topic are: Moore (1996), Swarzenski et al. (2001), Kelly & Moran (2002), Abraham et al. (2003), Lauria et al. (2004), Charette et al. (2004), and Burnett et al. (2006), to name a few.

Regarding innovative measurement techniques studies were done by Purkl (2002) and Dulaiova (2005).

Radium in groundwater has been investigated as a tracer by Krest & Harvey (2003). The authors studied radium disequilibria resulting from vertical transport of radium with groundwater that flows between the underlying aquifer and surface water. Here, they used a combined model of transport, production, decay and solid phases for determining the

vertical flow rate through wetland sediment.

Krishnaswami et al. (1991) wrote an article about the mobility of radium in groundwater, linking retardation factors for radium to salinity with a strongly negative correlation. Dickson (1984) conducted leach experiments on U-Th ore by NaCl solutions showing that all four radium isotopes were equally leached, while sulfate anions reduced the ^{226}Ra and ^{228}Ra leaching to a greater extent than for ^{223}Ra and ^{224}Ra, suggesting that the latter isotopes were being supported in solution by parent isotopes.

Hammond et al. (1988) and Tricca et al. (2000) write about radium isotopic ratios found in groundwater and its hosting rock explaining weathering and recoil mechanisms as sources for the specific activity ratios. Tricca et al. (2000) additionally consider desorption processes for elevated isotope ratios. King et al. (1982) did a study on radium geochemistry by sampling several boreholes within the Piedmont and the Coastal Plain aquifers of South Carolina, where they investigated the relationships of radium contents and activity ratios for determining sources of the radionuclides.

With respect to studies in Israel and the Dead Sea area this topic is also well researched. First Stiller & Chung (1984) and later Chung & Craig (2003) wrote about radium redux in the Dead Sea, examining radium depth-profiles and barium and radium data in order to determine mixing of the two layers of the Dead Sea. They found there to be no mixing and therefore the lower water mass can be regarded as a closed system.

Mazor wrote in (1962) about radon and radium in Israeli water sources and found anomalously high values within the Jordan Rift Valley, which were thought to indicate underground brines, oils and gases. Kronfeld at al. (1991) put forward an article on radium precipitation due to admixture of Dead Sea brines with fresher spring water and extreme ^{238}U-series disequilibrium sourcing from active and relict spring deposits along the Dead Sea coast. Kronfeld & Stiller (1997) investigated the uranium distribution in waters and sediments within the Jordan Rift valley.

Moise (1996) and Moise et al. (2000) published a comprehensive study on radium isotopes and radon in brines and ground waters of the Jordan Rift Valley with explanations on isotope enrichment and retardation, in which they ascribed high radium values in these waters to the mixing of fresh waters with brines.

1.3.3 Dead Sea Research

Articles relevant to the specific topics dealt with above with respect to the Dead Sea area can be found in the respective paragraphs. This section will only give an overview of Dead Sea-specific topics, which do not belong in those sections.

A large selection of articles by different authors covering the field of geology, hydrogeology and hydrochemistry of the Dead Sea can be found in: Niemi, Avraham & Gat (1997). The book deals with the structure of the basin, properties of the water and Quaternary environmental changes.

Yechieli et al. (1995) report on structural and hydraulic properties derived from the interaction between water levels of the Dead Sea and groundwater levels in the adjacent aquifer by a simplified one-dimensional flow model. This model allows predictions of future groundwater levels due to changes in lake levels. In (2000) Yechieli put forward results

of investigations about the fresh-saline water interface in the western Dead Sea margin. Using electric conductivity (EC) profiles he showed that the slope of the interface is 10 times shallower than normally expected near the ocean because of the greater density contrast, which makes the adjoining freshwater extremely prone to salinisation.

Yechieli (2006) and Shalev, Lyakovsky and Yechieli (2006) report on the change in Dead Sea levels and the associated response in groundwater levels with the result of salt dissolution and sinkhole formation along the Dead Sea shore. These processes were surveyed with TDEM (time domain electric traverses) and numerically modelled by Yechieli et al. 2001. A Dead Sea sinkhole study was also conducted by Arkin & Gilat (2000).

Historical Dead Sea level fluctuations calibrated with geological and archeological evidence has been put forward by Frumkin & Elitzur in (2001). The stability of the Dead Sea stratification based on observations over the years 1980-1987 is analyzed by Anati & Shasha (1989) with the proposal of a possible forecast for several months ahead. A detailed description of the geologic structure of the Dead Sea basin is given by Garfunkel & Ben-Avraham (1996). Recent trends in the hydrography of the Dead Sea as influenced by human activity and recent climate based on the monitoring during the years from 1992 to 2000 is forwarded by Gertman & Hecht (2002).

Hydrochemical aspects of the Dead Sea are discussed by Abu-Jaber (1998). The author describes the chemical evolution of Dead Sea water by a simple mixture and evaporation model, suggesting the waters to be of meteoric-continental origin with their salts having accumulated over the past 5000 years. Herut, Gavrieli & Halicz (1998) write about the co-precipitation of trace and minor elements in modern halites from the Dead Sea analyzing differences in distribution coefficients, which seem to be the result of kinetic factors and not of differences in the parent brine composition. Klein-BenDavid, Sass & Katz (2004) pay another tribute to the hydrochemistry of the Dead Sea. They show that the brines in the Dead Sea Rift originate from two different brines, which developed alternately in a dual-mode evaporation basin, distinguished by their Na/Cl and Br/Cl ratios. This model accounts for the deviations of brines from the marine evaporitic evolution by brine mixing, rather than due to a change in ocean chemistry.

Gavrieli, Starinsky & Bein (1989) used interaction coefficients calculated from ionic strengths of Dead Sea brine in order to predict the effect of temperature on halite precipitation. A study on the solubility of gypsum and halite in the Dead Sea with experimental solutions of Dead Sea water with Mediterranean seawater was conducted by Katz et al. (1981) and resulted in finding the Dead Sea to be saturated or supersaturated with respect to both minerals studied.

2. Methodology

This chapter gives an introduction to the methods used in this study. The first part describes the use of natural tracers for system analysis of the investigated area, and the second part explains the methods used in the laboratory.

2.1 Environmental Tracers

Natural tracers, such as geochemistry and stable isotope distribution in groundwater are an ideal tool for creating an understanding of the greater picture of the system under investigation. For this study, general chemistry, stable isotopes of the water molecule and of sulfur, as well as radium isotopes were analysed, not only to get an understanding of the occurring processes, but also to test, whether the chosen tracers are able to reflect these processes adequately. The theory behind these methods is explained in the following sections.

2.1.1 General Chemistry

The chemical composition of water is a basic yet highly valuable tool for understanding the processes determining the environment under investigation. The chemical composition of groundwater is the combined result of the composition of water that enters the groundwater reservoir and its reactions with minerals present in the rock that may modify the water composition.

The proper arrangement of the chemical data is crucial for creating a picture of the presented data. Together with different ionic ratios the graphical arrangement in plots of different ion species, is an easy-to-handle method for groundwater and geo-hydrological investigations. These methods have been described in detail by Mazor (2004).

The analysis of general chemistry in the samples taken for this study was carried out at the Geological Survey of Israel. SO_4^- was analysed by ICP (inductively coupled plasma analysis), HCO_3^- by titration, and all other ions by ion-chromatography.

The modelling of the hydro-geochemistry of groundwaters under investigation can be concluded by advanced computer programmes like Aquachem by Waterloo Hydrogeologic (1998-1999). This programme offers a variety of modules for the modelling of geochemistry. In this case saturation indices (SI) were used in order to underline the precipitation of ions due to the mixing of different water types. SI were calculated by the PHREEQC module using numerical solutions of the Davies equation, which is explained and derived in Appelo & Postma (1993) and URL 3.

The saturation index SI of an ion in solution is defined as:

$$SI = \log IAP / \log K \qquad 2.1$$

where IAP = ion activity product and K = equilibrium constant.

If SI > 0, supersaturation of the ion in solution can be assumed and precipitation can be the consequence, while if SI < 0 the solution is undersaturated with respect to the specific ion (or mineral phase) and the latter will be readily dissolved. A solution with a saturation

index of $-0.2 < SI < 0.2$ can be considered as being in equilibrium state.

An additional PHREEQC (version 2) component offers the possibility of calculating saturation indices using the Pitzer equation. The advantage of this equation is that it is a thermodynamic calculation considering high ionic strengths using virial coefficients. The Davies' equations are valid for solution ionic strength up to $I = 0.5$, which is greatly surpassed in the hypersaline waters of the En Gedi area. Detailed depiction of the Pitzer equations can be found on URL 4.

2.1.2 Stable Isotopes of the Water Molecule

Isotopes of atoms show identical chemical behaviour as the non-enriched atoms, but differ slightly in their physical behaviour. The reason is the greater atomic mass caused by one or more additional neutrons in the atomic core (making it the "heavier" isotope), which is indicated by a varied superscript number before the element symbol. Is the core's neutron/proton ratio out of relative balance the isotope becomes instable and forms a radioactive nuclide.

Variations in isotope abundance can be observed by means of modern measuring technique, either on gas- or solid-source mass spectrometers. The isotope abundance is the ratio R of the "heavier" (rare) to the "lighter" (abundant) isotope:

R = abundance of "heavier" isotope (e.g. ^{18}O) / abundance of "lighter" isotope (e.g. ^{16}O)

These ratios are altered by fractionation processes, caused by the transition from one state to another (for example from liquid to vapor). The reason is that the bonds between the lighter isotopes are broken more easily than equivalent bonds of heavier isotopes. Hence, the lighter isotopes react faster and become concentrated in the product, causing the residual substrate to become enriched in the heavier isotopes. For water this means that the heavier isotopes become enriched in the more dense or solid phase. An isotope fractionation factor is defined as:

$$\alpha = R_p / R_s \qquad 2.2$$

where R_p and R_s are the ratios of the heavy to the light isotope in the product and the substrate, respectively. An isotope enrichment factor ε is defined as:

$$\varepsilon = (\alpha - 1) * 1000 \; . \qquad 2.3$$

The fractionation process of isotopes in the water molecule results in different isotope effects, which are:

(1) Continental effect: heavy isotopes in precipitation water, originating from the ocean, deplete with increasing continentality.

(2) Temperature effect: the higher the temperature, the smaller the difference between the isotopic composition of any two species, because in higher temperatures, for example, heavy isotopes evaporate more easily. This effect results in two other phenomena: (a) Latitude effect: isotope ratios become smaller with decreasing latitude. (b) Seasonal effect: lighter isotope ratios in winter than in summer.

(3) Amount effect: the heavier isotopes become depleted with increasing amount

of rain during a single event.

(4) Altitude effect: is a combination of two phenomena; 1. adiabatic cooling of rising air masses, which triggers a decrease of heavy isotopes due to lower temperatures and lower evaporation rates, and 2. (secondary altitude effect) evaporation of falling rain droplets which leads to enrichment of heavy isotopes in the droplets falling the longer distance.

Variations in isotope abundance are reported as δ-values. This delta-value is defined as the relative deviation of the isotope ratio of the sample (R_x) to the isotope ratio of a given standard (R_s):

$$\delta = (R_x / R_s - 1) * 1000 \quad (‰) \qquad 2.4$$

There are different standards commonly used for different isotopes, such as Vienna Standard Mean Ocean Water (VSMOW), Standard Light Antarctic Precipitation (SLAP) for isotopes of the water molecule, or Peedee Belemnite (PDB) for carbonates and Canyon Diablo Troilite (CDT) for sulfur.

$\delta^{18}O$ versus $\delta^{2}H$ values of worldwide rainfall data are plotted relative to each other yielding the global meteoric water line (GMWL), which was first elaborated by Craig in 1961. It is described by the following equation:

$$\delta^{2}H = 8 * \delta^{18}O + 10 \qquad 2.5$$

The y-intercept of this line, called the deuterium excess, is changeable depending on the location. Typical ^{2}H-excess values range from 0 – 20; it is zero in the average composition of ocean water (VSMOW). The ^{2}H-excess is a result of ^{2}H being enriched by fractionation processes relative to ^{18}O, leading to an excess of approximately 10 ‰ during the evaporation of ocean water at an average humidity of 85 %. The slope of the line changes with evaporation conditions (humidity, temperature, etc.) and levels off as water re-evaporates after initial rainfall from evaporated ocean water.

The meteoric waterline of the Mediterranean and the Middle East put forward by Gat in 1971 has a relatively large deuterium excess. It is expressed by:

$$\delta^{2}H = 8 * \delta^{18}O + 22. \qquad 2.6$$

The analysis of stable isotopes for this study was conducted at the Institute for Hydrology Freiburg with an Isotope Ratio Mass Spectrometer (IRMS) Type Delta S, with a dual inlet system, produced by Finnigan Mat and with VSMOW as the reference standard. For the measurement of ^{18}O the probes are equilibrated with CO_2-gas. In order to get adequate results from the highly saline water samples equilibration time and temperature had to be adjusted and hence the samples were left to equilibrate for 12 hours at 36°C, instead of the usual 11 hours at 16 °C. The average error of measurement is 0.2 ‰ for oxygen-18 and 2 ‰ for deuterium.

H-isotopes are prepared for measurement by chromium reduction method, using 1 ml samples, of which 1 µl is injected to the chromium-reduction oven at a temperature of 900 °C.

The local meteoric isotope data for the area of this study were elaborated from data for Israel and the west of Jordan accessible through the ISOHIS programme of the IAEA (2004).

2.1.3 ^{34}S

The section below is based on Hoefs (1997).

Sulfur is present in nearly all natural environments. Sulfur is the major non-metal in ore deposits and it is abundant as sulfate in evaporites. It occurs as a minor component in igneous and metamorphic rocks and throughout the biosphere in organic substances. In marine sediments it occurs as both sulfide and sulfate and in ocean water as sulfate.

The most abundant stable isotope of sulfur is ^{32}S with an abundance of 95.02 %. ^{34}S has an abundance of 4.21 %. The two minor isotopes ^{33}S and ^{36}S can be neglected, as they are not of interest for this study.

Two types of fractionation mechanisms are responsible for the naturally occurring sulfur isotope variations:

1) Various chemical exchange reactions between both sulfate and sulfides and the different sulfides themselves, such as thermochemical reduction of sulfate and isotope exchange reactions among coexisting sulfide minerals.

2) A kinetic isotope effect during the bacterial reduction of sulfate, which produces the largest fractionations in the sulfur cycle. This fractionation process will be described in detail below.

Desulphovibrio are bacteria that transform sulfate to hydrogen sulfide under anaerobic conditions, while they gain their energy by coupling anaerobic oxidation of organic matter to the reduction of sulfate. The rate of sulfate reduction is limited by breaking of the first S-O bond, namely the reduction of sulfate to sulfite. Sulfides in sediments and euxinic waters are commonly depleted in ^{34}S by 45-70 ‰, while pure cultures of sulfate-reducing bacteria produce sulfide depleted in ^{34}S by 4-6 ‰.

Most of the sulfide produced by sulfate reduction is re-oxidized. Studies have shown that through a repeated cycle of sulfide oxidation to elemental sulfur and subsequent disproportionation, bacteria can generate the large ^{34}S depletion of many marine sulfides.

Another factor which may influence the sulfur isotope composition is whether sulfate reduction takes place in an open or a closed system. An open system has an infinite reservoir of sulfate in which continuous removal from the source produces no detectable loss of material. Typical examples are the Black Sea and local oceanic deeps. In such cases, H_2S is extremely depleted in ^{34}S while consumption and change in ^{34}S is negligible. In a closed system, the preferential loss of the lighter isotope from the reservoir has a feedback on the isotopic composition of the unreacted source material, leading to a steady increase of $\delta^{34}S$ in the residual sulfate with increasing sulfate consumption. This can be seen in figure 2.1. The curve for the derivative H_2S is parallel to the sulfate curve at a distance which depends on the magnitude of the fractionation factor. As shown in figure 2.1, H_2S may become isotopically heavier than the original sulfate when about two thirds of the reservoir has been consumed. The $\delta^{34}S$-curve for total sulfur asymptotically approaches the initial value of the sulfate.

Due to the activity of sulfate-reducing bacteria, most sulfur isotope fractionation takes place in the uppermost mud layers in shallow seas and tidal flats. As a result, sedimentary sulfides are depleted in ^{34}S relative to ocean water sulfate. The depletion is usually in the

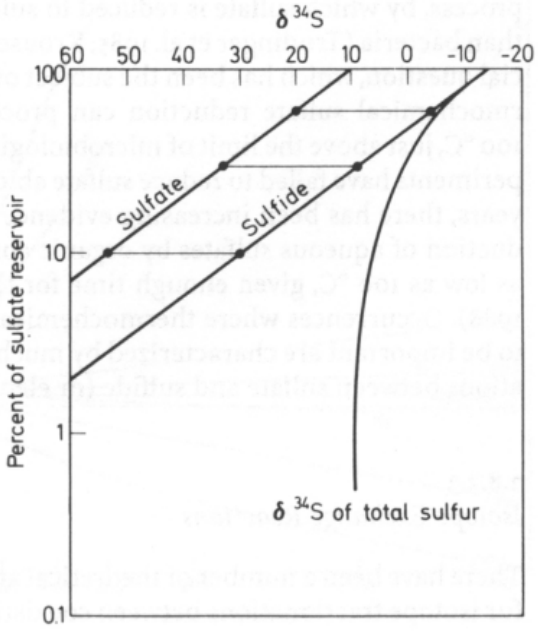

Figure 2.1: Rayleigh plot for sulfur isotope fractionations during the reduction of sulfate in a closed system. Assumed starting composition of initial sulfate, 10‰ (Hoefs, 1997).

order of 20-60 ‰.

Bacterial sulfate reduction is accomplished by the oxidation of organic matter:

$$2CH_2O + SO_4^{2-} \rightarrow H_2S + 2HCO_3^- \qquad 2.7$$

the resulting H_2S reacting with available iron, which is in the non-silicate bound form (oxyhydroxides).

The isotope fractionation between dissolved sulfate in (ocean) water and gypsum or anhydrite is negligible, whereby the isotopic composition of these evaporites is a reflection of sulfur isotope composition of marine sulfate through time. When water dissolves sulfatic evaporites the isotopic signature of dissolved sulfate within this water

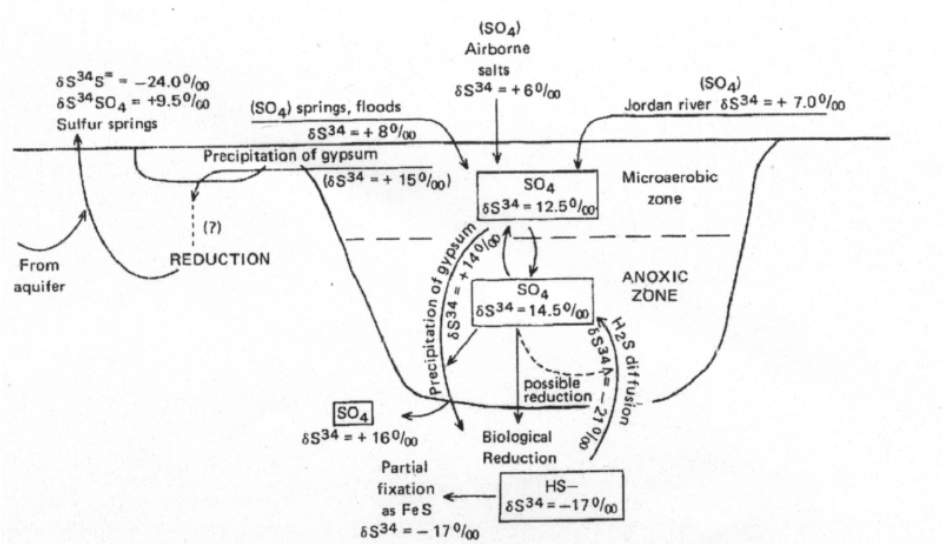

Figure 2.2: Sulfur cycle for the Dead Sea (Nissenbaum, 1975).

should represent the isotopic composition of these evaporites, which is then depleted by bacterial activity.

The sulfur cycle for the Dead Sea has been described by Nissenbaum (1975). It is controlled by the bacteria of the Dead Sea. While Dead Sea deep sediments show a scarcity of gypsum, shallow sediment traps contain large amounts. Referring to Neev & Emery (1967) he suggests that the precipitated sulfate is reduced to sulfide and that the bicarbonate produced in this process causes precipitation of $CaCO_3$. The interstitial water is highly depleted in sulfate and the isotope values in the iron sulfide in the sediment show depletion in $\delta^{34}S$ by 25 to 35 ‰, presumably reached by bacterial sulfate reduction. A schematic description of the sulfur cycle in the Dead Sea is given in figure 2.2.

Nissenbaum et al. (1990), stating findings of Neev & Emery (1967), points out that even though gypsum crystallised occasionally from the upper water mass and constituted a considerable portion of the deposits in sediment traps, it was almost completely absent from the deep, anaerobic sediments.

2.1.4 Radium Isotopes

2.1.4.1 Natural Decay Series of Uranium and Thorium

The following section is based on Kendall & McDonnell (1998).

Uranium and Thorium are long-lived radioactive elements naturally occurring in Earth material. During their decay they form other radioactive elements until finally, at the end of the decay chain they form stable plumb isotopes. The four different Radium isotopes ^{223}Ra, ^{224}Ra, ^{226}Ra and ^{228}Ra are radioactive elements formed as parts of the decay chains of ^{238}U, ^{232}Th and ^{235}U. ^{226}Ra with a half-life of 1601 years forms part of the ^{238}U decay series, ^{228}Ra with a half-life of 5.7 years and ^{224}Ra with a half-life of only 3.64 days both form part of the ^{232}Th decay series, and finally ^{223}Ra with a half-life of 11.1 days forms part of the ^{235}U decay series. These series are depicted in figure 2.3.

In a closed system the “parent” radionuclides ^{238}U, ^{232}Th and ^{235}U reach secular equilibrium with their “daughter” radionuclides when each daughter radionuclide reaches the same activity (referring to the number of disintegrations per unit time) as the parent radionuclide at the head of the chain. This activity is then proportional to the amount of parent radionuclide in the system. The time it takes to reach secular equilibrium is dependent on the longest-lived daughter in the chain, and is, as a rule of thumb, established after seven to ten times the half-life of that daughter radionuclide.

The relationship between the amount of a radionuclide and its activity is given by:

$$A = \lambda N \qquad 2.8$$

where A = activity,

λ = decay constant ($\lambda = \ln 2/t_{1/2}$, where $t_{1/2}$ is the radionuclide’s half-life) and

N = number of atoms of the radionuclide

The condition for secular equilibrium ($A_1 = A_2$ for two radionuclides A_1 and A_2 in the decay chain) can be written as:

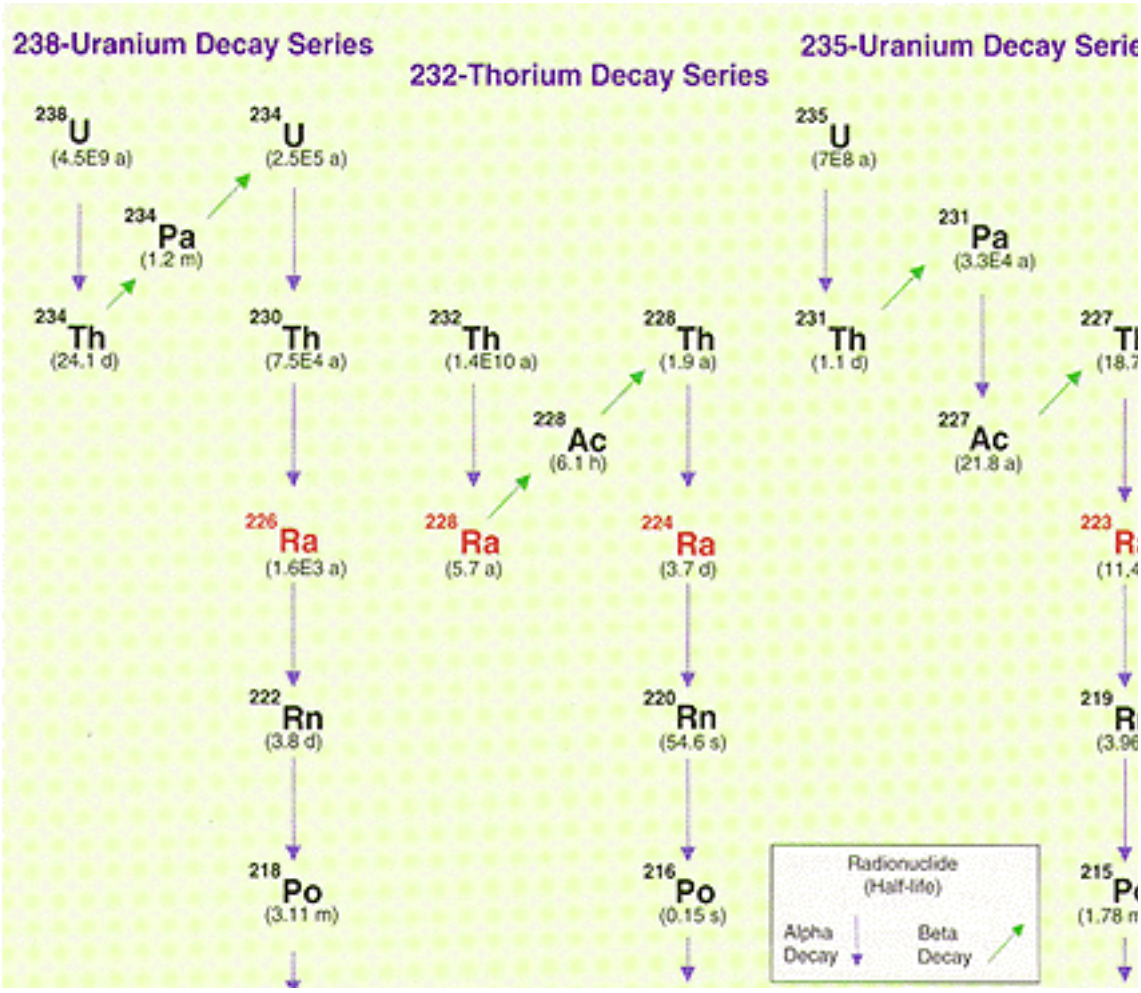

Figure 2.3: ^{238}U, ^{232}Th, and ^{235}U decay series (URL5).

$$\lambda_1 N_1 = \lambda_2 N_2 \qquad 2.9$$

and

$$N_1/N_2 = \lambda_2/\lambda_1. \qquad 2.10$$

Thus, the ratio of ^{238}U to ^{226}Ra at secular equilibrium is equal to the ratio of the decay constant of the latter to that of the former, 4.332×10^{-4} over 1.33×10^{11}, or 3.257×10^{-15}. Therefore, ^{226}Ra is about 10^{15} times more radioactive than an equal quantity of ^{238}U.

In nature, which rarely represents a closed system, elements are transported away from their origin by weathering of rocks, dissolving of minerals and transport of solutes, with water as its main agent. While some radionuclides are easily dissolved and transported by water, other elements of the same decay chain may have a strong affinity to adsorption to the rock material. The change in affinity from one element to the next is enormous.

In addition to chemical differences causing separation of decay-chain radionuclides during weathering, alpha-particle emission can also redistribute decay-chain radionuclides in a physical process. When an alpha-particle, consisting of two protons plus two neutrons, is ejected from a radioactive nucleus it causes the new nucleus to recoil up to several

hundred nanometers in the opposite direction, depending on its surroundings. If the atom is near a phase boundary the recoil can transport the atom across the boundary into a new environment. For instance, if the ^{238}U atom is located within a few nanometers of the surface of a quartz grain, the new nucleus may be ejected out of the grain into whatever lies on the other side, be it another grain or a pore filled with gas or liquid. This physical process causes the recoiled radionuclide to accumulate in the new phase without its immediate parent. Once the supply of the radionuclide to the new phase is stopped, the daughter product accumulated in the new phase will decay away at a rate determined by its half-life.

Whether the new radionuclide remains in solution, precipitates or adsorbs depends on the element itself and on the conditions it finds itself in. In order to understand what happens to the different radium isotopes, their geochemistry as well as that of their parent radionuclides will be explained in short below.

Thorium is one of the most insoluble elements in the decay chains. Its high charge (+4) and its high ionic potential cause it to form insoluble hydroxides under most natural conditions. For this reason natural waters contain very little Th and it is not transported very far in solution, as it becomes adsorbed onto colloidal or clay sized particles where it can be transported as suspended sediment in streams. Th is strongly adsorbed onto kaolinite and quartz.

Uranium can be present in oxidation states +6, +5 and +4. The +6 state is predominant in oxidizing environments and forms soluble complexes such as UO_2^{2+}, UO_2CO_3, $UO_2(CO_3)_2^{2-}$, and $UO_2(HPO_4)_2^{2-}$, depending on the anions present in the water and the pH, with the bicarbonate species usually being the most abundant. Bicarbonate charged waters are therefore very effective leaching and complexing agents for uranium.

Under progressively reducing conditions uranium is reduced to +5 and +4. This generally occurs as free oxygen is removed from the system, followed by the appearance of hydrogen sulfide. The result is the removal of uranium from solution due to the precipitation of insoluble uranium minerals (uraninite UO_2, coffinite $USiO_4*nH_2O$).

Uranium can also be removed from solution, even oxidizing ones, through adsorption onto solid substrates due to changing pH. Adsorption of uranium onto ferric oxyhydroxydes, clay minerals and even micaceous minerals at pH values common in natural waters is frequently observed.

These chemical characteristics allow uranium to be weathered from rocks, transported long distances in solution and then deposited by various means, far from the site of weathering, or to remain in solution for long periods of time.

2.1.4.2 Radium and its Isotopes ^{223}Ra, ^{224}Ra, ^{226}Ra and ^{228}Ra

The reactivity of radium takes up a position in between the reactivities of thorium and uranium in near-surface environments. With only one oxidation state (+2) it forms only weak complexes in solution. As a sulfate, however, it is highly insoluble and will precipitate with Ba or Ca, although it never reaches concentrations high enough to precipitate as pure $RaSO_4$. In most aqueous situations radium is subject to adsorption onto silicates, clays, and oxyhydroxydes, but not as strongly as thorium. It is therefore detectable in most waters.

Like the other uranium-series nuclides, radium enters the aqueous phase during the weathering of geological materials. Dissolution of silicates and carbonates is one mechanism that releases radium into solution. Alpha-particle recoil is a second means by which radium can enter solution, since the parents of all naturally occurring radium isotopes are alpha emitters and supply radium even if dissolution were not taking place. A third mechanism that supplies radium to groundwater, which takes place at high temperatures and salinities as in geopressured aquifers, is the continuous re-equilibration of silica between solution and a mineral grain surface such as quartz. When the silicate grain is continually exchanging silica with the solution it “uncovers” radium atoms which are then able to escape into the solution where they remain because the high ionic strength of the solution prevents adsorption.

In carbonate aquifers dissolution of the easily soluble matrix is the primary route of entry of radium into water. Featuring large fractures or conduit flow there is relatively little surface area for alpha-recoil in carbonate rocks. Because limestone is rich in uranium and lacks thorium, the radium in limestone and waters which originate from limestone aquifers will tend to be enriched in the ^{226}Ra isotope relative to ^{228}Ra.

Hammond et al. (1988) pointed out that the addition of radium to the brines by dissolution and leaching should depend on the abundance of the atoms in the solid phase and can be expressed by a first order reaction:

$$P_w = k * A_r / \lambda \qquad 2.11$$

where P_w = input of a radium isotope from rock to brine by weathering and leaching (atoms /(grams*second)),

k = rate constant for weathering and leaching,

A_r = isotope activity in the host rock (atoms / (grams*second)) and

λ = decay rate of the radium isotope in question (1/second).

Hence the effectiveness of adding isotopes by weathering (as opposed to recoil) depends on the ratio k/ λ. This ratio increases with half-life, so that the weathering supply may exceed the recoil supply for longer lived isotopes. This results in a lower ^{228}Ra/^{226}Ra ratio in the solute than in the aquifer rocks.

In clastic aquifers, dissolution is a rather limited way of entry of radium into the aqueous phase, because of the low solubility of silicates. Here, ion exchange would also be a limited source of radium in water. So the main route of entry appears to be alpha-particle recoil. Each Ra isotope will accumulate at a rate controlled by its half-life. Therefore, ^{224}Ra would accumulate fastest, followed by ^{223}Ra, ^{228}Ra and finally ^{226}Ra. The growth of each nuclide to its equilibrium value then follows the equation:

$$Ra_t = Ra_{eq} (1 - e^{-\lambda t}) \qquad 2.12$$

where Ra_t = radium activity at time t

Ra_{eq} = radium activity present at equilibrium

Here, ^{224}Ra, whose half-life is only 3.64 days, would build up to its equilibrium value after about 30 days, while ^{226}Ra would not reach its equilibrium value for thousands of years. This holds true for the growth of a radioactive daughter supplied to a system at a constant

rate when the only loss from the system is radioactive decay. The actual equilibrium values that the nuclides achieve depend on the rate of supply to the water, which in turn depends on the concentration of the parent nuclides in the matrix and on the surface area to volume relationship of the aquifer.

The result of this behaviour is that “young” water, which has been in the system for only several years, would have a high $^{228}Ra/^{226}Ra$ activity ratio, since ^{228}Ra would accumulate faster than ^{226}Ra. These radium isotope ratios can be used to “date” groundwater, meaning to determine a mean residence time of the water. What should be taken into consideration when doing so is the heterogeneity of the matrix in terms of grain size, U/Th ratio, and the absence of other sources of radium except alpha-recoil effects.

2.1.4.3 Mixing Processes Indicated by Radium Isotope Ratios

Mixing processes can be measured by analysing radium isotope ratios. This method can be used when two waters of different origin mix, for instance, one water type sourcing in a carbonatic aquifer would contain higher values of ^{226}Ra due to the abundant U and low Th in carbonate rock, while $^{226}Ra/^{228}Ra$ ratios picked up by waters weathering crystalline rocks are more equal, because the activities of U and Th are more equal. Conservative mixing is present when mixtures of two end-member waters with different $^{228}Ra/^{226}Ra$ ratios plot on a straight mixing line connecting the two end-members (figure 2.4, line connecting points A and B). The ratio of a water plotting mid-way between two end-members should contain 50 % of each end-member, while a water sample plotting three-quarters to one end of the mixing line contains one quarter of one end-member and three quarters of the other end-member.

In the case of non-conservative mixing soluble radium becomes adsorbed onto sediment particles or adsorbed radium gets released from sediment to solution due to changing conditions of pH or ionic strength during the mixing of the two waters. If non-conservative behaviour causes radium removal from solution it would affect each radium isotope to an equal degree. Therefore, as shown in figure 2.4, the resulting water mixture would lie on a line connecting the origin of the two axes with the point on the mixing line (dashed

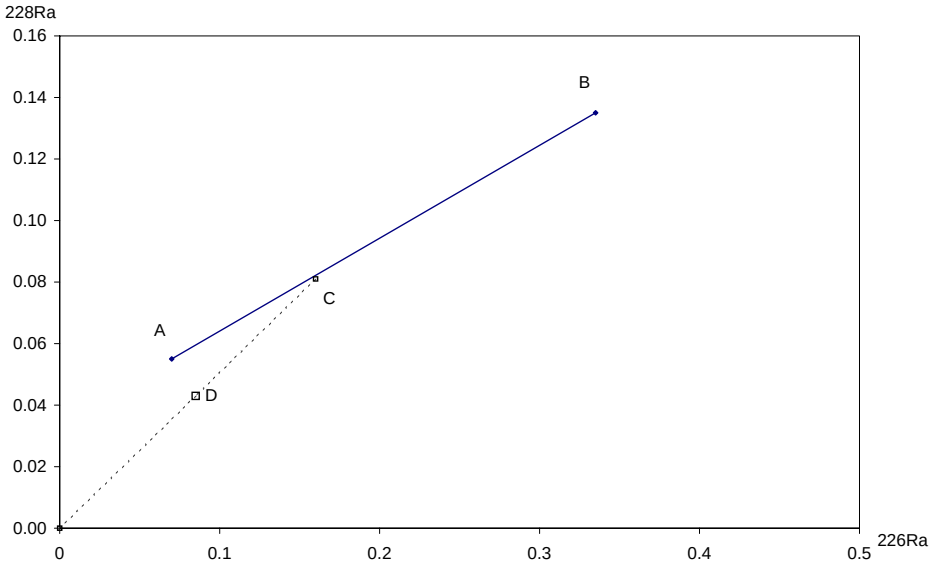

Figure 2.4: Schematic graph for non-conservative mixing of radium isotopes. For explanations see text (After Kraemer & Genereux, 1998).

line) where the mixture would have plotted if no removal had occurred. To correct for non-conservative removal of radium during mixing one has to extend the line connecting the origin of the graph and the non-conservatively mixed sample (point D) back to the conservative mixing line at point C. From here, mixing ratios can be calculated for point C, as for conservative mixing, representing mixing fractions for point D.

2.2 Fluorescent Dye Tracers

Fluorescent dyes are commonly used as tracers in surface and groundwater hydrology, as they are easily detectable at low concentrations. Their use and characteristics have been widely studied by Kaess (1998), Kasnavia, De Vu & Sabatini (1999), Smart & Laidlaw (1977), and many others. However, very little work has been done on the behaviour of fluorescent dye tracers in highly saline media.

Fluorescent dye tracers are characterised by a specific excitation wavelength which generates a response at a specific emission wavelength and can therefore be classified into three different groups according to their characteristic emission wavelength: blue dye tracers (Na-Naphtionate, Amino G acid) with an emission wavelength in the violet to blue range (380 - 490 nm), green dye tracers (Na-Fluorescein / Uranine, Pyranine) with an emission wavelength in the green range (490 – 570 nm), and red dye tracers (Rhodamines) emitting in the orange to red range (580 – 750 nm).

This fluorescence is controlled by various factors. Depending on which tracer is used, fluorescence is influenced by pH, the tracer can be depleted by light, and it can be adsorbed to the matrix or riverbed. Also, in the field background concentrations of these tracers may occur, especially in the green wave band (Smart & Laidlaw, 1977).

To date no detailed studies on salinity effects have been undertaken and these will be described in the course of this study.

2.2.1 Choice of Dye Tracers for Investigation

The choice of dye tracers for experiments in the laboratory or in the field were based on the known characteristics, some of which are listed below.

Eosin ($C_{20}H_6Br_4Na_2O_5$, C.I. number: 45380) and Uranine ($Na_2C_20H_{10}O_5$, C.I. number: 45350) are little adsorptive, Eosin slightly more than Uranine. The influence of pH increases below pH 5.5 for Eosin and from pH < 6 (8.5) for Uranine, resulting in a reduced fluorescent effect (see figure 2.5). Both are easily dissolved and non-toxic. Their detection limit is very low (Uranine: 0.001 µg/l, Eosin: 0.005µg/l).

The Uranine cation is highly adsorptive at very low pH-values and to organic substances due to the negative surface charge of these substances. While Uranine is a bivalent anion in aqueous solutions, in which state is fluoresces, in concentrated solutions it exists as a monovalent anion. In acid environments Uranine is present as a monovalent cation with low solubility, which explains its adsorptive behaviour under these conditions. Uranine is destroyed by chlorine dioxide and oxidizers as used in water purification systems (Kaess, 1998).

Excitation/emission wavelengths are 515/540 nm for Eosin and for Uranine: 490/520 nm.

Pyranine ($C_{16}H_7O_{10}S_3Na_3$,C.I. number: 59040) can be used in acidic groundwater, where Uranine is less suitable. Pyranine is strongly influenced by pH < 9, loosing a great part of its fluorescence intensity, however for laboratory experiments fluorescence intensity at pH values around 6-7 is still strong enough at concentrations above 1 ppm (parts per million by volume) to be easily detected by common spectro-fluorimeters. At values below approximately pH 5 Pyranine fluorescence can be read at a secondary emission peak around 455 nm (excitation 415 nm). The influence of varying pH to fluorescence of Pyranine and Uranine is portrayed in figure 2.5. Pyranine is non-adsorptive and highly soluble, but it is somewhat toxic (Benischke & Schmerlaib, 1986). Excitation / emission wavelengths at pH > 6 are 455/512 nm.

The Rhodamines, namely Amidorhodamin G (C.I. number: 45220), Rhodamin WT ($C_{29}H_{30}O_5N_2Na$, C.I.number: NA) and Rhodamin B ($C_{28}H_{31}N_2O_3Cl$, C.I. number: 45170), are highly adsorptive apart from Sulforhodamine B and G ($C_{27}H_{30}O_7N_2S_2Na_2$, $C_{25}H_{30}O_7N_2S_2Na_2$, C.I. numbers: 45100 and 45220, respectively), which are a little less adsorptive. Sulphorhodamine B and G show low solubility. Rhodamine dye tracers have been tested to be toxic. Excitation / emission wavelengths range from 530 - 560 / 550 -

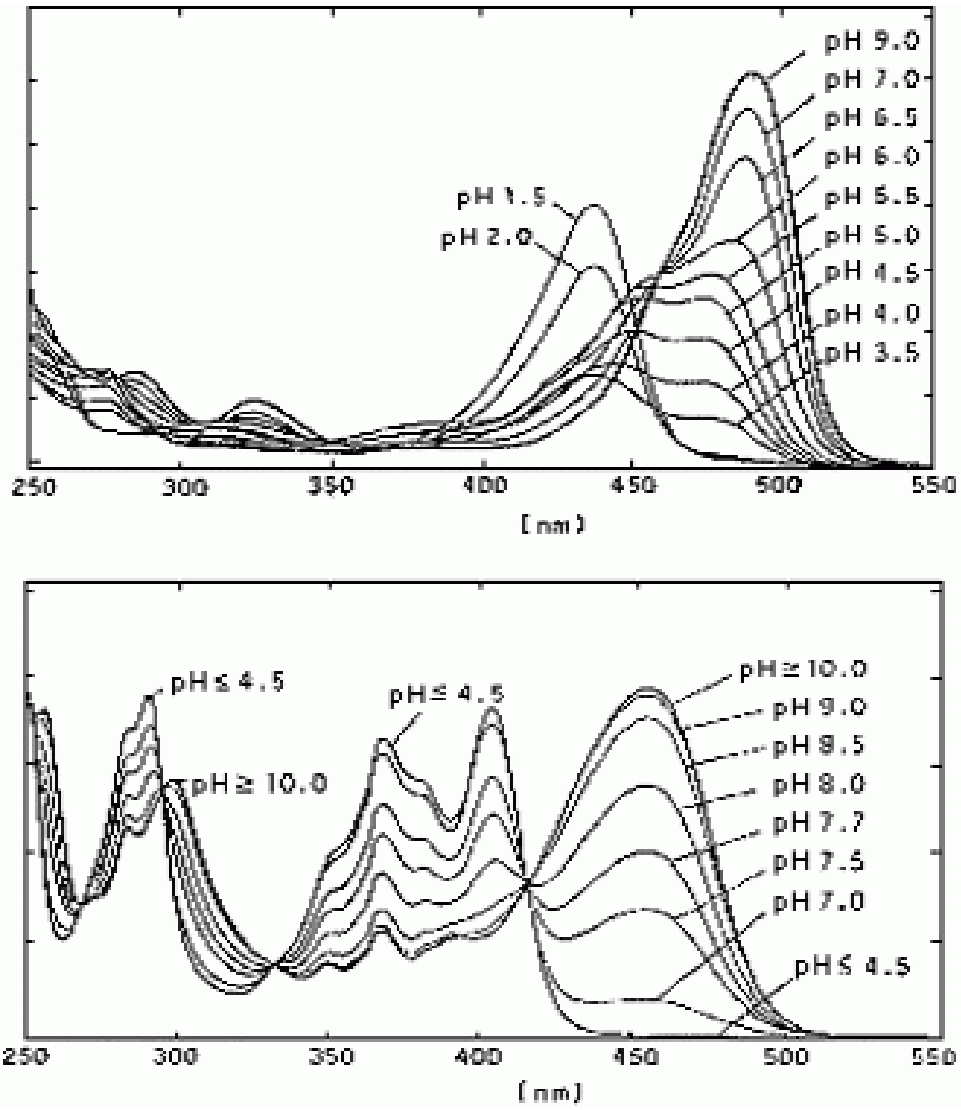

Figure 2.5: pH-dependence of fluorescence of Uranine (above) and Pyranine (below) (Behrens, 1986).

580 nm (Kaess, 1998).

Naphtionate ($H_2N(C_{10}H_6)SO_3Na$, C.I. number: N.A.) exhibits stable fluorescence between pH-values of 4 – 9. The very minor adsorption of Naphtionate is irreversible; velocities may be higher compared to Uranine due to the smaller molecular size of Naphtionate. The detection limit is comparatively high (0.3 – 0.5 µg/l) due to a large background in natural waters. In solution with water it is invisible in common concentrations. Recommended tracer quantity is > 10 times more than for Uranine under the same conditions (Leibundgut, 1986). Excitation / emission wavelengths are 325 / 425 nm.

The following tracers were analysed for their behaviour in highly saline media: Uranine, Naphtionate, Pyranine and Eosin.

2.2.2 Analysis of Dye Tracers

Water samples containing fluorescent dye tracers are easily analysed using a spectro-fluorimeter. These fluorimeters contain two monochromators which continuously move along the specified spectrum, allowing exact distinction between tracers with different excitation and/or emission wavelengths ($\delta\lambda$ > 20 nm). The configuration of a spectro-fluorimeter is depicted in figure 2.6. By scanning a broader spectral range than that of the tracer peak alone background fluorescence can be determined. With this method tracers can be detected at fairly low concentrations (0.5 µg/l for Uranine). Synchronous scanning or double-scanning allows detection of the ideal spacing of wavelengths and the exact location of the excitation and emission peaks. In this method both monochromators move along the spectral range keeping a fixed wavelength spacing, at the same time. The results of a synchronous scan can be seen in figure 2.7. A great advantage of modern spectro-

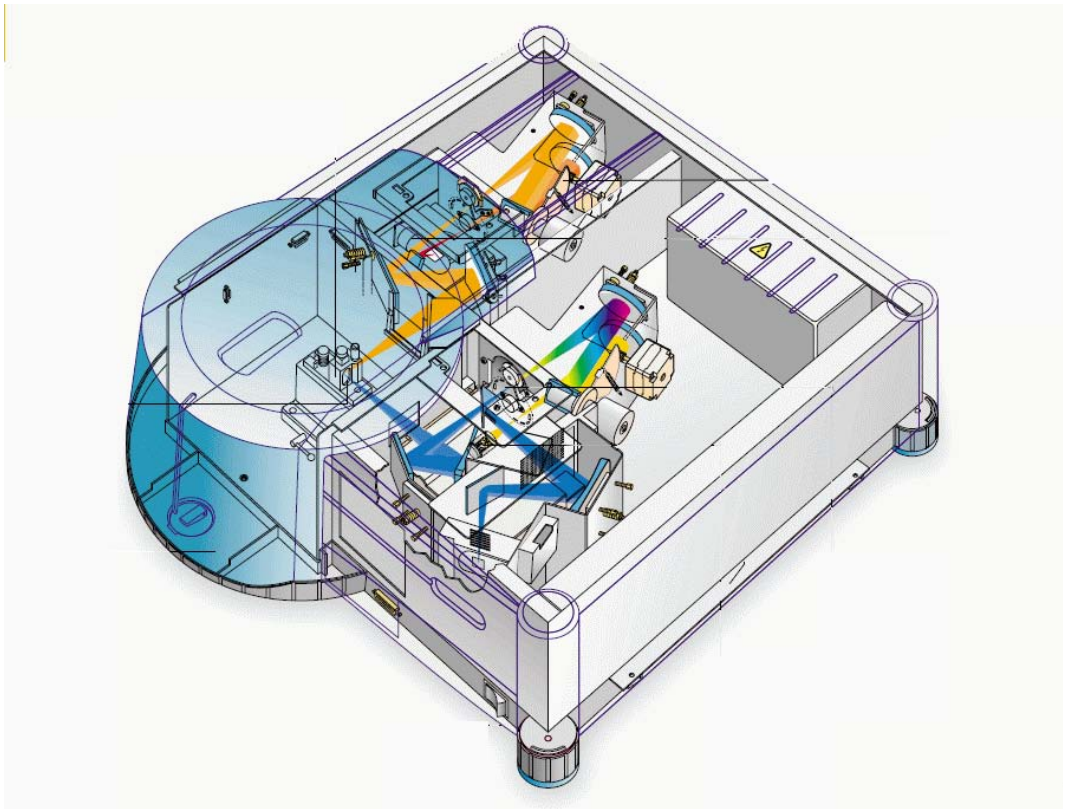

Figure 2.6: Configuration of a spectro-fluorimeter (URL5).

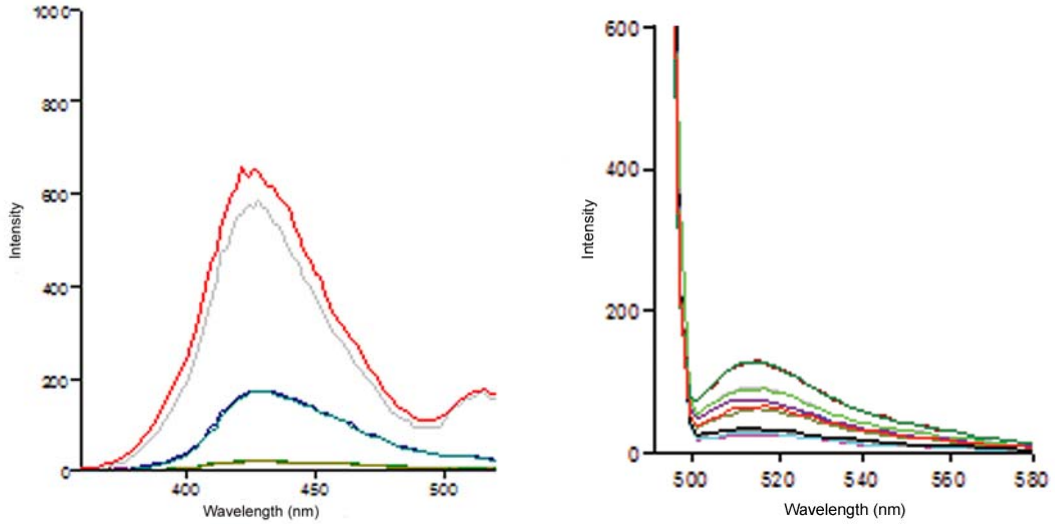

Figure 2.7: Emission scans of Naphtionate (left) and Uranine (right) at different concentrations: excitation wavelengths are fixed while emission spectra are scanned.

fluorimeters is that a large number of samples can be read in one run.

In this study fluorescent water samples were analysed with a Cary Eclipse Fluorescence Spectrophotometer by VARIAN at the Laboratory for Microalgae at Ben Gurion University, Blaustein Institutes for Desert Studies, Sde Boquer Campus. The average error of fluorescent measurements is 3 %.

2.3 Design of the Laboratory Experiments

The effect of salinity on the fluorescence of tracers can easily be determined by preparing tracer solutions in water with a varying degree of salinity.

Batch and column experiments are common methods for determining the behaviour of tracers under specified conditions, and to predict their fate in field experiments.

2.3.1 Batch Experiments

In batch experiments a specific amount of tracer solution is mixed with a specific amount of solid material and then is shaken for several hours. These experiments are used to determine adsorption coefficients (percentage of adsorbed tracer from the initial amount of tracer) or strain coefficients (ratio of yielded concentration to initial input concentration), or to characterise the interaction between tracer and different solid materials. The distribution coefficient K_d describes the tracer's affinity to adsorption. Adsorption is dependent on several factors, for example the charge of the surface elements of the solid material and the concentration of the tracer in solution. K_d is defined as:

$$K_d = \frac{C_2}{C_1} \qquad 2.13$$

where K_d = distribution coefficient (cm^3/g),

C_1 = tracer concentration in the solution (g/cm^3),

C_2 = adsorbed tracer (g/g).

It is calculated from:

$$K_d = \left(\frac{C_0}{C_1} - 1 \right) \cdot \frac{V_s}{m} \qquad 2.14$$

with C_0 = initial tracer concentration in the solution (g/cm³),

C_1 = tracer concentration in solution after contact with adsorbing material (g/cm³),

V_s = solution volume (cm³),

m = matrix dry matter (g).

2.3.2 Column Experiments

Column experiments are prepared by packing a cylinder with sediment or other solid material, and connecting the cylinder to a constant flow by a pump or a MARIOTTE-flask. The tracer is injected directly at the inlet. Breakthrough curves are acquired at the outlet by sampling over a certain period of time. From these, the flow velocity and retardation factor R can be calculated.

Retardation is the deceleration of the tracer with respect to water velocity, which is a result of adsorption and desorption processes.

$$R = \frac{v}{v^*} = 1 + \frac{\rho_b}{n_e} \cdot K_d \qquad 2.15$$

where R = retardation factor,

v = mean water velocity (velocity of the ‘ideal’tracer) (m/s),

v^* = pore velocity (mean tracer velocity) (m/s),

ρ_b = soil bulk density (g/cm³),

n_e = effective porosity,

K_d = distribution coefficient.

A retardation factor R > 2 indicates irreversible adsorption. The conversion of K_d values acquired from batch experiments into R does not show accordance with R determined directly from column experiments.

2.4 Theoretical Background for the Evaluation of Experimental Data

The breakthrough curves received from column experiments can be evaluated by fitting a theoretical curve to the measured data. By doing so characteristic parameters can be calculated.

2.4.1 The Equilibrium Convection-Dispersion Equation

The advection - dispersion model (CDE: convection – dispersion equation) describes the tracer's transport through the column with an advective term, which describes the tracer's transport in the direction of flow, and a dispersive term, which describes the dispersion of the tracer in the matrix, evoked by different flow paths and directions, which are forced upon the tracer by different pore sizes, friction on cavity walls, and tortuosity of inhomogeneous media. The equation put forward by Maloszewski & Zuber (1982) has the form:

$$c(t,x) = \frac{M \cdot x}{Q \cdot \sqrt{4 \cdot \pi \cdot D_L \cdot t^3}} \cdot \exp\left\{-\frac{(x - v \cdot t)^2}{4 \cdot D_L \cdot t}\right\} \qquad 2.16$$

where c = concentration of tracer in solution (mg/m³)

A = discharge area (m²)

Q = discharge (m³/s)

D_L = longitudinal dispersion coefficient (m²/s)

M = amount of tracer injected (mg)

x = flow distance (m)

v = average flow velocity of water (m/s)

This equation is an analytical solution to the one-dimensional convection – dispersion model for a DIRAC – impulse of tracer input, and delivers the tracer concentration as a function of time or space. D and v are the two parameters for adjustment of the fitting curve.

In case of adsorption of the tracer the equation is changed to:

$$c(t) = \frac{M}{Q} \cdot \frac{x}{\sqrt{4 \cdot \pi \cdot D_L^* \cdot t^3}} \cdot \exp\left\{-\frac{(x - v^* \cdot t)^2}{4 \cdot D_L^* \cdot t}\right\} \qquad 2.17$$

with

$$D_L^* = \frac{D_L}{R} \quad \text{and} \quad v^* = \frac{v}{R} \qquad 2.18$$

where D_L = dispersion coefficient of the ideal tracer (water),

D_L^* = dispersion coefficient of the real tracer,

v = flow velocity of the ideal tracer (water),

v^* = flow velocity of the real tracer.

This equation explains retardation but no tailings, since it only takes into account adsorption with immediate equilibrium. Zuber (1986) presents a further model which explains tailings by taking into account adsorption and desorption processes (first-order kinetic reactions). The theory is that equilibrium of adsorption and desorption between the solid and the liquid phase is reached ever faster the higher the concentration gradient.

2.4.2 The Non-Equilibrium Convection-Dispersion Model or the CXTFIT-Code

A similar model called CXTFIT, written by Toride et al. (1999) as an updated version of the original version by Parker and van Genuchten (1984) was used with STANMOD computer software by Simunek et al. (1999). The equation for this model requires the application of an ideal tracer, together with the real tracer as four (six) parameters are to be determined. Fitting parameters are: pore velocity v, dispersion coefficient D, retardation factor R, partitioning coefficient β, transfer coefficient ω, and first order decay coefficient μ (μ_1 and μ_2 for decay in the liquid / equilibrium and solid / non-equilibrium phase, respectively). Other coefficients may be added for production.

For calculations of the BTCs the one-site chemical non-equilibrium model with first-order kinetic adsorption sites was used. For steady-state flow in a homogeneous soil, transport of a linearly adsorbed solute is given by:

$$\frac{\delta c}{\delta t} = D \cdot \frac{\delta^2 c}{\delta x^2} - v \cdot \frac{\delta c}{\delta x} - \alpha \cdot \frac{\rho_b}{\Theta} \cdot (K_d \cdot c - s) - \mu \cdot c. \qquad 2.19$$

Where: D = dispersion coefficient (L^2/T)

v = pore velocity (L/T)

α = first-order kinetic rate coefficient (T^{-1})

ρ_b = bulk density (M/T^3)

θ = volumetric water content (L^3/L^3)

K_d = distribution coefficient

c = volume averaged concentration of the liquid phase (M/L^3)

s = concentration of the adsorbed phase (M/M)

μ = first order decay coefficient (T^{-1})

The first order decay coefficient μ in its reduced form appears throughout this course, as the same decay rate was assumed for the solid and the liquid phase ($\mu_1 = \mu_2$). Analytical solutions are found for different initial, boundary and production value problems and can be found in Toride et al. (1999). For a DIRAC delta input function as the boundary value problem and zero initial and production values the analytical solution is:

$$C_1(Z,T) = M^* f(Z,T), \qquad 2.20$$

where C_1 = dimensionless flux-averaged concentration (c/c_0) and

M = the dimensionless amount of applied solute for DIRAC delta input.

The system calculates all parameters as dimensionless and gives:

$$f(Z,T) = \Gamma(Z,T) \cdot e^{\frac{\omega T}{\beta \cdot R}} + \frac{\omega}{R} \cdot \int_0^T \sqrt{\frac{\tau}{\beta} \cdot (1-\beta) \cdot (T-\tau)} \cdot \Gamma(Z,\tau) \cdot H(\tau,T) d\tau \qquad 2.21$$

$$\Gamma(Z,\tau) = e^{-\frac{\mu \cdot \tau}{\beta \cdot R}} \cdot \frac{Z}{\tau} \cdot \sqrt{\frac{\beta \cdot R \cdot P}{4 \cdot \pi \cdot \tau}} \cdot e^{\left[\frac{-P(\beta \cdot R \cdot Z - \tau)^2}{4 \cdot \beta \cdot R \tau}\right]} \qquad 2.22$$

$$H(\tau, T) = e^{\left[-\omega \cdot \frac{\tau}{\beta} \cdot R - (\omega+\mu) \cdot \frac{T-\tau}{1-\beta} \cdot R\right]} \cdot I\left[2 \cdot \frac{\omega}{R} \cdot \sqrt{(T-\tau) \cdot \frac{\tau}{\beta(1-\beta)}}\right] \quad 2.23$$

ω = dimensionless mass transfer coefficient between equilibrium and non-equilibrium phase (α (R-1)L/v),

T = dimensionless time (vt/L),

β = dimensionless partitioning variable between equilibrium and non-eq. phase (1/R),

R = retardation factor ($1 + \rho_b K_d / \theta$),

Z = dimensionless distance (x/L),

P = Peclet number (vL/D),

I = modified Bessel function of order one.

3. Description of the Study Site

3.1 Geology and Hydrogeology

The Dead Sea with a water level about 417 m below sea level (b.s.l.) is part of the Syrian-African rift, one of the largest pull–apart basins in the world. This basin extends from the southern Jordan valley near Jericho to the central Arava valley reaching a length of approximately 150 km. To the east, lying in the Kingdom of Jordan, the area forms a plateau 1000 – 1400 m a.s.l., which descends gradually away from the transform. The Dead Sea area attained its recent structural shape during Late Pliocene to Early Peistocene (Garfunkel, 1996).

The sampling area is located on the western Dead Sea shore from where the area arches up reaching a height of 600 to 800 m a.s.l., with peaks reaching 1000 m a.s.l. Here, in the Judean Mountains, some 30 km to the west of the study area, water feeding this area is recharged.

The Upper Judea Group aquifer is composed mainly of limestone and dolomite, intercalated by the less permeable Beit Meir and Yorque'am formations, which in parts separate the upper and the lower sub-aquifer. These sub-aquifers have significant outcrops in the Judean Mountains where aquifer recharge takes place. The upper sub-aquifer is partly overlain by chalks of the Mount Scopus Group and the lower sub-aquifer, mainly built of sandstone, is underlain by aquicludal formations (Kronfeld et al., 1992; Yechieli & Gat, 1997).

The third aquifer borders the other aquifers along large normal faults of the western mar-

Figure 3.1: View from En Gedi spring over the alluvial fan deltas, the Judean Mountains to the west and the Dead Sea in the background on the left hand side.

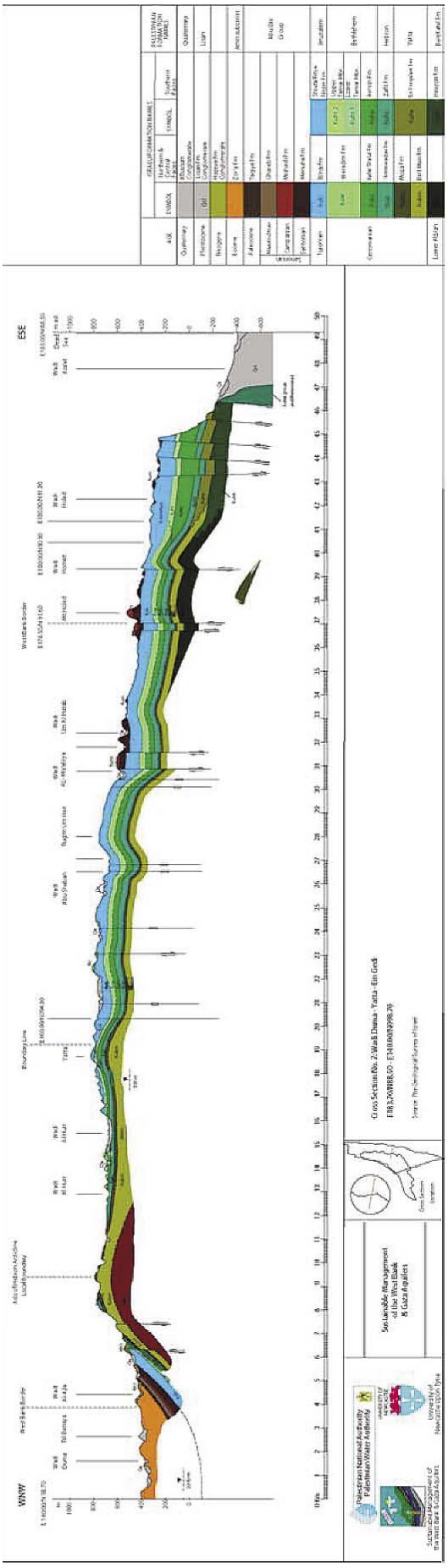

Figure 3.2: Geologic cross section: S/E - N/W from En Gedi via Yatta to Duma in the Westbank (Palestinian Water Authority, 2001).

gin of the Dead Sea rift. This aquifer, in direct vicinity of the Dead Sea, is an alluvial aquifer of Quaternary rocks and constitutes the coastal plain of the Dead Sea. Gravel, sand and clay deposited in fan deltas form several layers of this aquifer intercalated by lacustrine sediments: clay, gypsum and aragonite, as well as salt layers. Hydraulic gradients within the Quaternary Aquifer are between 0.002 and 0.007, varying along the coastal plain (Yechieli, 2000). Groundwater near the Dead Sea shore is mostly saline reaching salinities close to that of Dead Sea water. It mixes with fresh water intruding from the mountains to the west into the coastal aquifers resulting in a pronounced mixing zone. This zone is shifted towards the east as the Dead Sea shoreline recedes lakeward.

3.2 Geomorphology

This section is based on Bowman (1997).

Adjoining the fault escarpments to the west the Dead Sea Basin is shaped by distinctive alluvial fan morphology. Sediments covering the entire area are known as the Lisan Formation, which originate from the last deep-water body occupying the graben from 50000 to 12000 a BP.

The two large nahals, almost converging near the shore in the proximate area of study, are Nahal David and Nahal Arugot. The sublacustrine fan deltas are partly composed of limnic Lisan sediments, originally deposited in the canyons from where they were subsequently washed out, and of coarse fluviatile load of dolomite, limestone and flint. The sediments show crudely stratified and slightly cemented conglomeratic facies. The Lisan fan deltas at the foot of the escarpment are poorly sorted and layered, dipping moderately 3–6° lakeward with intercalations of transgressive beach units. Overlying these basal fan units are steeply inclined (24-34°), planar, and well sorted foresets of Gilbert-type delta with topset capping that demarcates the uppermost marginal facies of the Lisan Formation.

Since the lake level dropped, fan head entrenchment has been ongoing with forward and lateral growth of the fan units, with each entrenchment followed by basinward deposition of a younger fan, resulting in the formation of segmented telescopic alluvial fans, like the fan complex of the Ze'elim Formation. The main road along the lake is usually buried by winter floods, reflecting the migration of the depositional processes lakeward. Subsidence and the formation of sinkholes on some of the recent fans results from active piping and the dissolution of salt layers by the lakeward advancement of fresh water or wash-out of fine subsurface material.

3.3 Climate

The Dead Sea Basin, lying in the lee of the Judean Mountains, is the location of a hot, dry desert, yielding an average annual rainfall of 50-70 mm, which is limited to the months of December and January. Potential pan evaporation averages 2000 - 2300 mm per year, qualifying the local climate as arid to hyper-arid, although Alpert et al. (1997) found pan evaporation to amount more than 3500 mm per year in the southern Dead Sea area. Actual evaporation from the Dead Sea ranges from 1300 – 1600 mm per year. Relative humidity remains relatively low with an annual mean of 45 - 50 %. Mean temperatures lie between 20 – 24 °C with the hot, dry season lasting from February to mid-November,

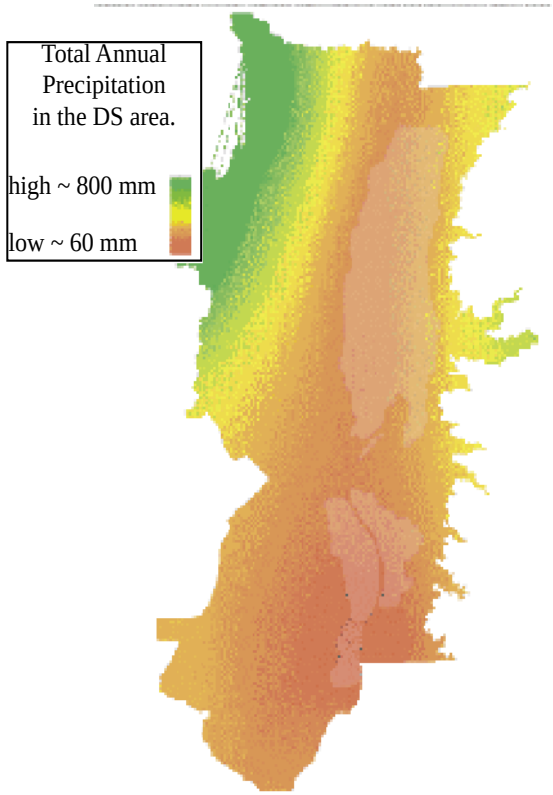

Figure 3.3: Total annual precipitation in the study area (URL2).

summer temperatures of 30 – 40 °C and a mean of 15 °C in January (Bowman, 1997).

The study area receives its water resources from the Judean Mountains, where the climate qualifies as Mediterranean / semi-arid with an average annual rainfall of 600 mm per year, and potential evaporation of 1700 mm per year. Here, the dry season lasts from mid-June to mid-September, with summer temperatures of around 26°C, dropping to about 9 °C in the wet winter. Mean annual temperatures here lie at 17 °C (URL2).

3.4 Soil, Land Use and Vegetation

'Soil' in common usage, meaning a layer developed from weathered bedrock and weathered plants, is, because of the lack of vegetation, not present within the study area of Dead Sea Basin, but rather it consists of the lacustrine sediments left behind by the retrieving Dead Sea, or sands and gravels washed down from the nahals (stream / wadi) which has sedimented in alluvial fans.

Plantations of date palms exist in patches along the coastal plain, irrigated by water diverted from the local springs. Other than that, the area is a tourist draw with hotels and health resorts scattered along the south-western part of the area.

A few settlements or kibbutzim are located within the study area, where people live from agriculture (dates) and tourism.

Natural vegetation is restricted to small areas around springs and oases, consisting of halophytes like Tamarix nilocita and tetragyna, reeds like Phragmites australis and shrubs.

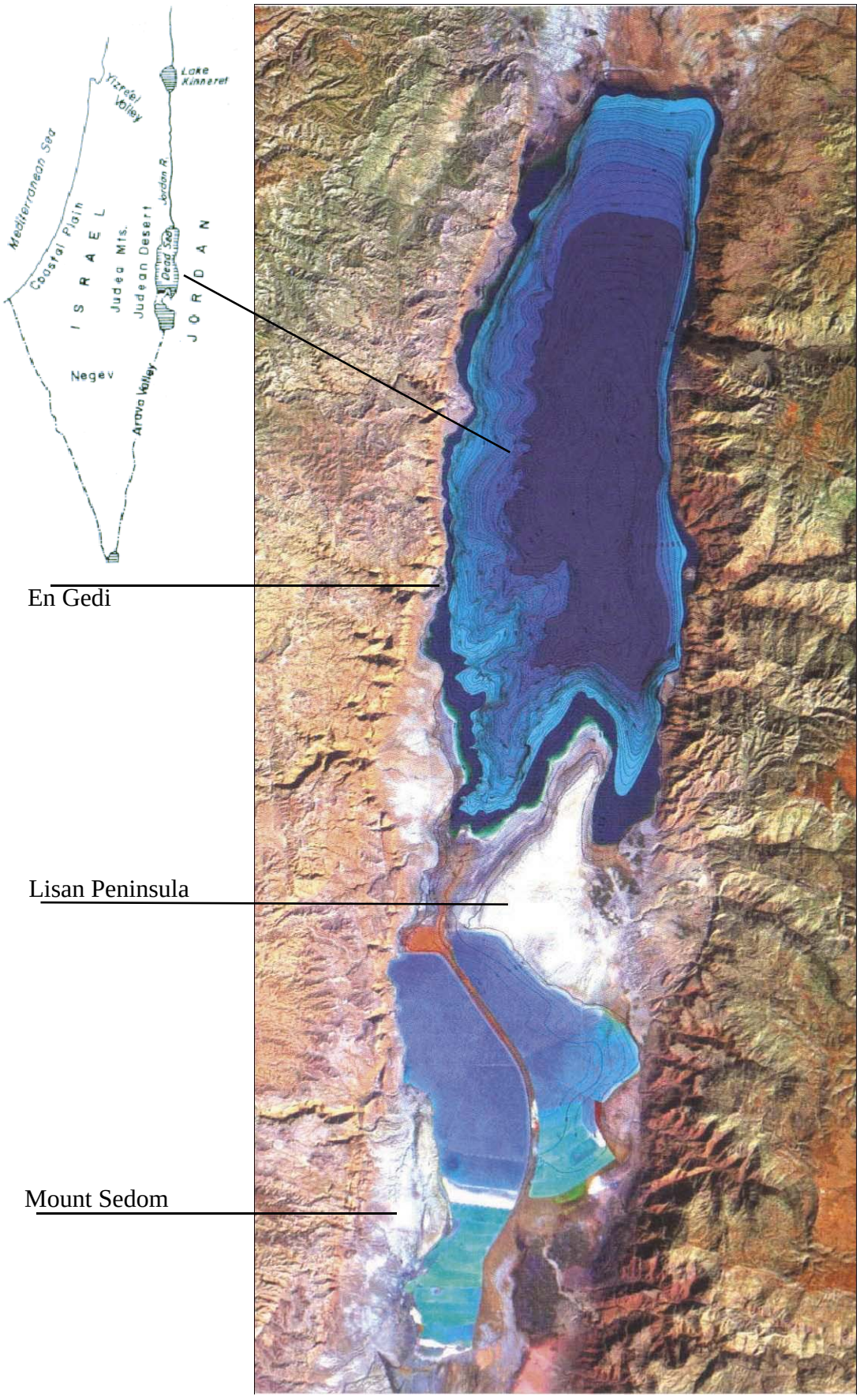

Figure 3.4: Topographic and bathymetric map of the Dead Sea Basin (Hall, 1997).

3.5 Hydrology

Due to the paucity of rainfall, the flow regime within the nahals of the Dead Sea Basin is one of flash floods, which originate in the Judean Mountains, occurring several times each winter. These waters locally infiltrate the Quaternary Aquifer, while direct recharge is negligible. Most of the water contained in the aquifer occurs through leakage from the Mountain Aquifer into the Quaternary Aquifer (Yechieli, 2000). Beyond the fault escarpment, canyons that cut their way westward into the steep limestone and dolomite rock, lead to springs and streams, whose waters are partly used for irrigation or bottled as drinking water, or diverted to the mineral industry south of the Dead Sea. The water that stems from these springs, once it reaches the Quaternary Aquifer, infiltrates and moves towards the Dead Sea as fresh groundwater until it reaches the fresh-saltwater interface. Small streams occur in the vicinity of near-shore oases, like the Enot Zukim (En Feshcha) oasis, and make way into the saline lake.

The lake itself currently has a surface area of 755 km², a maximum depth of 730 m b.s.l. (water depth is 310 m below surface), and a total volume of 128 km³. Only 50 years ago the surface area covered 1000 km², making a total volume of the water body of 143 km³. The loss in surface area is most extreme in the southern part of the Dead Sea, which is separated from the northern part by the Lisan Peninsula. The southern Dead Sea today consists of evaporation ponds, laid out by the Dead Sea works. Before the 1960's the main tributary of the Dead Sea was the Jordan River with an annual input of $1370 * 10^6$ m³. These days, the massive exploitation of the headwaters has reduced the total surface water input into the Dead Sea, including all sources to a mere $600 * 10^6$ m³. The other sources consist of large wadis / nahals like Nahals Nar, Draja, Arugot and Ze'elim on the western side of the rift and Wadis Walla and Moujib on the eastern side of the valley and smaller hot and cold springs and streams (Abu-Jaber, 1998). Locations of near-shore springs change over time, due to the drop of the terminal base level. The amounts of groundwater discharge into the Dead Sea are not well determined (Yechieli, 2006).

3.6 The Character of Dead Sea Water

The water of the Dead Sea is evaporated water of marine origin mixed with inflow from the Jordan River and various fresh and saline groundwater sources scattered around the lake shore. The high degree of evaporation results in saturation of various ions within the Dead Sea water and to total salinities of up to 330-350 g/l in the northern part of the Dead Sea and more than 400 g/l in the southern part, which is made up of evaporation ponds, thus containing ten-fold the amount of salt compared to regular seawater.

Unlike sulfatic seawater, the Dead Sea brine has essentially a Ca-chloridic composition ($Ca^{2+} > HCO_3^- + SO_4^{2-}$), saturated with respect to carbonate and sulphate, both present in very small concentrations, and is close to halite saturation. Basically the Dead Sea brine is of an Mg-Ca-K-Na and Cl-Br type, derived from the highly evaporated seawater of the Gulf of Sedom. The residue underwent modifying and mixing processes, combined with multiple progressive and regressive evaporation cycles, with periodic precipitation of halite and occasionally of carnallite (potassium-magnesium-chloride salt, $KMgCl_3 \times 6H_2O$) (Zak, 1997).

Table 3.1 shows the composition of major ions in Dead Sea water, analysed in the analyti-

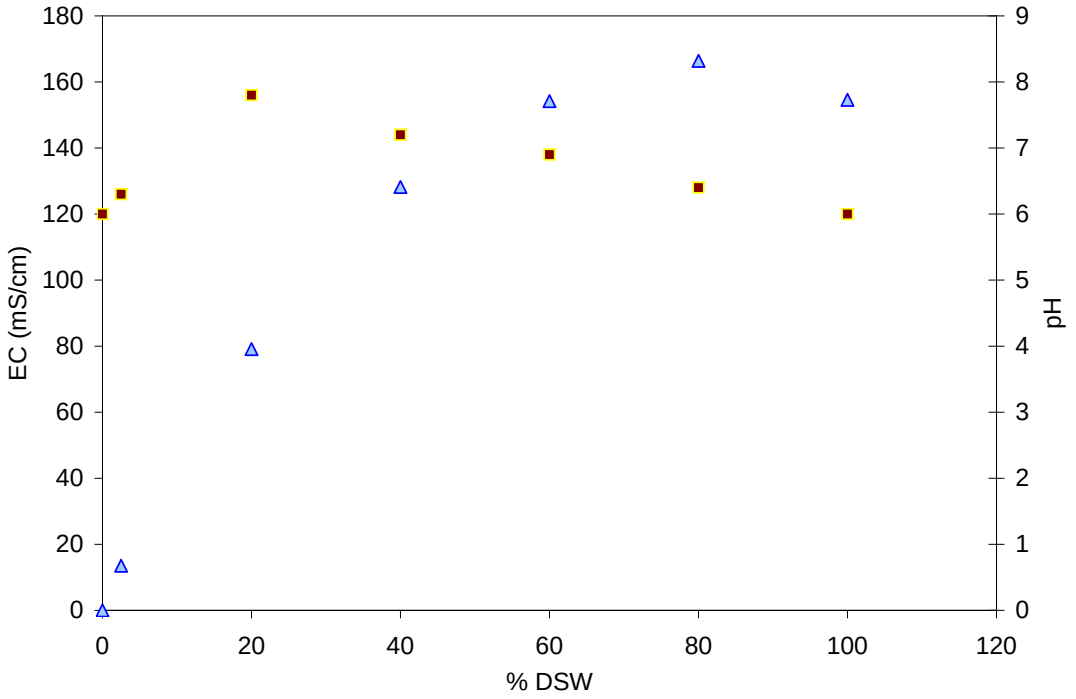

Figure 3.5: Electric conductivity (EC) and pH versus salinity in % DSW.

Table 3.1: Composition of major ions of Dead Sea water.

K^+	Ca^{2+}	Mg^{2+}	Na^+	Cl^-	Br^-	SO_4^{2-}	HCO_3^-	PO_4^-	NO_3^-	TDS
mg/l										
6280	17448	33200	43600	205600	5160	1660	318	0.387	0.1	313266

cal laboratory of the Department of Environmental Hydrology and Microbiology, Blaustein Institutes for Desert Research. Major ions were analysed by ion chromatography, PO_4 and NO_2 by spectro-photometry, and alkalinity was determined by titration.

Due to the extremely high salinities and ionic strength, Dead Sea water and groundwater in immediate vicinity of the Dead Sea shows a modified behaviour in various aspects. For instance, HCO^{3-}-concentrations determined by alkalinity titration method, without corrections for borate are shifted from the realvalue and are therfore an estimation,only. Apart from that the measured pH of Dead Sea water is not actually (the negative logarithm naturalis of) the amount of H^+ ions, as the great ionic strength distorts this value. Another physical property differing from common expectations is the trend of electric conductivity (EC), which shows a non-linear trend with increasing percentage of DSW, so that EC-values level off from around 70 – 80 % DSW. This fact has been discussed by Yechieli (2000 and 2006). Figure 3.5 depicts these properties.

3.7 The Fresh-Saline Water Interface in the Dead Sea Area

This section is based on Yechieli (2006).

The zone of density contrast between fresh and saline water bodies is defined as the fresh-saline water interface. The location of the interface is critically important in coastal aquifers as a basis for optimal water management. The fresh-saline interface around the

Dead Sea and other saline lakes is somewhat different to that near the ocean.

The depth of the interface between the two water bodies of contrasting density near saline lakes can be approximately defined by the Ghyben-Herzberg equation:

$$H_s = \rho_f / (\rho_s - \rho_f) * H_f \qquad 3.1$$

where H_s = depth to the interface below sea level (or lake level),

H_f = head of the water table above the saline water body,

ρ_f = density of the fresh groundwater, and

ρ_s = density of the saline groundwater.

Normal seawater is characterized by $\rho_s = 1.025$, and thus $H_s = 40 * H_f$, whereas for the Dead Sea, $\rho_s = 1.23$ and therefore $H_s = 4.35 * H_f$.

As a result, the interface in the Dead Sea area is very shallow, around ten times shallower than its depth near normal seawater. In the vicinity of the evaporation ponds of the southern Dead Sea, the brine density is even higher ($\rho_s = 1.28$), leading to $H_s = 3.57 * H_f$. Thus, higher density of the saline component is accompanied by a shallower interface and a thinner lens of overlying fresh groundwater.

Investigations in the Dead Sea area showed that, regions that were covered by the Dead Sea brine until recently (~10 years ago) already show a distinct fresh-saline water profile, which means that the flushing of the brine occurred here at a very rapid rate, but is still incomplete, with a salinity of ~20 % of the original Dead Sea brine.

Simple estimates of the locations of the interfaces are in general agreement with the predicted shallow depths. This correspondence is true also for the interface near the evaporation ponds, where the base level has decreased in the past (until the 1970's) and has been increasing in the past 20 years. Thus, the interface in the Dead Sea coast responds rapidly to changes in the base level.

Irregularities within the fresh-saline water interface could be recognized using the TDEM (time domain electromagnetic) method in several traverses (Kafri et al., 1997; Yechieli et al., 2001). These traverses detected the fresh-saline water interface near the expected equilibrium position, consisting of a westward dipping interface with some deviations due to: 1) an unflushed brine body, 2) a steepening of the interface in the western portion of the traverse close to the basin boundary fault, and 3) irregularity of the interface attributed to the existence of several subaquifers and / or the non-steady state conditions of the continuous drop in the Dead Sea level.

3.8 Conclusions

The study area lies in an arid to hyper-arid climate with temperatures averaging 20-24 °C, with peak summer temperatures reaching 40-45 °C and annual rainfalls averaging 50-70 mm, while potential evaporation lies around 2000-2300 mm per year. During the winter a regime of flash-floods shapes the local landscape.

The Judean Mountains, mostly made up of limestone and marl, arching up to the west, falling steeply from the Judean Desert with an altitude of up to 800 m down to the level of the Dead Sea, as low as -417 m within in a few tens of kilometers, are the source of fresh

springs and groundwater in this area. The receding Dead Sea increasingly reveals parts the Quaternary Aquifer that is made up of clayey, silty material. The Quaternary Aquifer is a heterogenic complex of lacustrine sediments and sands and gravels in the fan deltas, washed down from the nahals by winter floods.

Vegetation is scarce and succeeds to grow only around springs and in oases, or when artificially irrigated and used for agriculture.

This landscape of intense altitudinal contrasts hosts some of the most saline groundwaters. Through the receding of the Dead Sea, these groundwaters are mixed with fresh waters moving lakeward with the lowering of the lake level. Dissolution of subsurface salt layers lead to the formation of large sinkholes and subsidence of the ground along the western Dead Sea shore (figure 3.6). Because the influence the drop in the Dead Sea level on its surroundings does not always correspond to calculations and as the changes that take place, do so, so rapidly, reliable investigation methods are needed to predict their influence.

Figure 3.6: Sinkholes on the western Dead Sea shore.

4. Results

Following the overall structure of this work, the results chapter is divided into two major parts: the evaluation of the samples taken in the field and results of the laboratory experiments.

4.1 Environmental Tracers

On a field trip to the Dead Sea area in August 2006 five sites in two boreholes and one spring in the En Gedi area were sampled for different tracers in order to get a picture of what processes take place in the fresh-saline water interface and which tracers are able to capture these processes.

4.1.1 Sampling Sites

Sampling locations were chosen in order to get a profile of the fresh-saline water interface. Two samples were collected as the two end-members, one fresh and one saline and a further three samples were taken as a vertical profile within one borehole located between the two end-members. Sampling locations are marked in figure 4.1. Sample numbers are listed below, followed by a description of the sampling location.

EG/SP The sample defined as the fresh end-member was taken at En Gedi spring, just below the tapping of the spring, where part of the source water remains as a natural spring. It is located approximately 1.5 km from the Dead Sea shore at 211 m b.s.l. The spring serves as a major source of drinking water, and part of it is diverted through a pipe to the bottling location downhill.

EG 11/1, 2, 3 The vertical interface profile was taken in borehole number EG11, at an elevation of 403.6 m b.s.l. approximately 50-60 m from the Dead Sea shore. The borehole tubing is 7.5 cm in diameter. This borehole as well as borehole number EG16/3 (see below), were drilled by the Geological Survey of Israel and serve research purposes, only. Figure 4.2 gives a detailed description of the profile and figure 4.3 shows a depth profile of electric conductivity on the left and a depth profile of chloride content on the right. These depth profiles were taken approximately one week before the sampling, and were used as a basis for choosing sampling depths. EG11/1, 2, and 3 were taken at depths of 14.5, 15.75, and 19.5 m below well head (b.w.h.), respectively. The water table levelled at 13.95 m b.w.h., and total borehole depth was 20 m b.w.h. In order to ensure that the profile shown in figure 4.3 remained stable, density, pH, electric conductivity and temperature were measured several times throughout the sampling in each depth (see table 4.1).

EG 16/3 The sample assigned as the saline end-member was sampled in a borehole approximately 8 m from the Dead Sea shore at an elevation of 414.7 m b.s.l. In its chemistry and its ion content, the composition of this water equals that of DSW and can be regarded as that of the saline end-member (TDS = 330 g/l). The water table levelled at 4.42 m below well head, and the sample was taken at 11 m b.w.h. The borehole tubing has

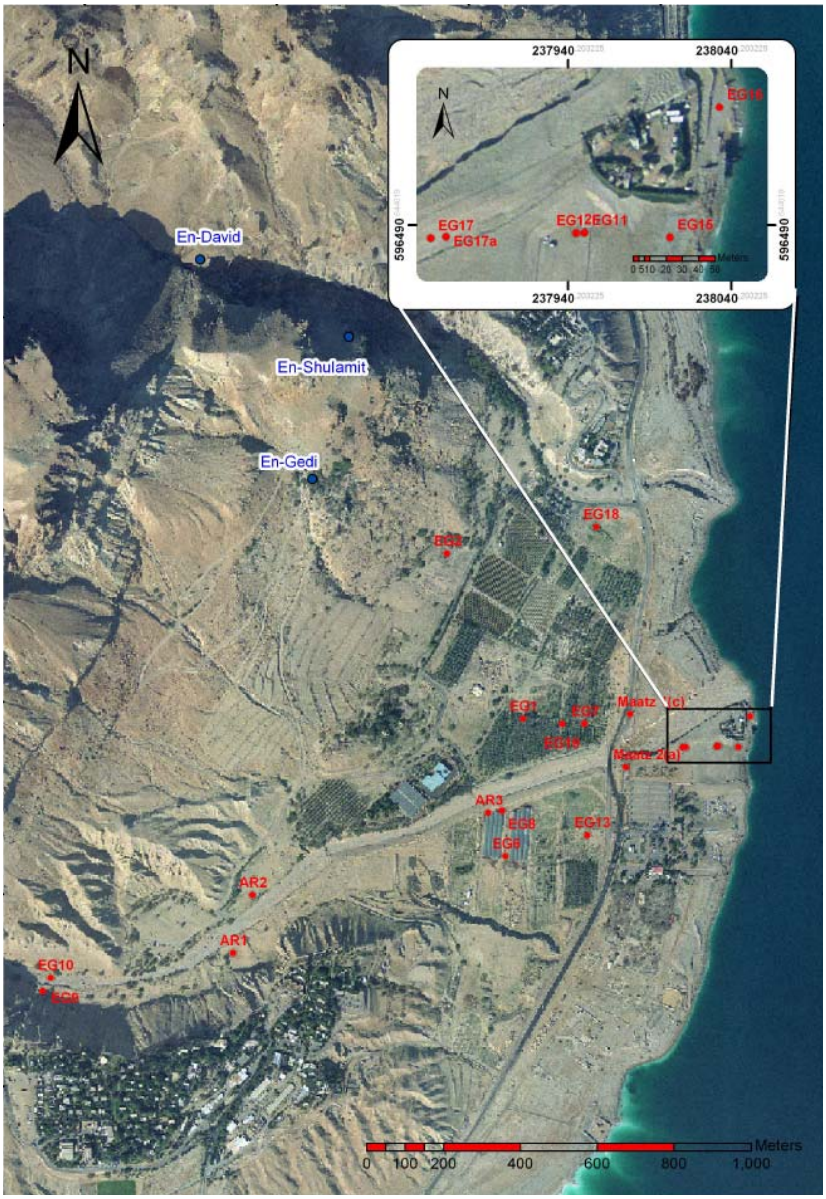

Figure 4.1: Map of the En Gedi area with the respective sampling sites (Lewenberg, 2005)

a diameter of 5 cm and reaches down to a depth of 12 m b.w.h. Table 4.1 lists the detailed data of the sampling.

The samples were analysed for environmental tracers described in the following sections.

Table 4.1: Sampling details

sample ID	density (g/cm³)	pH	EC (mS/cm)	T_w (°C)	T_{air} (°C)	sampling depth (mbwh)	GW-surface (mbwh)	altitude (mbsl)
EG/SP	0.998	8.2	0.700	28.0	31	surface	-	211
EG11/1	1.064	6.2	114.1	30.9	38	14.5	13.95	403.6
EG11/2	1.118	6.1	172.0	30.7	38	15.75	13.95	403.6
EG11/3	1.164	5.9	195.5	28.5	38	19.5	13.95	403.6
EG16/3	1.234	5.6	193.15	28.8	35	11	4.2	414.7

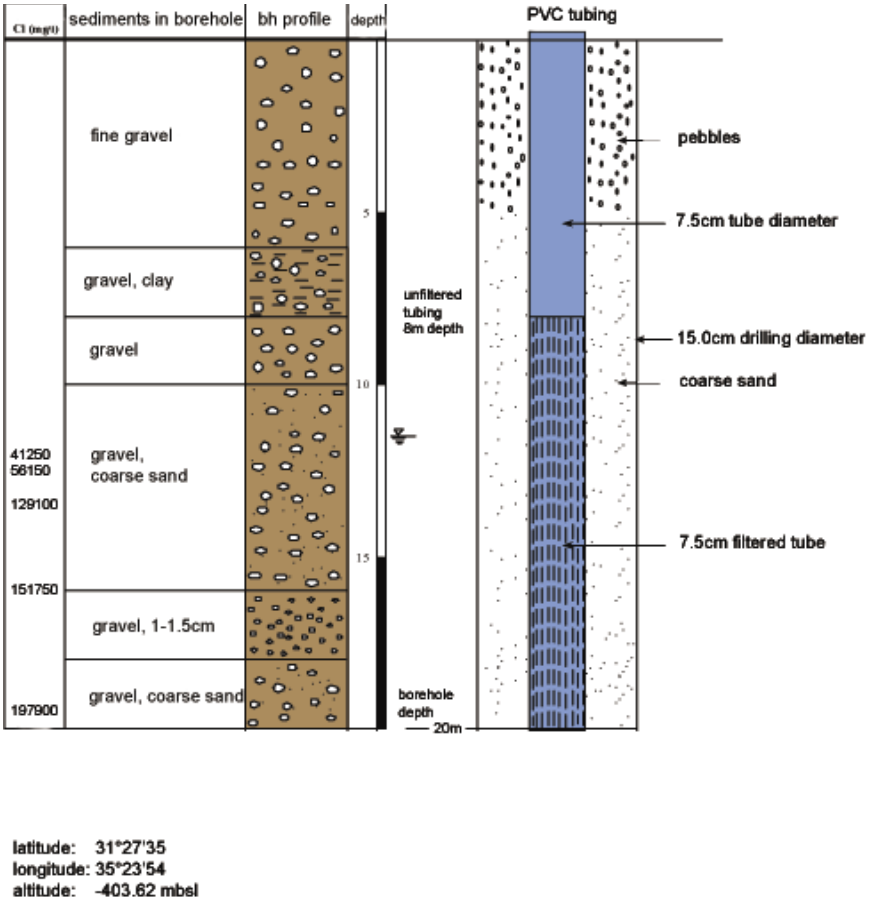

Figure 4.2: Borehole profile of EG 11 (Lewenberg, 2005).

4.1.2 Sampling Procedure

Water sampling was conducted by pumping water from the boreholes with an electric pump with a pipe of 1 cm in diameter. For general chemistry and stable isotope samples 50 ml PET bottles were filled to the overflow and carefully closed so as not to trap air inside. A double-lid system prevented evaporation. ^{34}S samples were collected in 100 ml PET bottles, closed thoroughly and wrapped with Teflon-tape to prevent leaking. All sample bottles were stored in the dark and at the end of the day wrapped in boxes and sent to the IHF from were they were distributed to the respective laboratories.

For Radium analysis water samples of 5 liters volume were taken. In the laboratory of the Geological Survey of Israel these samples were weighed and filled into large porcelain bowls, which were then placed on hot plates under hot lamps, in order to evaporate the samples as quickly as possible without any losses. The heat was constantly kept just below boiling point, so as not to lose any of the sample by spilling. Sample EG11/1 and EG11/3 were fully evaporated after 14 and 19 hours, respectively. Sample EG11/1 weighing 5064.9 g yielded 614 g of damp salt; EG11/3 weighing 5602.2 g yielded 1477.8 g of salt. The salt was filled into PET containers and sent to the IHF.

Samples were also taken for CFCs and noble gases. Care must be taken to prevent contamination while collecting samples for the analysis of gaseous compounds in water.

Water samples for CFCs were collected in glass bottles with glass lids and metal closure clips and were placed in metal cans. Sampling was carried it out in 8 litre buckets. The

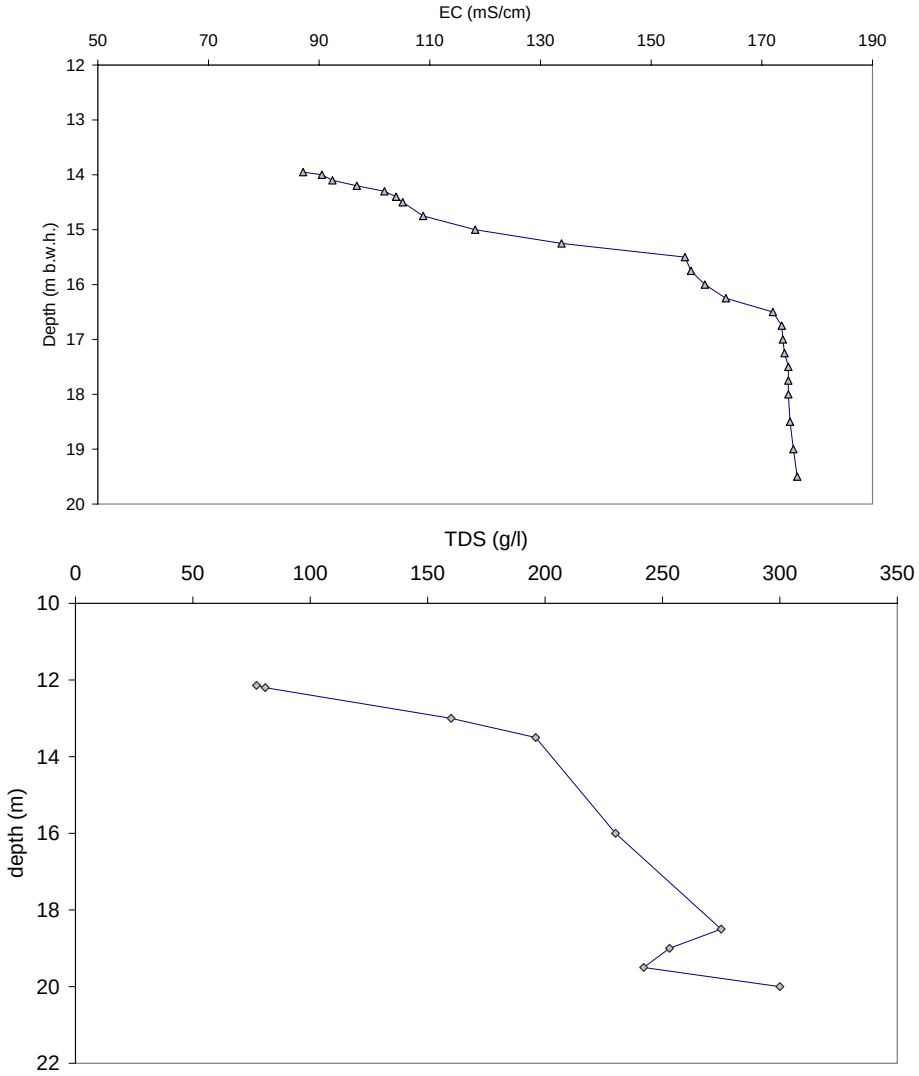

Figure 4.3: Depth profile of electric conductivity (above) and of TDS (below) in borehole EG11.

pipe was placed inside at the bottom of the bottle and left until the water overflowed in the bottle, the can, and the bucket. The lids and closure clip were also placed inside the bucket. When all parts had been flushed with water from the borehole and after ensuring that no air bubbles had been caught inside or on the lids, the bottle was closed under water with the glass lid and the metal clip and the can was closed with the tin lid. After the can had been tightly closed it was removed from the water-filled bucket.

Noble gas sampling was carried out in copper tubes. The tubes were connected to the water-pumping pipe, so that the water from the borehole flushed the tubes in direct contact with the pipe. The copper tubes were held vertically so as to let air bubbles rise and escape out of the tubes. Each tube was placed on the ground horizontally and the screws on both ends were tightly closed with a spanner. A picture of the sampling can be found in the Annex.

Both, CFC and noble gas samples were packed and shipped after sampling.

The evaluation of CFCs and noble gases could not be carried out as part of this thesis, as the laboratory analysis of the noble gases had not been completed at the time of writing. Noble gas data are needed for the successful analysis of CFCs for excess air calculation.

4.1.3 General Chemistry

The results of the general chemistry analysis are displayed as a fingerprint diagram in figure 4.4a. The major cations are sodium, magnesium, calcium, potassium and strontium. Cations of the four of EG11 and EG16 (and DSW) plot on parallel lines, which indicates mixing of two end-members, a fresh and a saline one. On the right the plots for SO_4^- and HCO_3^- differ somewhat from that pattern. The fresh end-member contains very little SO_4^- and HCO_3^-, whereas the intermediate samples contain a significant amount of both cations, which is again reduced in the highest salinities of samples EG11/2, 3 and EG16/3.

Saturation indices (SI) were calculated with the PHREEQC-routine in the modelling programme Aquachem, using the Davies equations for dissolution equilibrium calculation, which is valid for low ionic strengths (I) up to I = 0.5. These were compared to SI calculated with a PHREEQC-routine using the Pitzer equations, considering the specific ionic strength of the water. Both calculations showed that all samples, apart from the fresh end-member, are saturated with respect to carbonates and sulfates. The values resulting from the Pitzer equations give a more precise picture representing the assumed processes. Therefore the saturation indices of carbonates and sulfates in the saline samples (EG11/1-3, EG16/3 and DSW), calculated with the Pitzer equations are depicted in figure 4.5. According results for the deep water mass of the Dead Sea were calculated by Krumgalz (1997), also using the Pitzer equations.

Samples EG11/1, 2 and 3 are all undersaturated with respect to halite. The water samples only become saturated with this mineral the closer the proximity to the Dead Sea, as in sample EG16/3 and in the Dead Sea itself. All three samples collected in borehole EG11,

Table 4.2a: Major ion distribution in the En Gedi samples.

sample ID	Sr^{2+}	K^+	Ca^{2+}	Mg^{2+}	Na^+	Cl^-	SO_4^-	Br^-	HCO_3^-	TDS
					mg/l					
EG/SP	0.5	2.7	55	26	42	75	30	0.2	215	368
EG11/1	92	2014	5196	9627	11500	56590	2600	1108	268	89097
EG11/2	154	3500	8350	18700	21000	106300	1650	2285	146	162194
EG11/3	211	5000	11500	28300	29850	154650	988	2994	93	233991
EG16/3	274	7473	17210	42180	35660	219240	246	4741	< 20	330198

Table 4.2b: Mixing percentages calculated from different ions and ionic ratios.

sample ID	% of saline end-member (=EG16/3)					ion ratios					
						mg/mg			molar		
	K^+	Na^+	Cl^-	Br^-	mean	Na/Cl	Br/Cl	Ca/SO_4	Na/Cl	Br/Cl	Ca/SO4
EG/SP	0	0	0	0	0	0.56	0.002	1.8			
EG11/1	27	32	26	23	27	0.203	0.020	2.0	0.313	0.0087	4.8
EG11/2	47	59	48	48	51	0.198	0.021	5.1	0.305	0.0095	12.1
EG11/3	67	84	71	63	71	0.193	0.019	11.6	0.209	0.0086	27.9
EG16/3	100	100	100	100	100	0.163	0.022	70.0	0.251	0.0096	167.7
DSW						0.212	0.025	10.5	0.327	0.011	25.2

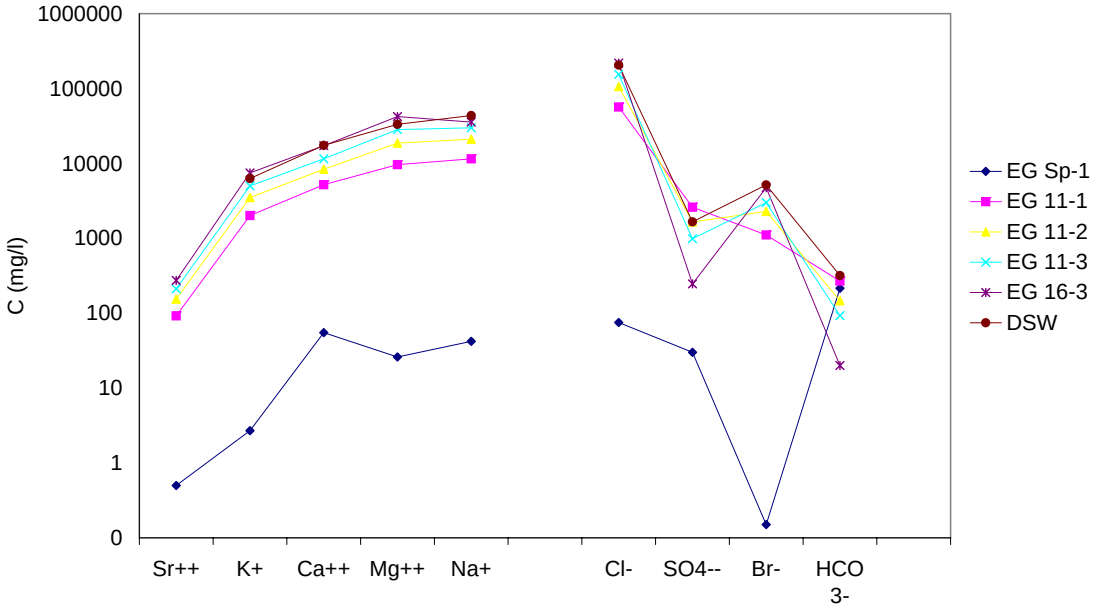

Figure 4.4a: Fingerprint diagram of major ions.

as well as the DSW, plot in parallel lines. EG11 samples lie somewhat within the supersaturated range with regard to anhydrite, aragonite, calcite, celestite, gypsum and magnesite, while dolomite is considerably within the supersaturated range for all samples. The DSW sample shows the same trend as the do EG11 samples with the carbonates being the most saturated compared to the sulfates.

Sample EG16/3 has decreased SI for carbonates aragonite and calcite, but is decidedly supersaturated regarding halite, anhydrite and celestite, as well as dolomite. Values exceeding zero by only small amounts is not necessarily an indicator of precipitation taking place. Rather, SI-values of around zero can be considered to be an indicator for the occurrence of equilibrating processes. Therefore, the decreased SI of aragonite and calcite in

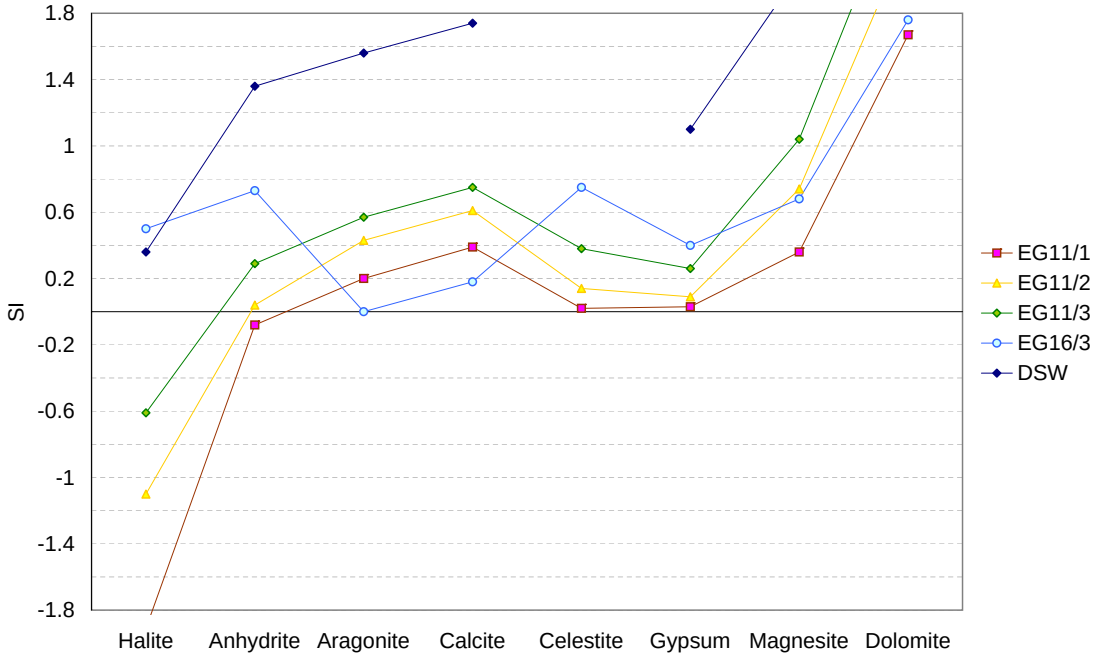

Figure 4.5: Saturation indices calculated using the Pitzer equations.

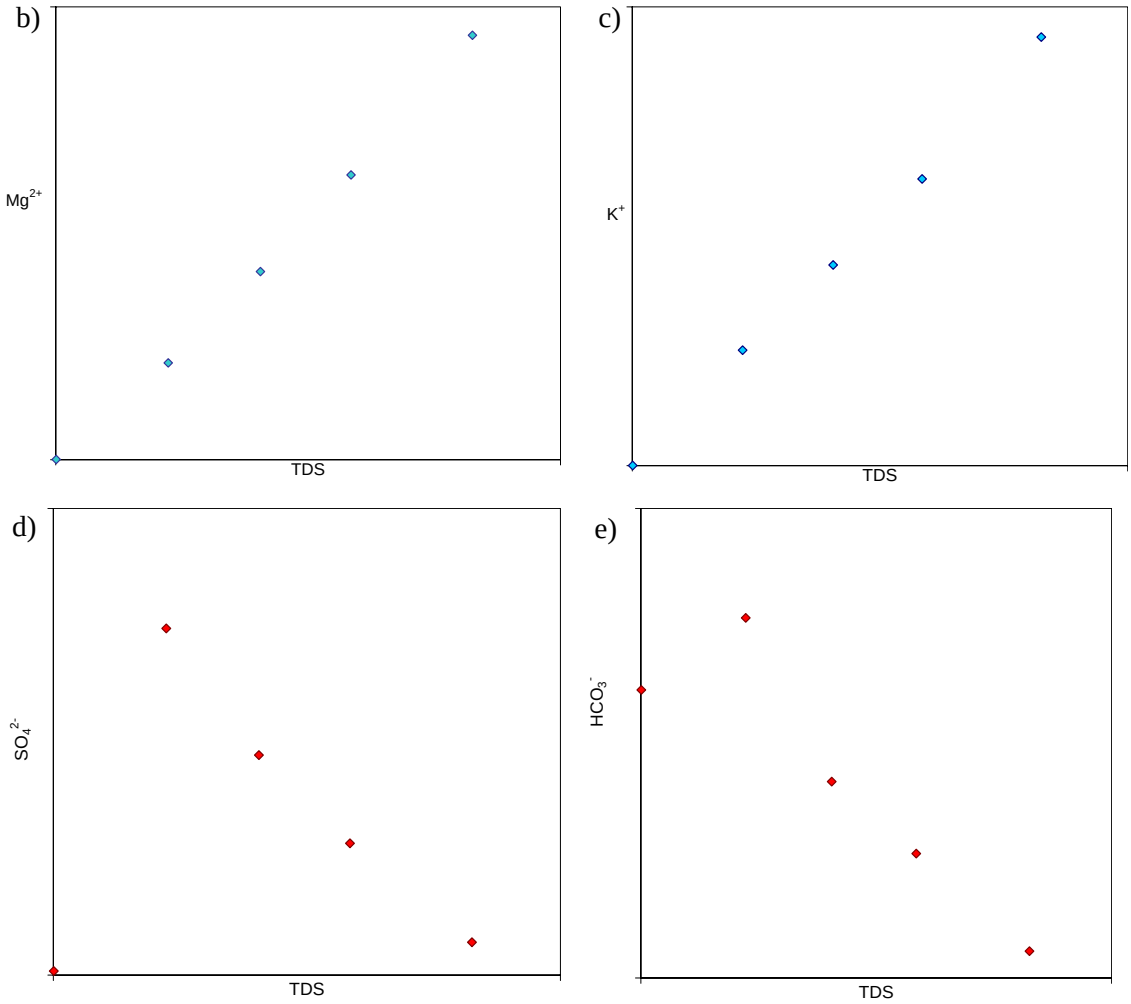

Figure 4.4 b-e: Composition diagrams of some major ions.

sample EG16/3 could imply that saturation in this sample has reached a level leading to precipitation of the different carbonates.

As can be seen from the composition line of sample EG/SP in figure 4.4a, both end-members contain a certain amount of ions, with the saline end-member being the sole contributor of Br^-.

Na/Cl ratios gave 0.56 (equivalents) in the sample taken at the spring (EG/SP), it is approximately 0.2 for the three samples taken in EG11 and 0.16 for the EG16 sample and 0.21 for the Dead Sea. Br/Cl molar ratios were approximately 0.009 for the borehole samples and 0.01 for DSW. The molar ratios of Ca/SO_4 ranged from 5 (EG11/1) to more than 160 (EG16/3).

Tables 4.2 a) and b) list ion contents and ion ratios for all samples, as well as mixing percentages calculated from Cl^-, Br^-, K^+ and Na^+.

Conclusions

Mixing of two end-members, both containing a significant amount of ions, is indicated by the straight plotting lines of cations and chloride and bromide versus TDS. In figure 4.4 b) and c) magnesium and potassium versus TDS are depicted as examples for the plots showing straight mixing lines. Precipitation of carbonates and sulfates is assumed as sa-

linity increases, which is depicted in figures 4.4 d) and e). The other plots of major ions can be found in the Annex.

The high HCO_3^- content in the fresh end-member together with Ca^{2+} and Mg^{2+} as major cations, are indicators of the fresh end-member originating from a limestone / marl aquifer. The HCO_3^- content initially rises with increasing salinity, but then decreases as the salt content rises further, most probably through precipitation together with Mg^{2+}, Ca^{2+} or Sr^{2+} anions, and therefore it reaches lower values.

The reason for the sulfate pattern is quite similar: fresh water coming from the west represented by sample EG/SP meets the saline end-member in the fresh-saline water interface, resulting in increased SO_4^- contents (together with an increase in all the other ions). Sulfate is then precipitated as the water reaches higher salinities and/or is decomposed by biological activity, which was visibly indicated by red algae growth in sample EG16/3. Bacterial activity and its influence on sulfate concentrations are further investigated in section 4.1.5.

The assumption of carbonate and sulfate precipitation is supported by the SI calculation using the Pitzer equations. The results imply that considerably higher precipitation rates are reached in sample EG16/3.

4.1.4 Stable Isotopes of the Water Molecule

Figure 4.6 shows a plot of ^{18}O data vs. elevation, indicating the altitude effect for Israel and western Jordan. The data were taken from the ISOHIS data bank of the IAEA (2004). Because only 4 relevant sampling stations that had been monitored for a longer period were accessible for Israel, data from the same source for western Jordan, on the other side of the graben, were chosen to support these data. The trend of the data for Israel had a slope of -0.0018 and for western Jordan it was -0.0023. Plotting the fresh end-member EG/SP amongst these data, it can be assumed that precipitation in higher altitudes forms the recharge of the water sampled at the spring.

Figure 4.7 shows a plot of $\delta^{18}O$ vs. $\delta^{2}H$. The blue dots are the samples taken from the groundwater in the En Gedi area. The values connect the fresh end-member originating in the Judean Mountains, which can be seen precisely as it plots among the green squares, which are the data of stable isotopes of rainfall in Israel and Jordan. These rainfall data plot along the Mediterranean and Middle Eastern Meteoric Waterline (MMWL, continuous line). The dashed line represents the GMWL. On the other end of the sample line, the red circle gives the average surface composition of Dead Sea water, which plots at the saline end of the mixing line.

Mixing or dissolution of "evaporites"?

In figure 4.8, a plot of $\delta^{18}O$ vs. salinity (TDS) of the five samples taken is depicted. A straight line connects the samples indicating a mixing of the two end-members. Regarding the processes of underground salt dissolution and sinkhole formation along the western Dead Sea margin, this straight yet sloping, mixing line would rule out the option that the increase in salinity on approaching the Dead Sea shore from sampling location EG/SP via EG11/1-2-3 to EG16/3, is the result of only one water source, namely EG/SP, dissolving salt evaporites. This process would result in a line of constant ^{18}O values with

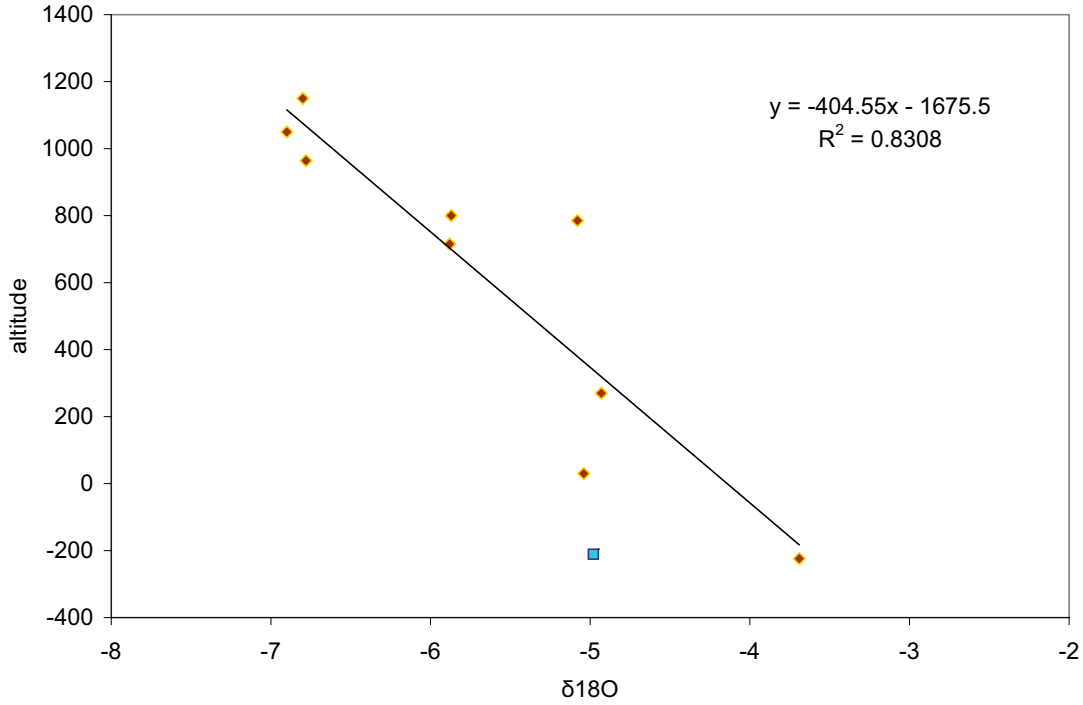

Figure 4.6: $\delta^{18}O$ data indicating the altitude effect for Israel and western Jordan. The blue square represents the fresh water sample collected at the En Gedi spring.

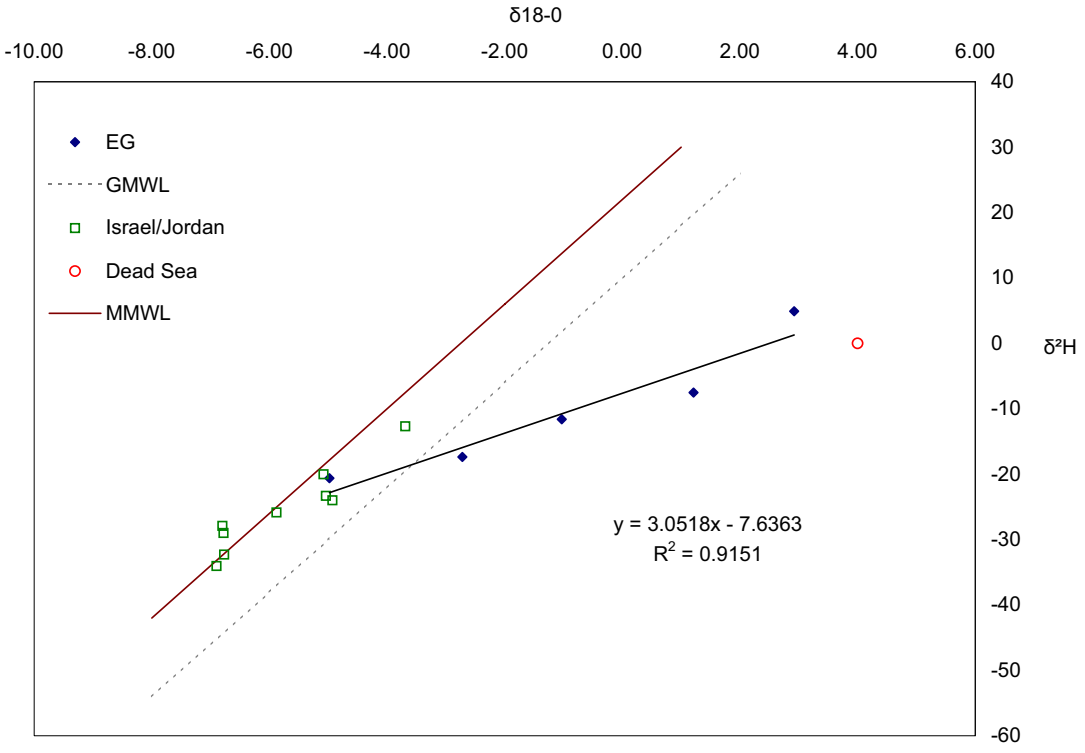

Figure 4.7: Plot of $\delta^{18}O$ versus ^{2}H data of the samples in relation to rainfall data from Israel and western Jordan and the isotopic signature of the Dead Sea.

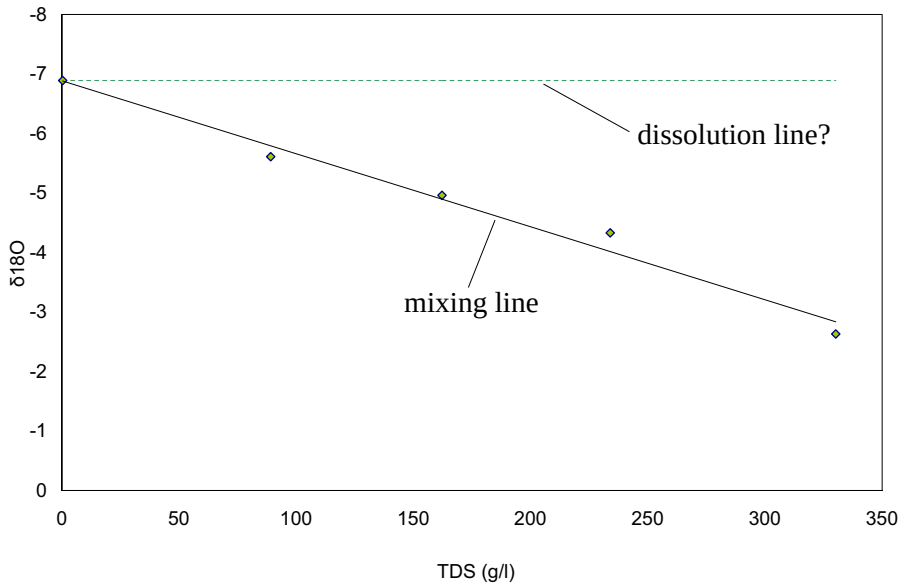

Figure 4.8: Plot of $\delta^{18}O$ versus TDS indicating the mixture of two end-member waters.

increasing salinity, which is indicated by the dashed green line.

This would be the case for dry evaporites. Full evaporation of DSW, on the other hand, is hard to achieve under natural conditions. Although salt crusts develop on exposed surfaces, such as rocks around the Dead Sea shore, salt sludges are more likely to be found on flat surfaces or underground.

Clays and silt deposits exposed by the receding Dead Sea dry up through the heat of the sun during the day, but during the night, even in summer when temperatures do not drop below 30 °C, these silty, clayey deposits absorb the humidity of the air, causing pronounced slurrying.

This effect was re-enacted with pure DSW (without sediments). 100 g of DSW were left to evaporate in the drying oven at 40 °C for 48 hours. The result was a residue of 37 % water within the remaining salts and this state was reached after approximately 10 hours. The measured evaporation line is depicted in figure 4.9. These results would support the theory that evaporites, which lie close to the Dead Sea shoreline or even below the saline groundwater table, consist of salt sludge contributing a specific isotopic ratio of H- and O-isotopes. This would make the distinction between one fresh water type dissolving evaporites and two end-member waters mixing rather difficult.

4.1.5 ^{34}S

^{34}S-values in the SO_4—cations in the spring sample gave 10 ‰ and in the borehole samples ^{34}S-values ranged from 13.6 in sample EG11/1 to 21.6 in EG11/3. There was very little change in ^{34}S-value between the two most saline samples EG11/3 and EG16/3. The results of the sulfate and ^{34}S analyses can be seen in figure 4.10. Sulfate concentrations rise from the fresh end-member to the EG11/1 sample, reaching a value of 2600 mg/l and continuously drop off from there to one tenth of this concentration in sample EG16/3. Presumably bacterial activity leads to an increase of the heavier sulfur isotope in the sulfate, but reaches a steady level in the two most saline samples.

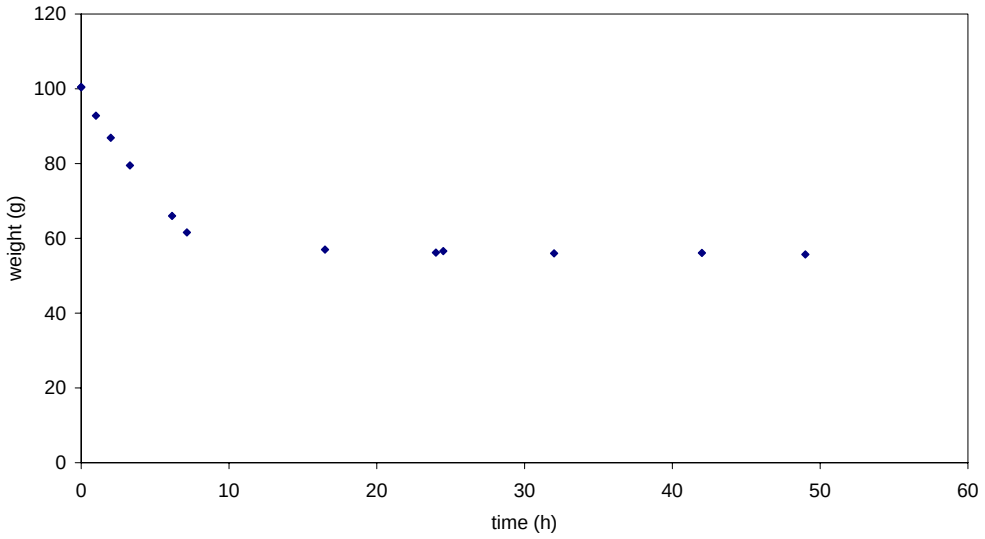

Figure 4.9: Evaporation of Dead Sea water at 40 °C.

The decrease in sulfate cannot be explained by bacterial reduction, alone. We know from the general chemistry analysis that a decrease in bicarbonate was also observed and that saturation indices calculated with Aquachem and PHREEQC levelled around zero for most carbonates and sulfates.

Conclusions

The non-corresponding evolution paths of ^{34}S and sulfate demonstrate that there must be more than one process influencing these two tracers. Looking once again at Figure 2.1 showing a Raleigh plot for sulfur isotope fractionations during the reduction of sulfate in a closed system, we can see that from the starting point at a $\delta^{34}S$ value of 10 ‰ for 100 % initial sulfate, which resembles the fresh end-member sample having a $\delta^{34}S$ value of 10 ‰, a drop in the sulfate reservoir to one tenth of the initial value would lead to a $\delta^{34}S$ value of about 54 ‰. Yet the measured fraction of the sulfur-34 isotope is only 21 ‰. This

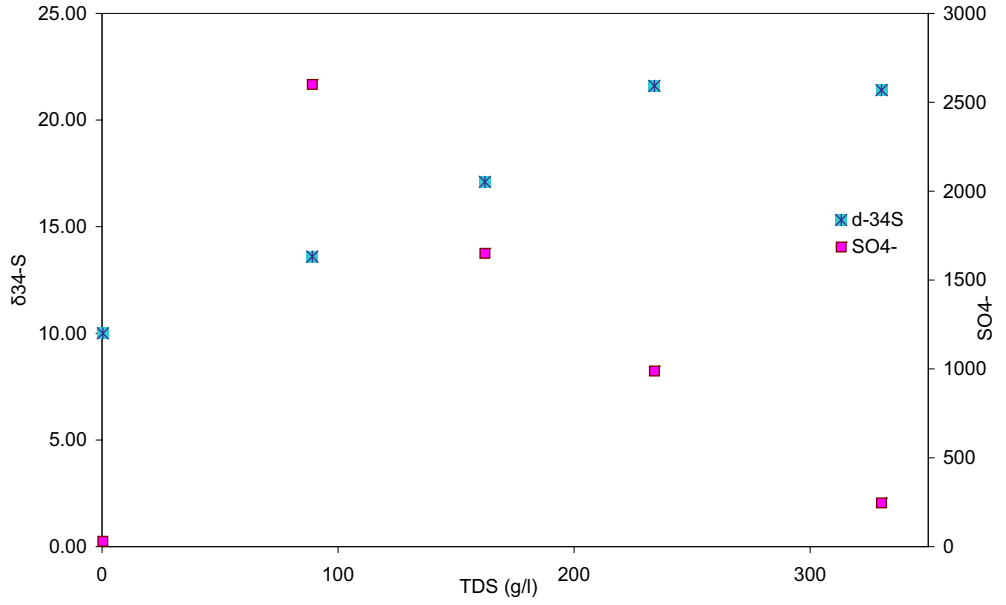

Figure 4.10: Distribution of sulfur isotopes along the fresh-saline water interface.

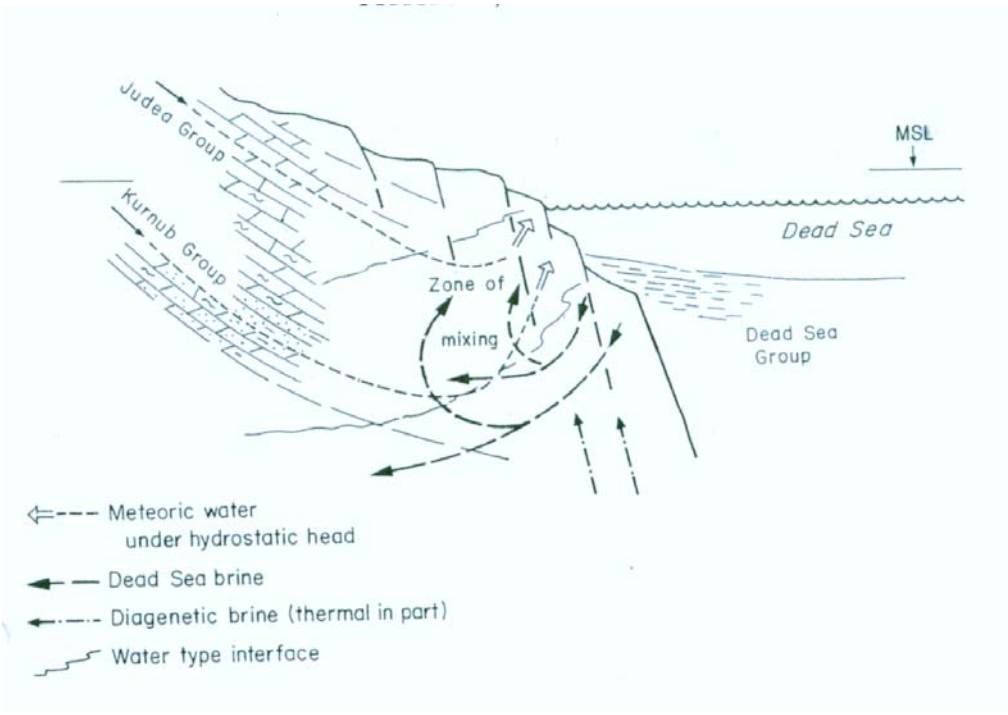

Figure 4.11: Near-shore water circulation leading to distinct $\delta^{34}S$-signature (Zak, 1997).

supports the assumption that a second process, namely the precipitation of sulfates, leads to the reduction of sulfate content present in EG11/1 with increasing salinity in samples EG11/2, EG11/3 and EG16/3.

The constant level in $\delta^{34}S$ in samples EG11/3 and EG16/3 demands another explanation. In a study on nutrients in pore waters from Dead Sea sediments, Nissenbaum (1990) presented results from the analysis of $\delta^{34}S$-values. Here, an almost complete absence of these isotopes in deep, anaerobic sediments from the Dead Sea was stated. This was attributed to post-depositional reduction by sulfate-reducing bacteria. In an earlier study by Nissenbaum and Kaplan (1976), quoted in Nissenbaum (1990), the sulfate concentration of pore water in deep sediments was found to be about 10 % (or 30-50 %, stated by Levy (1980), quoted in the same study) of the values in the overlying water.

In 1975 Nissenbaum presented in a study on the biogeochemistry of the Dead Sea distributions of $\delta^{34}S$. He found ^{34}S of the SO_4^--ion to amount 8 ‰ in waters originating from springs and floods, and sulfur springs to have a ^{34}S-value of 9.5 ‰, while Dead Sea water showed a signature of 12.5 ‰. ^{34}S-values in precipitated gypsum were found to level at 15 ‰. Neev and Emery (1967), quoted in Nissenbaum (1975), suggested that the precipitated sulfate is bacterially reduced to sulfide and that the bicarbonate which evolves in this process causes precipitation of $CaCO_3$. Sulfate in precipitates is frequently enriched in ^{34}S, according to Nissenbaum (1975). These observations present a good basis of interpretation for the results of this study.

Although major dissolution processes are not assumed to be occurring in the investigated system, the sulfur isotopic signature of 13.6 ‰ in sample EG11/1 corresponds well with the quoted $\delta^{34}S$-value of 15 ‰ found in precipitated gypsum. Since the SI of the saline samples are all in the range of saturation, and since fresher water is thought to have been replacing more saline water through the admixture of the former with the latter, gypsum precipitates can be presumed to be dissolved by the approaching fresh water. This process

is implied by the $\delta^{34}S$-value found in sample EG11/1, which is then increased by bacterial sulfate reduction. This assumption coincides with the theory put forward by Hoefs (1997), introduced in chapter 2.1.3. Even though in this study dissolved oxygen was not measured, as sample number EG11/1 was taken only half a meter below the water table it is also possible that the sulfate-reducing bacteria are not active in this shallow depth, since conditions here may not be anaerobic. With increasing depth and therefore increasingly anaerobic conditions, bacterial sulfate reduction is initiated.

What is significant in figure 4.10, are the $\delta^{34}S$-values of samples EG11/3 and EG16/3. The $\delta^{34}S$-value of 10 ‰ at the spring (sample number: EG/SP) roughly corresponds with the value for fresh springs of 8 ‰ found in the above mentioned study. The increase in ^{34}S, following the initial increase in sulfate, would be caused by equilibration with the sulfate in the more saline environment. This value increases assumedly through bacterial reduction of sulfate in samples EG11/2 to EG11/3. A possible explanation is depicted in figure 4.11. In sample EG16/3 admixture of an additional “water type” could be the reason for the change in trend in ^{34}S. Knowing from field observations that only a few meters from borehole EG16, saline springs emerge almost at the shoreline of the Dead Sea, a circulation of Dead Sea water (containing larger amounts of sulfate than EG16/3) into depths under ground is possible, where the anaerobic zone, being greatly depleted in sulfate and ^{34}S, is located. This re-circulated water then rises up and mixes with the water coming from the other sampling sites. This would explain the concurrence of trend in TDS and ion composition of samples EG11/3 and EG16/3 with the simultaneous discrepancy of trend in ^{34}S. With an admixture of deep, ^{34}S-depleted water having the same salinity as EG16/3, the ^{34}S-value of sample EG16/3 could be explained. Such a circulation of near-shore lake- and groundwaters has been described by Zak (1997) and by Mazor (1997), who found this process indicated by isotopic concentrations of ^{2}H and ^{18}O.

4.1.6 Radium Isotopes

Two samples were taken for the analysis of radium, one at site EG11/1 and one at EG11/3. Radium concentrations throughout this work will be stated in dpm/kgH_2O (disintegrations per minute per kilograms of water), in short, dpm.

For technical reasons concentrations of the short-lived isotopes ^{223}Ra and ^{224}Ra present in the samples at the time of collection could not be measured or reconstructed, so that an evaluation of ^{226}Ra and ^{228}Ra is given below.

^{226}Ra and ^{228}Ra in the sample collected from EG11/1 gave 8.1 and 2.46 dpm, respectively. For EG11/3 the concentration of ^{226}Ra amounted 28.98 and of ^{228}Ra 8.82 dpm. While the absolute concentration of both radium isotopes is decreased in the less saline sample EG11/1 as compared to EG11/3, the ratio of ^{228}Ra to ^{226}Ra is the same in both samples.

Without the data of the short-lived radium isotopes and with two samples only, dating of the water samples is impossible, but a characterisation of the latter can be based on the long-lived radium isotopes, especially when compared to regional data investigated by other authors.

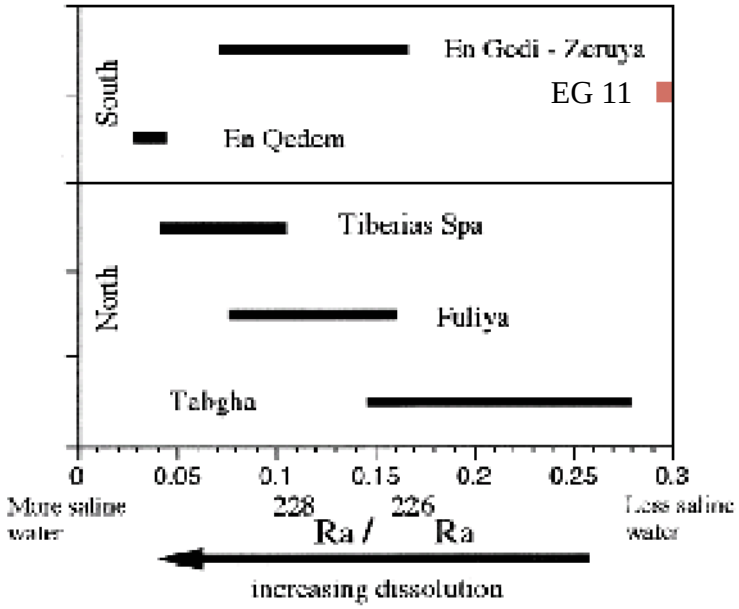

Figure 4.12: EG11 Ra-ratios plotted amongst $^{228}Ra/^{226}Ra$ activity ratios in various water types found in the region (after Moise et al., 2000).

Conclusions

A decrease in absolute radium concentrations with constant $^{228}Ra/^{226}Ra$ ratios is an indicator of mixing of fresh water, devoid of radium, with a saline end-member supplying the sample with radium.

Both samples, showing a greater ^{226}Ra, a daughter within the ^{238}U series, than the ^{228}Ra, a daughter in the ^{232}Th series, are consistent in indicating the host rock being of a limestone character, as limestone is rich in uranium and lacks thorium. This coincides with radium isotopic ratios found in the Dead Sea valley by Moise et al. (2000), who found $^{228}Ra/^{226}Ra$ ratios to have a value of 0.3-0.4 in waters originating from limestone and sandstone aquifers, while they found waters in contact with evaporites to have a $^{228}Ra/^{226}Ra$ ratio of 0.6-0.75. This would imply that the waters sampled in EG11/1 and EG11/3, having a $^{228}Ra/^{226}Ra$ ratio of 0.3, are in equilibrium with the local rocks.

In fact, Moise et al. (2000), who found the $^{228}Ra/^{226}Ra$ ratio in samples taken in the Dead Sea valley to be very similar to expected values found in the local rocks, suggest the equilibrium of groundwaters with their respective host rock to be the dominating factor controlling $^{228}Ra/^{226}Ra$ ratios.

A relatively high $^{228}Ra/^{226}Ra$ ratio can also be the result of another process, namely preferential dissolution and leaching of the longer-lived isotope, as presented in the theory by Hammond et al. (1988) (see chapter 2.1.4.2). Moise et al. (2000) found the rock-water activity ratios $^{228}Ra/^{226}Ra$ in wells near Lake Kinneret to be slightly lower in the water than in the host rock, and their samples taken in the Dead Sea basin showed lower values than air-radiometric Th/U data published in a study by Vulkan & Shirav, quoted by Moise et al. (2000).

Figure 4.12 presents findings of Moise et al. (2000). The diagram shows $^{228}Ra/^{226}Ra$ ratios of various water types as a function of changing chloridity. The right-hand side of the diagram represents recoil predominance, the left-hand side represents dissolution. The samples taken for this study are plotted amongst the other local data. Waters sampled in

the Dead Sea area show $^{228}Ra/^{226}Ra$ ratios ranging from 0.03 to 0.258. The authors plot these data in groups of sampling areas and thus by chemical composition. Looking at the horizontal axis this graphic suggests that a saline solution that derives its salinity from salt dissolution should have a small $^{228}Ra/^{226}Ra$ ratio, because of preferential dissolution of ^{226}Ra, while a less saline water type should show a higher $^{228}Ra/^{226}Ra$ ratio, as the two isotopes will be diluted (or not dissolved) to the same extent, both having low solubilities in relatively fresh water.

The samples taken for this study are highly saline, yet they plot on the right hand side of figure 4.12. This means that the waters are in equilibrium with the host rock and the salinity found in these samples does not originate from salt dissolution, but from mixing with a saline end-member water. When no dissolution or leaching takes place, radium isotopes are supplied to the solution by recoil effects only, and therefore they are introduced to the solution relative to their quantitative existence in the aquifer rock. The constant $^{228}Ra/^{226}Ra$ ratios once again underline the theory of continuous mixing of two end-member waters, as the radium isotopic ratio would be in disequilibrium with the host rock when it is not mixing but dissolution that is the reason for the change in salt content, resulting in a lower $^{228}Ra/^{226}Ra$ ratio.

4.1.7 Syntheses

The general chemistry analysis suggests the different salinities found in the samples to be the result of admixture of two end-member waters, one fresh and one saline. The calculations of the Pitzer equations show that the groudwater in the study site is close to saturation or supersaturated with respect to sulfatic and carbonatic mineral phases. Therefore the precipitation of sulfates and carbonates would be an explanation for the decrease in sulfate and bicarbonate observed from sample EG11/1 to EG16/3.

The observations made in the stable isotope chapter lead to questions about how evaporites in direct vicinity of the Dead Sea can be defined. Are the subsurface salt-layers, by their dissolution leading to the formation of sinkholes, dry deposits of salt as found in the Mount Sedom area or rather salt-sludge or salts in saturated brine? Salts in saturated brine will not be dissolved, but will still contain a high degree of humidity. If the evaporites are salt-sludge, with the water within this sludge having a particular (strongly enriched) isotopic signature, the process of mixing of two end-member waters could not be easily distinguished from a fresh end-member water re-dissolving salt evaporites. A dry salt would not contribute any isotopic signature of the water molecule, as water would be absent within this salt.

These considerations lead to the conclusion that the evaluation of stable isotopes of the water molecule alone, is not an ideal tool for characterising the processes taking place in the subsurface environment of the Dead Sea, especially when salt layers lie within the saturated zone.

With the help of ionic ratios, though, there might be a way towards a more evident explanation. According to Lewenberg (2005), Na/Cl ratios in groundwaters from salt layers in the Dead Sea basin lie at 0.55, which is indicative of salt dissolution, while he found the water of the Dead Sea to have a Na/Cl ratio of 0.25. Precipitation of halite leads to a decreased Na/Cl ratio, while dissolution of halite leads to an increased Na/Cl ratio. The samples taken from the saline groundwater for this study had Na/Cl ratios of 0.2 or smal-

ler, which is too low for indication of salt dissolution.

Other ion ratios support the assumption of admixture: Br/Cl ratios of the borehole samples and DSW lie quite close to each other (0.009 / 0.01). Dissolution of halite is indicated by a Br/Cl ratio of around 0.0003. Barth (2000) found halite dissolving groundwaters to have a Br/Cl ratio of at least one order of magnitude below the ones found in the samples from the En Gedi boreholes.

With respect to gypsum dissolution, waters indicating this process should have a Ca/SO_4 ratio close to unity, while the samples analysed in this study lay manifold times above unity which, according to Barth (2000), may be the result of interactions of these waters with carbonates.

The results and interpretation of sulfur isotopes open up another dimension to the understanding of the processes found in the groundwater of the En Gedi area. To start with, $\delta^{34}S$-values of 15 ‰ found in gypsum precipitates in the Dead Sea area by Nissenbaum (1975), correspond to the measured value in sample EG11/1 of 13.6 ‰. This sample is the 'freshest' sample within the fresh-saline water interface, least saturated with respect to sulfates, so that this water would be capable of dissolving sulfates that have been precipitated by the receding saline water. Since conditions in this shallow part of the groundwater presumably are aerobic, bacterial sulfate reduction is probably not taking place. Therefore this sample carries an isotopic signature close to that of the precipitates. For the carbonate phase the same process can be assumed.

Sulfate reduction is visible from samples EG11/1 to EG11/2 and EG11/3. The $\delta^{34}S$ value in sample EG16/3 staying at level with the value found in EG11/3 indicates mixing with waters of a lower ^{34}S-value. DSW having a ^{34}S-value of around 12.5 ‰, yet having a much higher sulfate concentration cannot be the immediate source of mixing, but is possibly active in the process by re-circulating through the deeper, anaerobic zone, hence being depleted in sulfate and having the ^{34}S signature of this deep layer, being depleted with respect to the overlying water column by 10-50 %. Through mixture of this re-circulated water with water moving from upstream (EG11/3), EG16/3 obtains its distinctive $\delta^{34}S$-value.

The long-lived isotopes of radium approve the theory of mixture of two end-member waters in two ways: firstly, absolute radium activity is decreased in the fresher water sample as opposed to the more saline water sample, which may be the result of dilution of these tracers during which there is no fractionation process. Secondly, the constant $^{228}Ra/^{226}Ra$ ratio reconfirms conservative mixing without any dissolution processes, as these would result in a preferential ^{226}Ra accumulation through leaching effects as proposed in the theory by Hammond et al. (1988). A further result from the radium analysis is that the isotope ratios, suggesting equilibrium with the aquifer rocks, reflect the local lithology with uranium rich and thorium poor rocks dominating.

With this background it seems reasonable to conclude that the varying salinity of waters along the horizontal / vertical sampling profile taken for this study is the result of mixing of two end-member waters, with a minor circulation taking place within a very narrow range from the lake westwards in the deeper parts of the shoreline and flowing back to the lake via springs and admixture with the fresher waters coming from the west, flowing into the Dead Sea. Minor dissolution effects by the approaching fresh water, indicated by sulfur isotopic signatures, is restricted to precipitated sulfates and carbonates of the receding hypersaline water due to supersaturation regarding these phases.

4.2 Laboratory Experiments

In order to get a profound understanding of the behaviour of fluorescence of the different tracers in saline media, tracer experiments were conducted with saline solutions, sediments and saline solutions in batch experiments, and sediments and saline solutions in column experiments.

Two different equations were used for fitting theoretical curves to the measured values of the column experiments: an equilibrium convection-dispersion equation (CDE) developed by Maloszewski & Zuber (1982) and a non-equilibrium CDE called CXTFIT by Toride et al. (1999).

4.2.1 Response of Fluorescence to Varied Salinity

4.2.1.1 Procedure

Initially, the four chosen dye tracers were dissolved in waters with varied degrees of salinity.

These waters were prepared by diluting water from the Dead Sea (TDS approx. 330 g/l) with de-ionized water to levels of 100, 80, 60, 40, 20, and 2.5 % Dead Sea Water (DSW). Therefore, salinity in this case refers to the amount of TDS composed of a variety of ions found in the Dead Sea, and not to NaCl concentration alone (for ion composition of DSW see chapter 3.1). Table 4.3 lists TDS values representing the respective DSW percentages.

Instead of using 0 or 1 % DSW, 2.5 % DSW-concentration was chosen in order to achieve stable, neutral (7.0 +-0.2) pH. Tracers could not be directly dissolved in highly concentrated Dead Sea water, where the dry tracer would not dissolve, even after 24 hours on a shaker. Therefore all tracers were dissolved in small amounts of de-ionized water before added to DSW, or standard solutions were prepared in de-ionized water and were diluted in DSW. Calibration lines of the tracers can be found in the Annex.

Table 4.3: Conversion of salinity in % DSW to TDS (g/l).

% DSW	2.5	20	40	60	80	100
TDS (g/l)	8.25	66	132	198	264	330

4.2.1.2 Evaluation

In figure 4.13 the response of fluorescence of the four tracers, Uranine, Pyranine, Naphtionate and Eosin to increasing salinity at a concentration of 1000 µg/l is depicted. The measured intensity of fluorescence is plotted against the percentage of DSW.

Eosin shows very instable characteristics to increasing salinity. The extinction relative to fluorescence intensity at 2.5 % DSW amounts 57 % at 40 % DSW and therefore was not analysed for salinities above 40 % DSW at this concentration (see below).

Uranine shows a negative trend with increasing salinity. Fluorescence remains stable between 2.5 and 20 % DSW and decreases continuously from there. The drop-off becomes

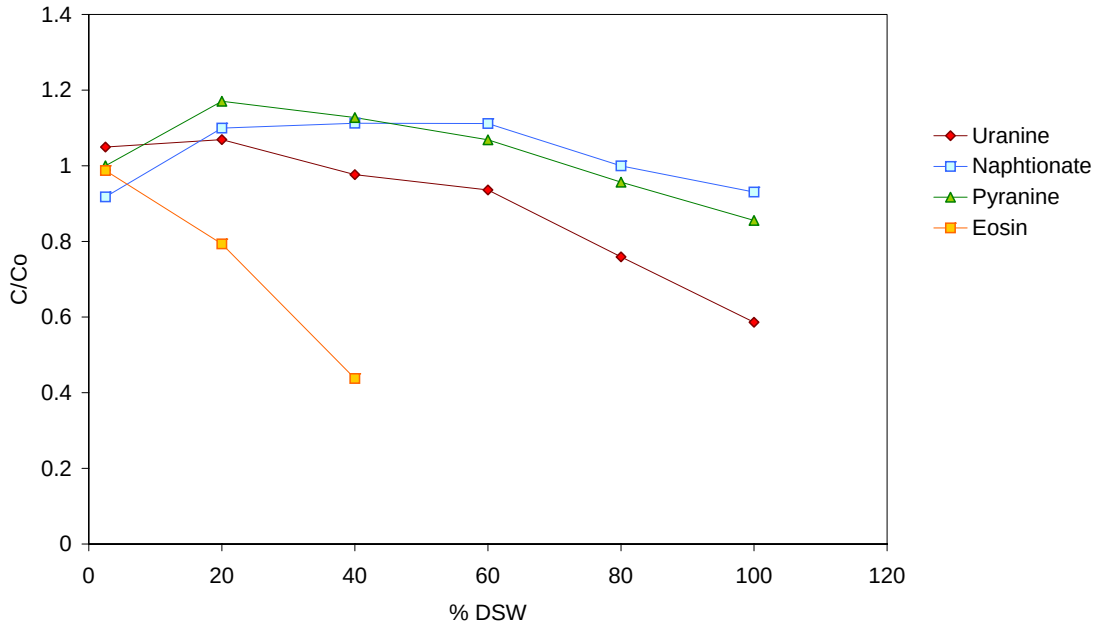

Figure 4.13: Response of fluorescence to varied salinity.

slightly steeper at salinities above 60 % DSW. Fluorescence yield relative to 2.5 % DSW-solution amounts 94 % at 60 % DSW, and drops to 60 % at 100 % DSW.

The behaviour of Pyranine is quite similar to that of Uranine in DSW-solutions. At 2.5 % DSW fluorescence intensity is slightly lower than at 20 % DSW, where intensity peaks, intensity levels off linearly from 20 % DSW. The fluorescence yield is slightly higher than that of Uranine.

For Naphtionate intensity remains stable over a wide range of salinities and only drops off at salinities above 60 % DSW. An increase in fluorescence from 2.5 to 20 % DSW can also be observed, as seen in the Pyranine curve.

Fluorescence yield remains quite stable throughout the whole range of salinities, and yields a good 85 % and 93 % at 100 % DSW for Pyranine and Naphtionate, respectively, when related to 2.5 % DSW. When related to the 20 % DSW intensity-peak / plateau, yields amount 74 % and 85 % at 100 % DSW for Pyranine and Naphtionate, respectively.

4.2.2 Batch Experiments

4.2.2.1 Setup

Batch experiments were conducted with sediments taken from the Ze'elim formation in the Dead Sea valley. The sediments were washed with tab water and sieved with sieves by Ari J. Levi ltd. with pore diameters of 150, 300, 600, 840, 1190, and 1400 µm. Afterwards they were dried in the drying oven at 75 °C for 48 hours. This temperature was chosen instead of the standard of 105 °C, in order not to change any of the mineral structures of present evaporites. The sediments consisted of coarse to fine sands and coarse silt, and grain sizes of around 2 mm to less than 150 µm were selected for the laboratory experiments. X-ray diffraction analysis (XRD) conducted at the Geological Survey of Israel

showed that the composition of the sediments used was made up of around 50 % calcite, 30 % quartz and 20 % dolomite in the coarser fractions, and 40 % calcite, 40 % quartz, 10 % dolomite, 5 % potassium feldspar and 5 % phyllosilicates for the fine grain fractions.

15 ml batch tubes were filled with 5 g of sediments, 2.5 g of grain sizes smaller 150 µm and sizes 150 – 300 µm each. To this 7.5 ml of tracer solution was added. These experiments are in the following referred to as „fine".

50 ml batch tubes were filled with 19.6 g of sediments, 4 g each of grain sizes 300 – 600 µm, 600 – 840 µm, 840 – 1190 µm, 1190 – 1400 µm and 3.6 g of 1400 – approximately 2000 µm. This lavish grain size distribution was chosen in order to represent a range of grain sizes present in the field projected to a small-scale laboratory environment. The same grain size distribution was used in the column experiments. To the 50 ml tubes 15 ml of tracer solution was added. These experiments are in the following referred to as „coarse".

Concentrations of 1, 10, 100, 1000 and 10000 µg/l were used for Uranine, 100, 1000, 10000 and 100000 µg/l for Naphtionate, each in (2.5), 20, 40, 60, 80, and 100 % DSW-dilution. Because of the strong decrease in fluorescence for Eosin in salt water solution, the amount of batch experiments was reduced for Eosin, but a few were still conducted in order to confirm the unfitness of Eosin as a water tracer in highly saline water. The results correspond to earlier findings of E. Magal, unpublished.

Pyranine was chosen, also after findings of E. Magal, unpublished, who had used Pyranine in batch experiments with a variety of natural and artificial sediments in high salinities. Her results showed good fluorescent yield for Pyranine. Therefore batch experiments were conducted with Pyranine as a preparation for the column and field experiments at a concentration of 1000 µg/l (see below). Only one concentration could be analysed for reasons of time restriction.

All samples were left in the dark on a platform shaker Innova 2300 by New Brunswick Scientific at 129 rotations per minute (rpm) for 24 hours. Before measuring fluorescence all samples were filtered through a 0.45 µm MILLEX-HV PVDF syringe driven filter unit. Sample solutions were measured for their pH with a Cole & Parmer pH 100 Series pH, mV, °C meter by Cole – Parmer Instrument Company, produced in Singapore; and for their EC with a Cyber Scan 100 con by EUTECH Instruments, manufactured in Singapore.

4.2.2.2 Evaluation

Uranine

Figure 4.14 shows the results of the batch experiments for a 1000 µg/l Uranine solution, in comparison to the initial solution („solution"). The behaviour of the tracer was consistent over a range of concentrations from 10 to 1000 µg/l. „coarse" and „fine" refer to coarse-grain batch experiment and fine-grain batch experiment, respectively. The fluorescence signal is constant between 2.5 and 20 % DSW and drops off from there. The trend is similar for the solution, and both coarse and fine fraction experiments, showing decreasing fluorescence with increasing salinity. The differences in fluorescence between different salinity levels, is obviously triggered by the salinity itself, whereas the differences between solution, coarse and fine is the result of sorption and therefore a function

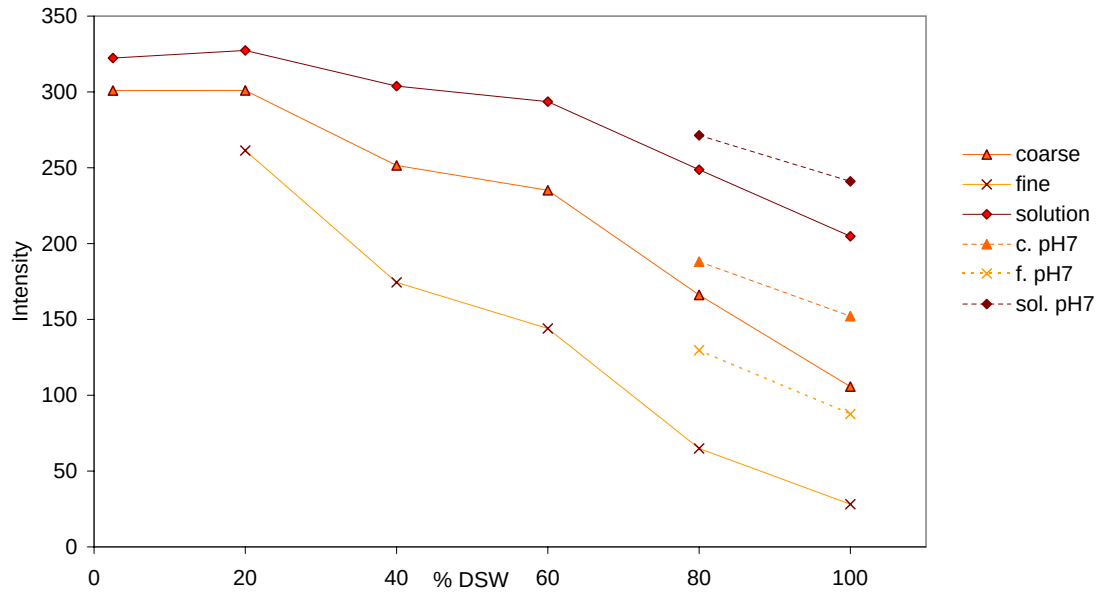

Figure 4.14: Results of the batch experiments using Uranine (C = 1000 µg/l) in comparison the solution.

of surface area.

The dashed lines „coarse pH 7“, „fine pH 7“ and „sol. pH 7“ are the results of experiments conducted with 80 and 100 % DSW, which was neutralized with 0.1 N NaOH-solution.

17 ml of 0.1 N NaOH-solution were needed to raise the initial pH of 5.91 of DSW to 7.08. More concentrated NaOH-solution could not be used as any concentration above 0.1 N crystallised out immediately. Although it should be remembered that this pH is a measured value, only, and does not reflect the real pH, yet there is no other efficient method that can be routinely used for identifying real pH. pH was measured before and after all batch experiments; the values are displayed in table 4.4.

As can be seen, the pH dropped again during the experiments, but it becomes clear that raising the measured pH improves fluorescence yield. The differences between pH neutral and the initial result are 5 % at 100 % DSW for the solution, 16 % at 100 % DSW for the coarse grain, and 24 % for fine grain batch experiment. Fluorescence yield gains most from changing the pH in the fine grain batch experiment, as Uranine is most adsorptive in low pH solutions. So the change in pH decreases adsorption, and it also slightly increases fluorescence yield in solution without the sorptive material, as can be seen from the upper „solution“-line in figure 4.14. Overall fluorescence extinction amounted 67 % in the coarse grain fraction and 91 % in the fine grain fraction as compared to 2.5 % DSW.

Distribution coefficients calculated from the batch experiments are presented in chapter 4.2.4 together with retardation factors calculated from both, batch and column experiments. The diagrams depicting the other concentrations of tracer solution used in the

Table 4.4: pH-values measured before and after the Uranine batch experiments.

% DSW	20	40	60	80	80	100	100
pH, solution	7.8	7.2	6.9	6.4	7.3	6	7.1
pH, batch, coarse	6.8	6.8	6.7	6.3	6.7	6.0	6.5
pH, batch, fine	7.1	6.7	6.5	6.2	6.5	5.8	6.3

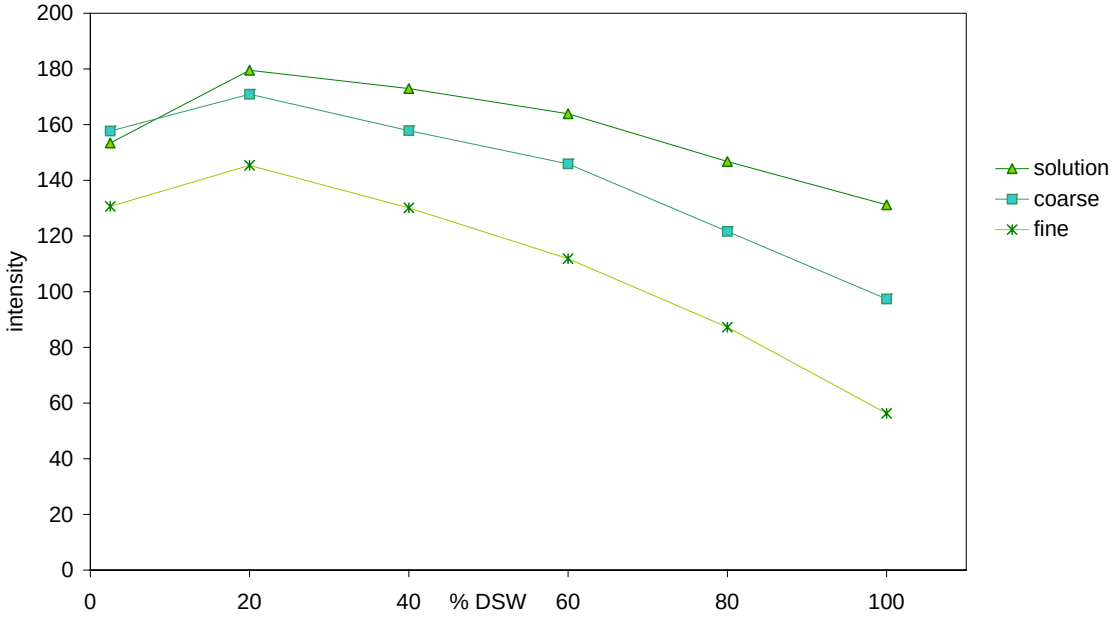

Figure 4.15: Results of the batch experiments using Pyranine at C = 1000 µg/l in comparison to the solution.

batch experiments for all tracers can be found in the Annex.

Pyranine

In figure 4.15 the results of the batch experiments conducted with Pyranine are presented. Here, fine-grain batch experiments were additionally conducted at 2.5 % DSW-concentration. Fluorescence intensity is lower at this salinity, reaches a peak at 20 % DSW and then drops off linearly. Like for Uranine the lines lie more or less parallel, indicating a similar behaviour with increasing salinities as the Uranine. The lower fluorescence intensity at 2.5 % DSW could possibly be explained by the relatively low real pH of 7.1 at 2.5 % DSW, as Pyranine is strongly sensitive to changes in pH (see figure 2.5). This theory is supported by the intensity value at 2.5 % DSW after contact with the coarse grain fraction. The pH after the batch experiment is slightly increased compared to the original solution, assumingly through release of carbonates from the sediment, and hence the fluorescence yield remains the same as in the solution, although part of the tracer might become adsorbed as seen in all other salinity levels.

Extinction at 100 % DSW reached 39 % for „coarse“ and 57 % for „fine“ relative to 2.5 % salinity, and 43 % and 61 % for „coarse „and „fine“, respectively, when related to 20 % salinity.

When looking at the results of the experiments with Pyranine, one should keep in mind that the pH-values were not at their optimum for the measurement of fluorescence of Pyranine. But as the laboratory experiments were used as studies for understanding the fate of the used tracers in field experiments, and in particular for the measurement of fluorescent tracers with an online (in-situ)-fluorimeter, the results are therefore highly valuable.

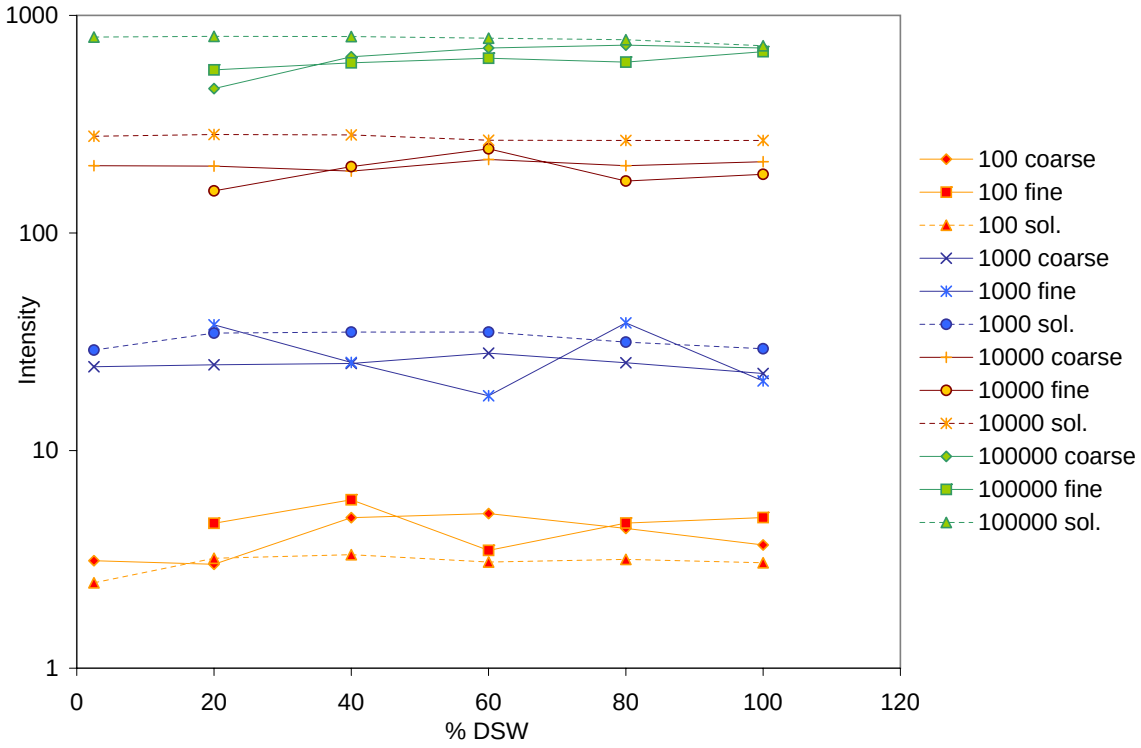

Figure 4.16: Results of the batch experiments using Naphtionat at concentration of 100, 1000, 10000 and 100000 µg/l.

Naphtionate

Naphtionate fluorescence remains steady in all salinity levels. Changing behaviour in batch experiments depending on tracer concentration can only be observed with fine sediments, as shown in figure 4.16. At the lowest concentration of 100 µg/l, both batch experiments resulted in higher fluorescence yields than the original solution in most salinity levels. Differences are quite little, though, and may be attributed to noise or some sort of

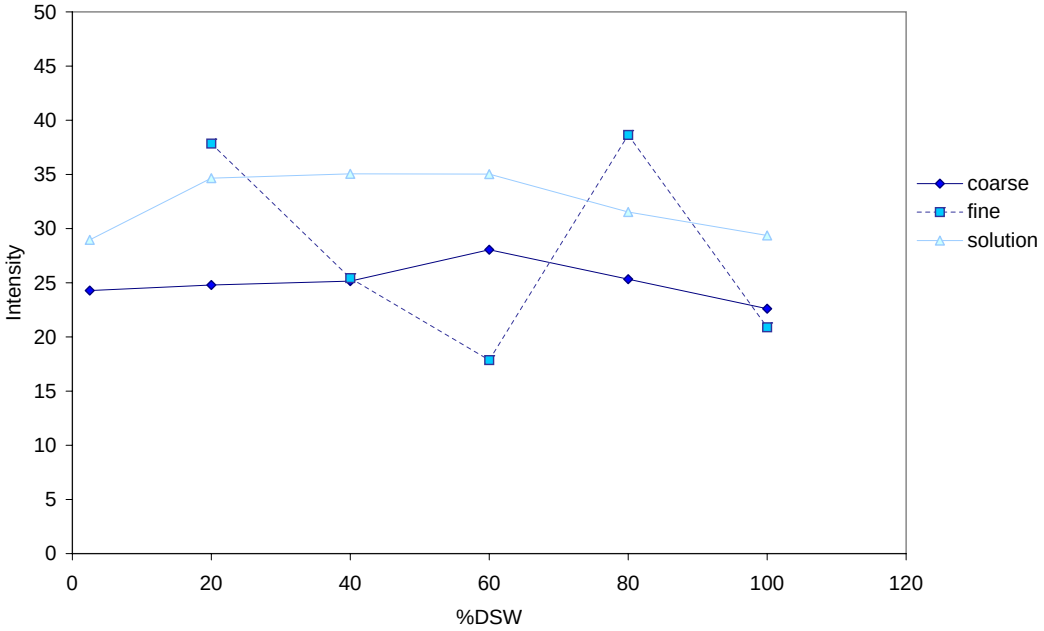

Figure 4.17: Fluorescence of Naphtionate resulting from batch experiments at C = 1000µg/l.

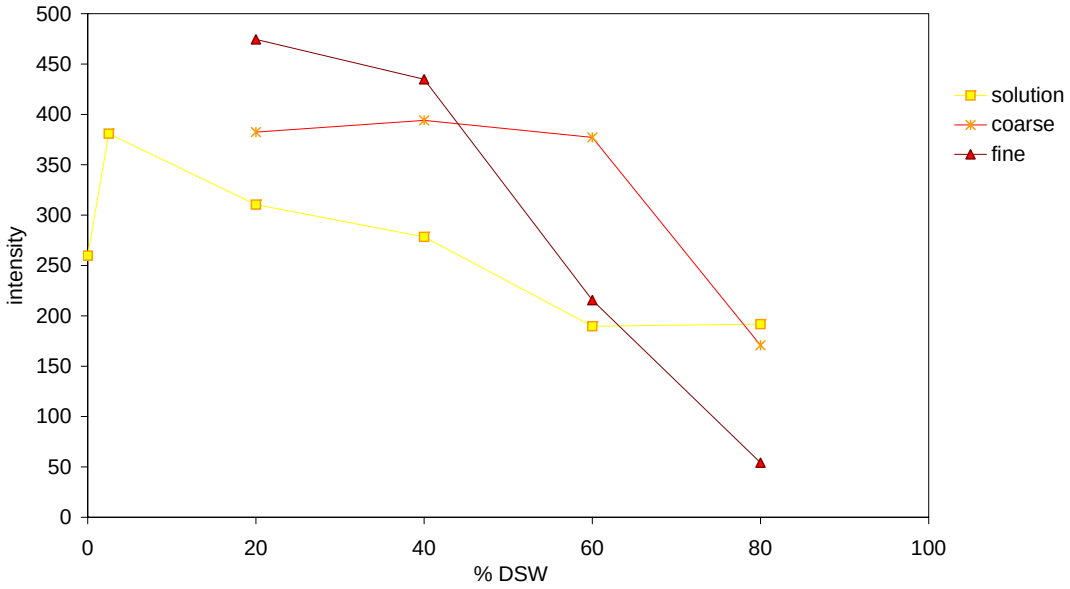

Figure 4.18: Fluorescence of Eosin after batch experiments and in solution at C= 10000 µg/l.

background. At tracer concentrations of 1000 to 100000 µg/l increasing salinity has very little influence on the fluorescence of Naphtionate, and there is no trend of behaviour. The 1000 µg/l concentration is depicted in figure 4.17 as an example. For the solution and the coarse fraction fluorescence intensity stays very stable, whereas for the fine fraction the signal is variable without any visible trend. This fluctuation of the fine fraction also varies between different tracer concentrations and only smoothens at very high tracer concentrations of 100000µg/l (100 ppm). However, there is quite a visible loss of fluorescence in the batch solutions as compared to the initial solution. This loss remains steady, though, and is not increased with higher salinities.

Eosin

Eosin batch experiments were conducted at a concentration of 10000 µg/l in 20, 40, 60 and 80 % DSW dilutions. They are depicted in figure 4.18. Fluorescence increases after contact with the sediments, or there is a release of substances from the sediments which fluoresce in the same wavelength. The trend of fluorescence is strongly negative with increasing salinity, although there is an increase in fluorescence between the solution in de-ionized water and in a 2.5 % DSW dilution. Adsorption increases considerably to the fine fraction above 40 % salinity, and from 60 % to the coarse fraction. In the solution there is no further decrease in fluorescence yield between 60 to 80 % DSW.

Extinction rates are 50 % for the solution, 55 % for „coarse“ and 86 % for „fine“, all at 80 % DSW relative to a 2.5 % solution.

4.2.3 Column Experiments

4.2.3.1 Setup

Column experiments were conducted in two identical plexi-glass columns, which were run simultaneously. Their height was 20 cm and the diameter 5.4 cm. An overflow outlet

Figure 4.19: Setup of the column experiment. The column (1) is connected to the peristaltic pump on the right and to the fraction collector on the left.

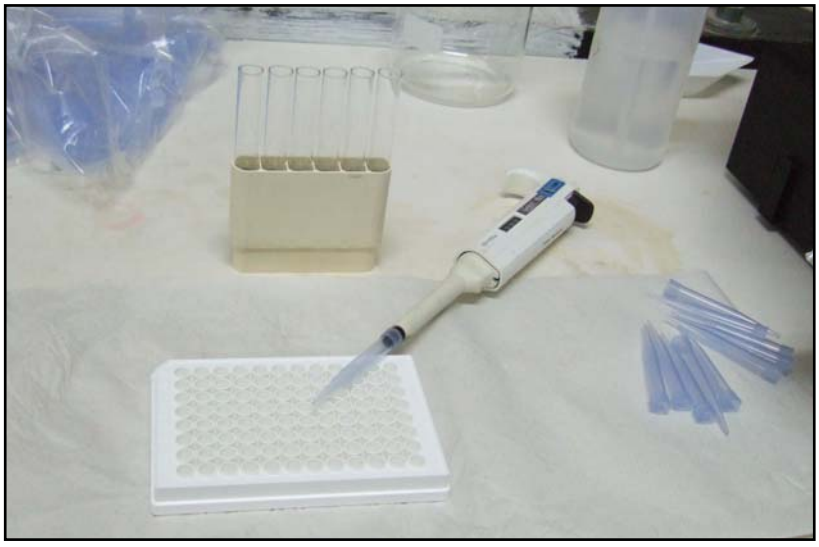

Figure 4.20: Wellplate for fluorescence measurement in the spectro-fluorimeter.

was located at a height of 17.5 cm, and the outflow pipe at the bottom of the column had a diameter of 5 mm, which was covered with 200µm filtering net, in order to keep sediments from flowing into the conducting pipes.

Allowing a constant head of 0.5 cm, the columns were filled to a total height of 17 cm with the same dried sediments as the „coarse“ batch experiments (see above), resulting in a total volume of 4.1

$\pi * r^2 * h = 389.34\ cm^3$.

Sediments were distributed as follows:

100 cm^3 of grain sizes 300 – 600 µm, weighing 119.3 g,

100 cm^3 of grain sizes 600 - 840 µm, weighing 134.0 g,

100 cm^3 of grain sizes 840 – 1190 µm, weighing 137.5 g,

80 cm^3 of grain sizes 1190 – 1400 µm, weighing 98.9 g, and

70 cm^3 of grain sizes 1400 – 2000 µm, weighing 105.6 g.

Sediments were weighed to an accuracy of 0.05 g resulting in a total dry weight of 595.2 g and 595.4 g for column 1 and 2, respectively.

Porosity was calculated by weighing the columns filled with the dry sediments, then filling them carefully with water. When no air-bubbles were seen through the walls of the column, and upon shaking the column no air-bubbles came to the surface, the columns were weighed again. Total dry weight subtracted from total wet weight resulted in a porosity of 20.7 and 21.3 % for column 1 and 2, respectively, or 81.7 cm^3 pore volume.

Inflow to the columns was regulated by a peristaltic pump Minipuls 3 by GILSON, with conducting pipes of 2 mm diameter connected to the in- and outflow pipes of 5 mm diameter. The columns were kept in a saturated condition throughout the experiments. Outflow again was regulated by the same peristaltic pump. The outflow pipes were lead to automatic fraction collectors Spectra/Chrom CF-1 by Spectrum Chromatography, making a total pipe length of approximately 1 m. The fraction collectors collected water volumes of 3.75 ml into glass tubes counted as 65 drops per tube into a total of 174 tubes per run.

Experiments were run with Uranine and Naphtionate in multi-tracer experiments in 2.5, 20, 40, 60, 80, and 100 % DSW, as well as pH neutral dilutions of 80 and 100 % DSW, in two different concentrations each. The tracer input was injected at the top end of the columns as a DIRAC – impulse of 1 ml tracer solution. Concentrations of 1000 µg/l (1 ppm) and 10000 µg/l (10 ppm) were used for Uranine and 10000 µg/l (10 ppm) and 100000 µg/l (100 ppm) for Naphtionate.

Pyranine column experiments were run in the same DSW – concentrations with a 1 ml DIRAC impulse of 10000 µg/l input concentration.

For fluorescence analysis a sample of 300 µl was conveyed from each sampling tube into wellplates of 96 wells each for reading in the spectro-fluorimeter.

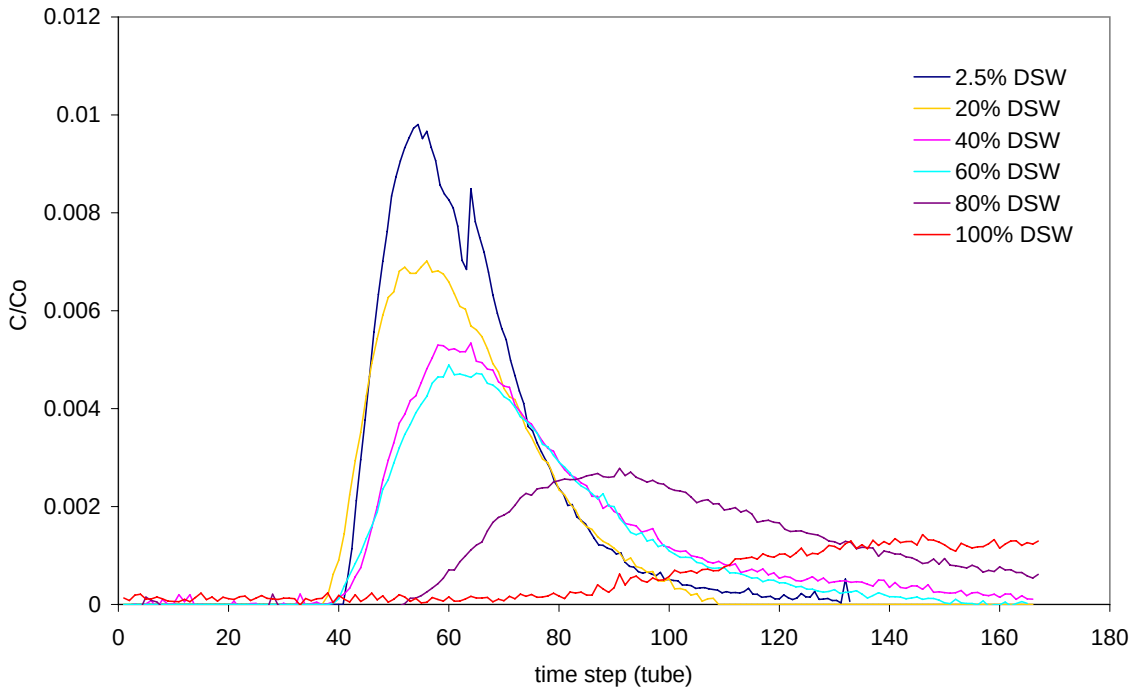

Figure 4.21a: Uranine breakthrough curves of an injected tracer mass of 1 µg.

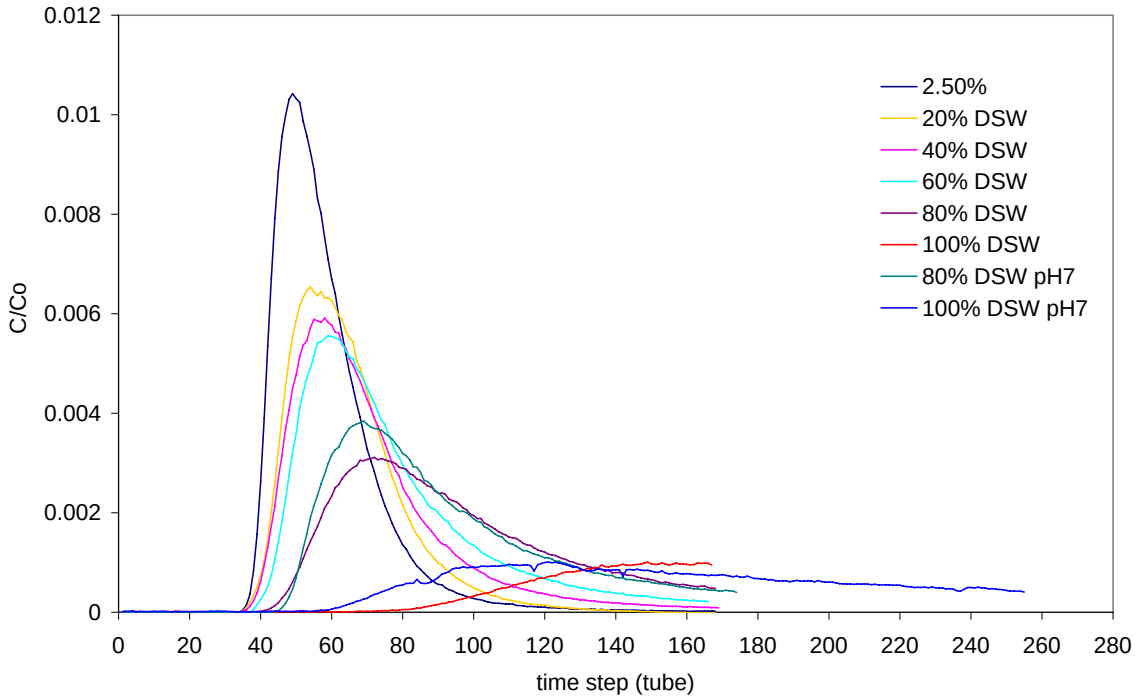

Figure 4.21b: Uranine BTCs of an injected tracer mass of 10 µg.

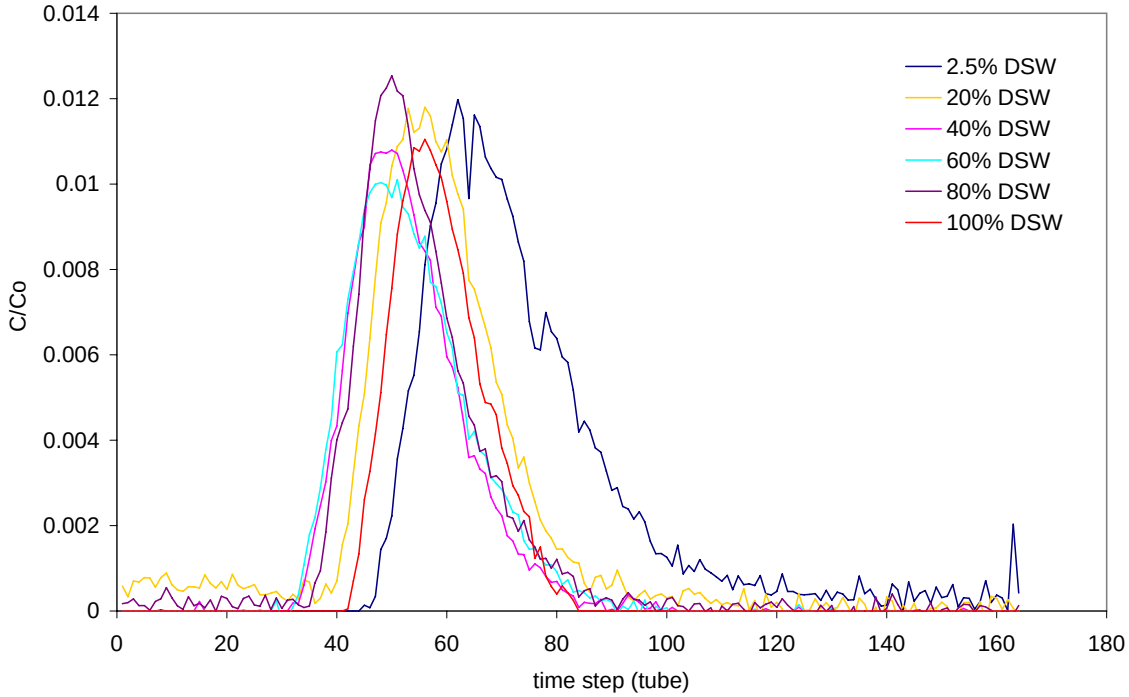

Figure 4.22 a: Naphtionate breakthrough curves of an injected tracer mass of 10 µg.

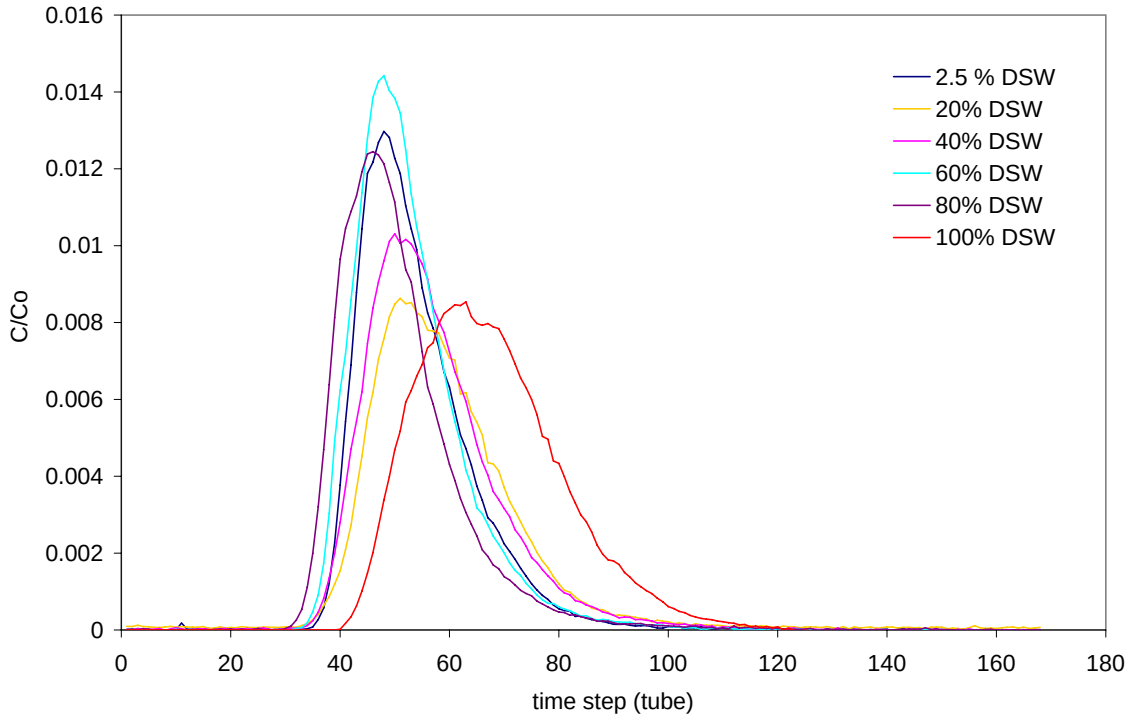

Figure 4.22 b: Naphtionate breakthrough curves of an injected tracer mass of 100 µg.

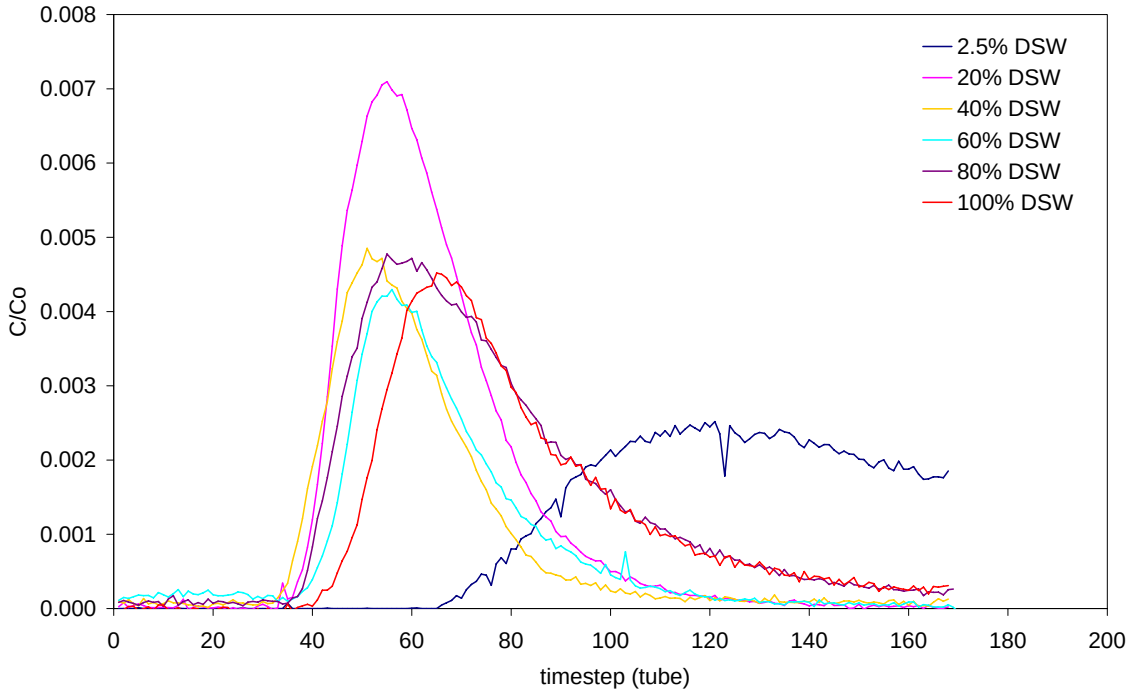

Figure 4.23: Pyranine breakthrough curves resulting from an injected tracer mass of 10 µg.

4.2.3.2 Evaluation

Uranine

The results of the column experiments for Uranine can be seen in figure 21a and b, presenting the breakthrough curves for injected tracer concentrations of 1000 µg/l and 10000 µg/l (tracer mass: 1 µg and 10 µg), respectively. All experiments at 1000 µg/l concentration were accomplished in column 1, and all experiments at a concentration of 10000µg/l were accomplished in column 2. The good concurrence between both concentrations is a proof for the reproducibility of the results. Each two curves at the same salinity (1 and 10 µg traecr input mass, respectively) can be found in the Annex.

A distinctive trend is observed for increasing salinities: retardation increases steadily and yield decreases with increasing salinity. Total yield lies between 80 to 98 % up to 60 % DSW, and is less at 80 and 100 % DSW, because the tracer breakthrough was not registered in the whole.

Naphtionate

The breakthrough curves (BTCs) for the two injected tracer concentrations of Naphtionate are shown in figure 4.22 a and b. The rather disperse distribution of the BTCs on the time axis and the seemingly arbitrary amplitude of the curves may lead to questions about why the behaviour of the tracer is so diverse in relatively constant conditions. At this point it may be necessary to say that conditions of the column experiments, especially flow rates, varied slightly from one run to the next. The reason, for one, being the increase in viscosity of the fluid due to increasing salt content having an influence on the fluid conveyance of the peristaltic pump, and secondly, that due to the high corrosiveness of DSW all tubes and pumps had to be thoroughly cleansed in between runs, involving opening of

valves etc., and therefore their settings may have varied slightly from one run to the other. Due to the smaller size if the Naphtionate molecule these differences may have a greater effect on the Naphtionate BTCs than they do on the Uranine.

A slight tracer loss was observed in the higher input concentration of 100000 µg/l at salinities of 20 and 40 % DSW, while a peak amplitude can be seen in the 60 % DSW BTC. Both observations are not in agreement with the BTCs resulting from the lower concentration of 10000 µg/l, and are therefore also assumed to be the result of the aforementioned varying flow conditions.

Despite these effects, yields are very constant ranging from almost 90 to 100 %, proving the fitness of Naphtionate as a water tracer in variable salinities. Each two curves at the same salinity (10 and 100 µg traecr input mass, respectively) can be found in the Annex.

Pyranine

Pyranine breakthrough curves are presented in figure 4.23. Greatest retardation is observed at the lowest salinity of 2.5 % DSW, whereas least retardation is observed at 20 % DSW. Yields amount 68 % for the 2.5 % DSW dilution, while the breakthrough was not registered in the whole, and 86 % for 20 % DSW dilution. BTCs at 40 – 100 % DSW are more similar, yet present distinctive differences: 40 % and 60 % show a relatively low yield of 57 and 54 % respectively, while 80 % and 100 % BTCs are more decelerated, but show relatively high yields of 75 % for 100 % DSW, and the 80 % DSW BTC shows the highest yield of 90 %.

For reasons of time restriction the results of Pyranine have to be regarded as preliminary results, as all experiments are yet without repetition, and therefore need to be reconfirmed.

Figure 4.24 presents the breakthrough curves of the three dye tracers in comparison to each other, showing their relative behaviour in each salinity level. Table 4.5 gives an overview over total yields achieved in the column experiments.

Table 4.5: Total yields in percent resulting from the column experiments.

Tracer	M_0 (µg)	% DSW					
		2.5	20	40	60	80	100
Uranine	1	(105)	86	93	74	65	34
	10	98	80	83	87	72	3
Naphtionate	10	(108)	(120)	93	97	(103)	84
	100	97	87	94	(106)	98	100
Pyranine	10	69	86	57	54	90	75

4.2.4 Distribution Coefficients and Retardation Factors

In the figure 4.25 K_d values of Uranine, Pyranine and Naphtionate determined in the batch experiments for two different tracer concentrations are presented together with results from fresh water experiments found by Leibundgut & Wernli 1986.

The distribution coefficients K_d reflect the tracers' affinity to sorption. Leibundgut &

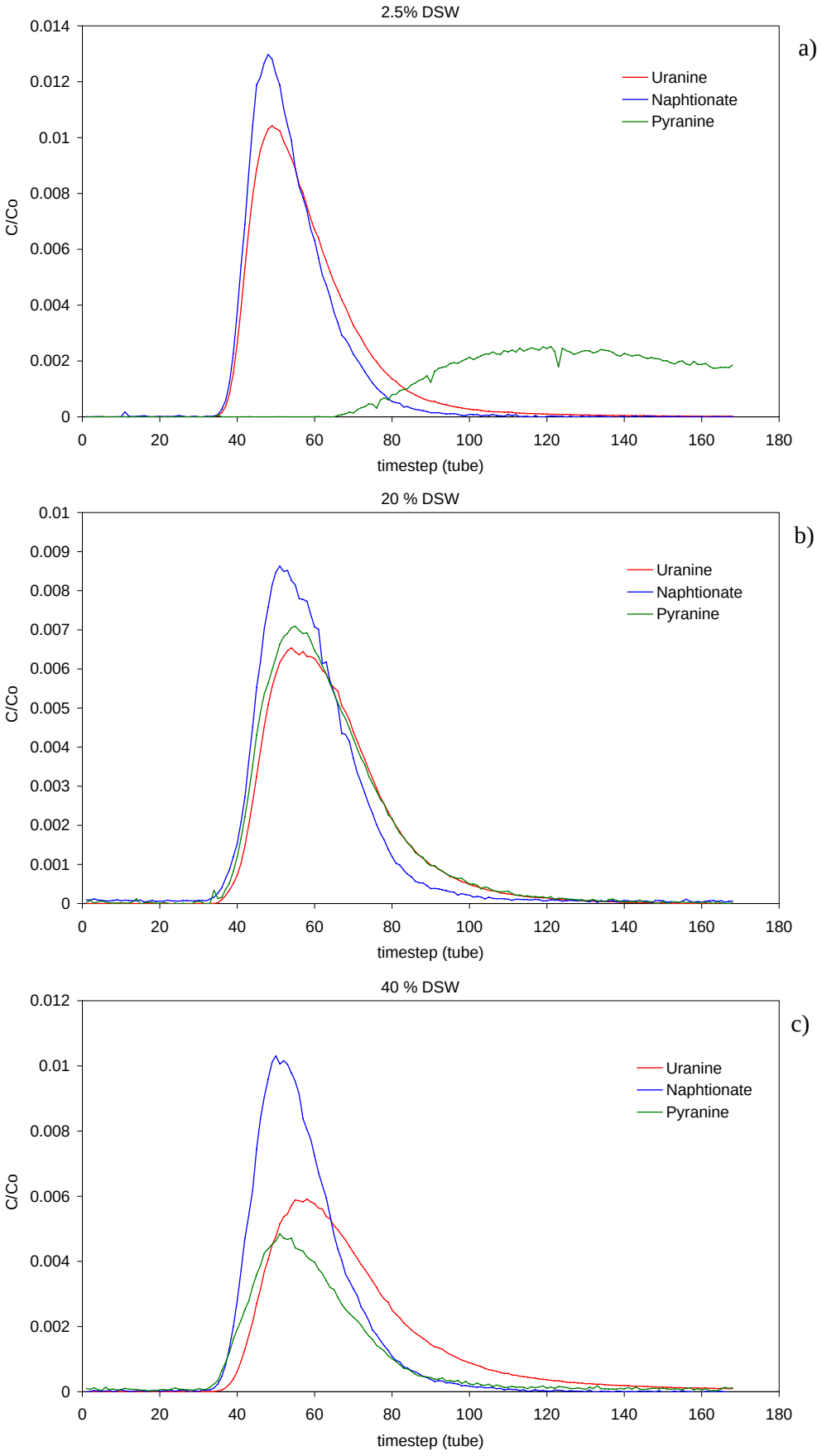

Figure 4.24 a-c: Breakthrough curves of Uranine, Pyranine and Naphtionate at: a) 2.5 % DSW, b) 20 % DSW and c) 40 % DSW.

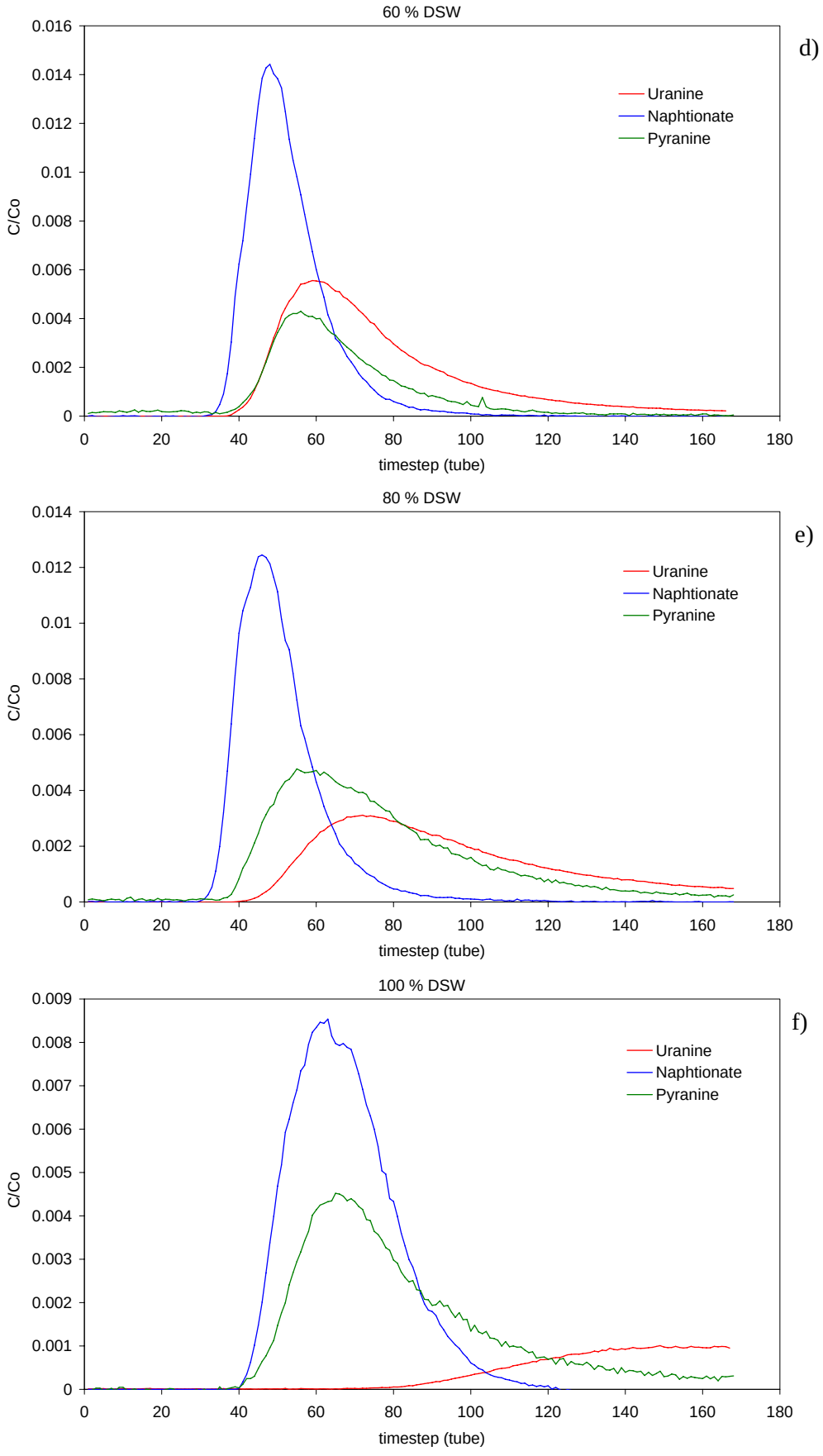

Figure 4.24 d-f: Breakthrough curves of the three tracers at:
d) 60 % DSW, e) 80 % DSW and f) 100 % DSW.

Wernli 1987 used fresh water for determining K_d-values of fluorescent tracers in this medium. They added 100 g of dry matter plus 250 ml of tracer solution to a 1l glass bottle, leaving it to shake for 24 hours at 140 rpm. K_d-values resulted to be small (0-0.25) for the tracers used in this study.

The K_d-values calculated from the measured fluorescence in the saline water are in rough agreement with the small K_d-values when extrapolating the trend of K_d towards low salinities.

The curves for Uranine start at low values in low salinities, remaining at $K_d < 0.5$ and at 100 % DSW they rise up to values of approximately 2 for a 100 µg/l solution and about

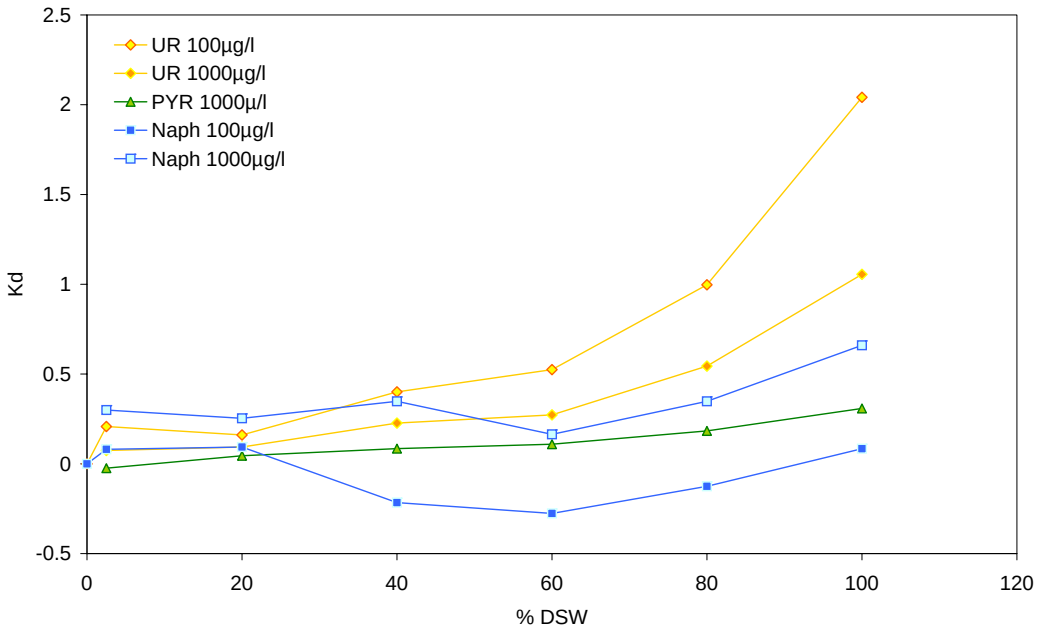

Figure 4.25: K_d-values calculated from the batch experiments

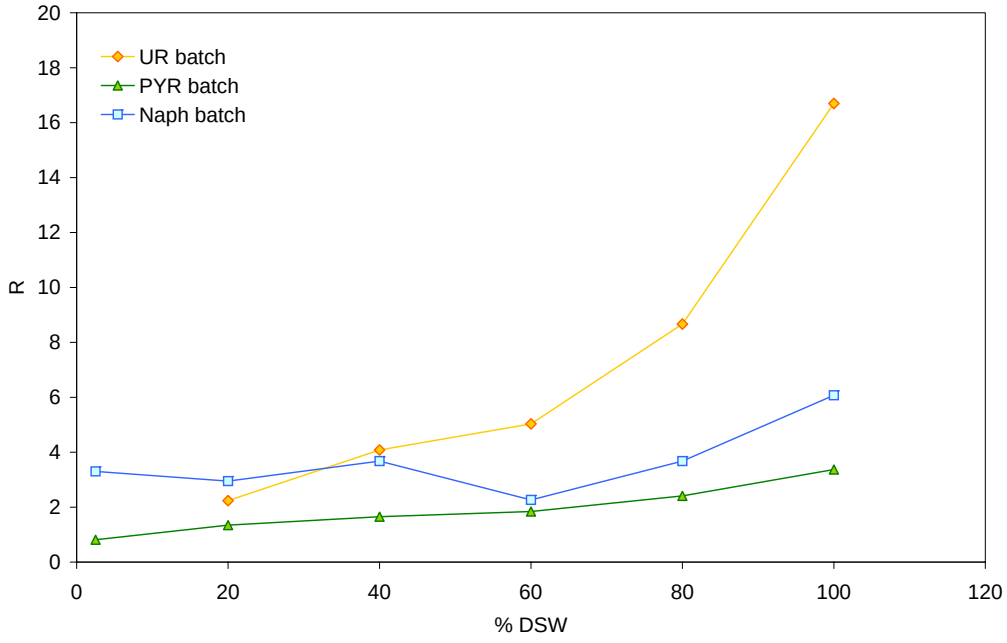

Figure 4.26: Retardation factors calculated from K_d-values (C = 1000 µg/l).

1 for a concentration of 1000 µg/l. Both concentrations of Naphtionate solutions keep a more or less constant level of approximately 0.15 moving upward and downward by 0.2 without any visible trend. K_d becomes < 0 for the batch experiments conducted at C = 100 µg/l, which means that higher tracer intensities were measured than could be expected from the initial tracer solution; K_d is usually >= 0.

The Pyranine curve shows even more constant values with a slightly sloping trend towards higher values with increasing salinity. The values range from 0 at 2.5 % DSW to 0.26 at 100 % DSW.

Retardation factors R calculated from the K_d-values from the batch experiments for a concentration of 1000 µg/l are shown in figure 4.26. R is calculated from (2.15):

$R = 1 + /n_e * K_{d,}$ with ρ_m = soil bulk density (g/cm³) and n_e = effective porosity.

Since R is a function of K_d the trend of the curves of the retardation factors is similar to that of the K_d-values.

The batch tubes were left on the shaker for 24 hours, with the sediments being more or less suspended in the tracer solution, so that full contact of the tracer solution with the adsorbing and desorbing material should have taken place. Therefore, tracer and sediments are assumed to be in equilibrium after this contact time.

The column experiments only took 3-4 hours each, which means that an equilibrium state between liquid and solid phase within the columns was probably not reached. Leibundgut suggests that R-factors can be determined from BTCs directly when 100 % tracer yield is achieved by using the cumulative frequency curve. In the column experiments 100 % tracer yield was not always achieved, wherefore retardation factors were calculated from curve fittings. The results from the curve fittings are presented in the next chapter.

It has been proposed that R-factors attained directly from column experiments do not comply with retardation factors calculated from K_d in batch experiments. The reasons might be the difference in contact time and the difference between the ratios of solution volume to dry material in the batch and and in the column experiments. Further investigations into this topic are eligible, i.e. researching for valid parameters inter-connecting the outcomes of batch and column experiments. Such investigations were not carried out, as this would have gone beyond the scope of this study.

4.2.5 Modelling

4.2.5.1 Parameter Estimation

The breakthrough curves received from the column experiments were modelled with an advection- (convection) dispersion model (CDE), written by Maloszewski & Zuber (1982), describing retardation and dispersion of the tracer. Only one tracer concentration was modelled for each tracer for reasons of time restriction, but as will be explained below the fitting parameters reflect the observed curves very clearly, so that knowing the fitted parameters for the modelled curves, an optical comparison of the two respective BTCs in the same salinity should be a reasonable measure of validity for the BTCs and their specified parameters.

The same BTCs were also modelled with the CXTFIT – code by Toride et al. (1999) and

Simunek et al. (1999). This code additionally considers non-equilibrium reactions between tracer and matrix. Because this model uses a minimum of six parameters for curve fitting (pore velocity v, dispersion coefficient D, retardation factor R, partitioning coefficient β, transfer coefficient ω, and decay coefficient μ), an ideal tracer should be injected in order to determine v and D. As there is no known ideal tracer for highly saline brines, Naphtionate BTC at 2.5 % DSW was used for determining the necessary parameters of the 'ideal' tracer for modelling of all tracers in the different salinities.

As a final step the different fitting parameters, received from fitting the calculated to the measured curves were compared for characterizing the tracers' behaviour in the different salinities.

4.2.5.2 Discussion of the Models

Figures 4.28, 4.29 and 4.30 depict the calculated BTCs from both models, equilibrium CDE and non-equilibrium CDE or CXTFIT, in comparison to the measured curve for the three tracers. As an 'ideal tracer' for the determination of pore velocity v and dispersion D, the 2.5 % DSW BTC of Naphtionate was used in the non-equilibrium model, as this tracer shows least effects towards influence of salinity variations: $D = 3.42 * 10^{-4}$ m²/s, v = 0.1548 m/s. It can be seen that the fit with the CXTFIT – code is of higher quality in all cases. This shows that, even in small scale laboratory experiments like the present one, non-equilibrium reactions between tracer and matrix take place in increased salinity levels. Calculated R, β, ω and μ –values for the non-equilibrium and D, v and R for the equilibrium model are listed in the tables below (table 4.6a and b) and the parameters for the CXTFIT-code are also depicted in figure 4.27.

For the more simple CDE-model the dispersion coefficient D is, when there are other effects influencing the tracer breakthrough, an overall parameter expressing the shape of the BTC. The relatively good fittings were achieved by adjusting pore velocity and D. As the discharge was measured during the experiments it was kept a fixed value and was not a function of pore velocity v. However, calculated retardation factors and dispersion parameter D can be regarded as preliminary estimates, but as the model is based on the assumption of a complete yield, and several factors shaping the BTC in saline media are neglected, it is not sufficient for accurate parameter determination.

Table 4.6a: Fitting parameters determined by the CXTFIT-code.

Tracer	% DSW	2.5	20	40	60	80	100
Uranine	R	1.10	1.25	1.40	1.43	2.10	4.20
	β	0.900	0.846	0.800	0.760	0.640	0.545
	ω	3.0	7.0	10.0	6.6	10.0	20.0
	μ	0	0.77	0.67	0.55	0.80	1.20
Naphtionate	R	1.10	1.20	1.16	0.90	1.00	1.24
	β	0.87	0.87	0.90	0.99	0.87	0.90
	ω	0.10	2.0	2.0	0.001	0.80	7.0
	μ	0	0.35	0.15	0	0	0
Pyranine	R	3.00	1.45	1.42	1.44	1.66	1.88
	β	0.700	0.830	0.800	0.805	0.700	0.720
	ω	2.0	1.0	1.0	1.0	1.0	8.0
	μ	0.30	0.40	2.00	2.20	0.50	0.70

Table 4.6 b: Fitting parameters determined by the equilibrium CDE.

Tracer	% DSW	2.5	20	40	60	80	100
Uranine	D (m²/s)	$1.3*10^{-7}$	$2.1*10^{-7}$	$2.1*10^{-7}$	$2.3*10^{-7}$	$2.2*10^{-7}$	$2.0*10^{-7}$
	v (m/s)	$1.09*10^{-4}$	$1.09*10^{-4}$	$1.05*10^{-4}$	$1.20*10^{-4}$	$1.13*10^{-4}$	$1.17*10^{-4}$
	R	1.062	1.001	0.951	0.923	1.000	1.045
Naphtionate	D (m²/s)	$9.50*10^{-8}$	$1.60*10^{-7}$	$1.30*10^{-7}$	$1.00*10^{-7}$	$1.08*10^{-7}$	$1.10*10^{-7}$
	v (m/s)	$4.30*10^{-5}$	$3.93*10^{-5}$	$3.85*10^{-5}$	$4.90*10^{-5}$	$4.75*10^{-5}$	$3.55*10^{-5}$
	R	1.06	2.11	1.47	1.00	1.13	1.00
Pyranine	D (m²/s)	$1.40*10^{-7}$	$1.65*10^{-7}$	$1.60*10^{-7}$	$1.50*10^{-7}$	$2.60*10^{-7}$	$1.60*10^{-7}$
	v (m/s)	$1.42*10^{-5}$	$3.00*10^{-5}$	$3.00*10^{-5}$	$2.90*10^{-5}$	$2.80*10^{-5}$	$2.50*10^{-5}$
	R	1.43	1.06	1.03	1.06	1.06	1.06

Uranine

Regarding the parameters fitted with the equilibrium CDE (table 4.6b) , dispersion D marks a linear increase for increasing salinities for the Uranine. Retardation R has no trend, but remains more or less constant around 1.

Looking at the parameters fitted with the non-equilibrium CXTFIT-model, Uranine BTCs show quite a clear trend towards increasing salinities, which this is visibly portrayed in the fitting parameters of the non-equilibrium model, shown in figure 4.27 a. Retardation R is close to 1 in lower salinities and increases significantly from salinities higher than 60 % DSW. The partitioning variable β is close to 1 in low salinities, but becomes smaller the higher the salt concentration in the water. A stronger decrease is yet observed at salinities higher 60 % DSW. This means that the higher the salt content, the more tracer remains in the non-equilibrium phase, that is the matrix. The transfer between the two phases reaches higher values in increasing salinities, marking enforced transfer from the liquid to the solid phase. Decay or degradation coefficient μ shows the same trend, increasing with increasing salinities, signalling degradation of the Uranine in increasing salinities.

Naphtionate

Naphtionate parameters for the equilibrium model D and R all more or less have the same value with a peak value each at 20 % DSW (explanation see below), and otherwise staying at level, portraying the steady behaviour of Naphtionate in all column experiments.

Like the breakthrough curves, the parameters of Naphtionate BTCs received from the non-equilibrium model (figure 4.27b) are rather arbitrarily distributed (i.e. without a clear trend with increasing salinity). Retardation R stays more or less constant around 1, whereas the partitioning variable β is 1 at 60 % DSW, and has smaller values in both higher and lower salinities. The transfer parameter ω remains low, but peaks at 100 % DSW with a value as high as 7. Decay coefficient μ is zero in most cases, but reaches higher values at 20 and 40 % DSW.

Taking a closer look at the behavior of μ and ω in comparison to the Uranine BTCs, which

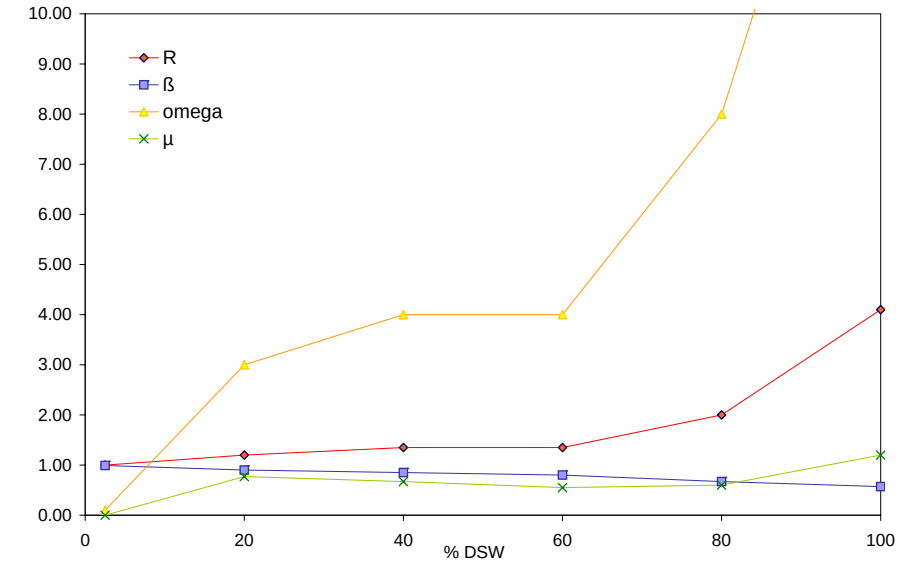

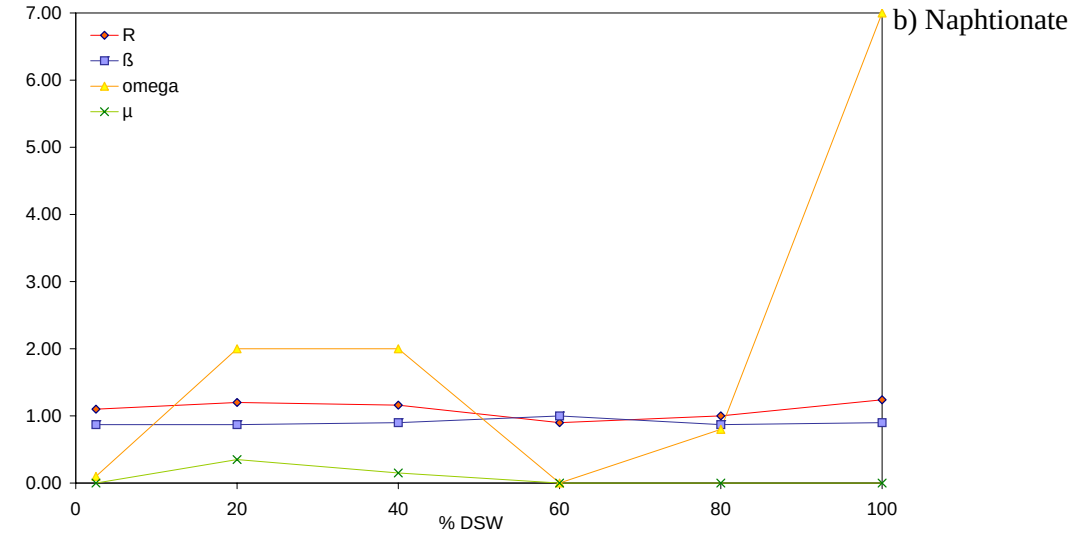

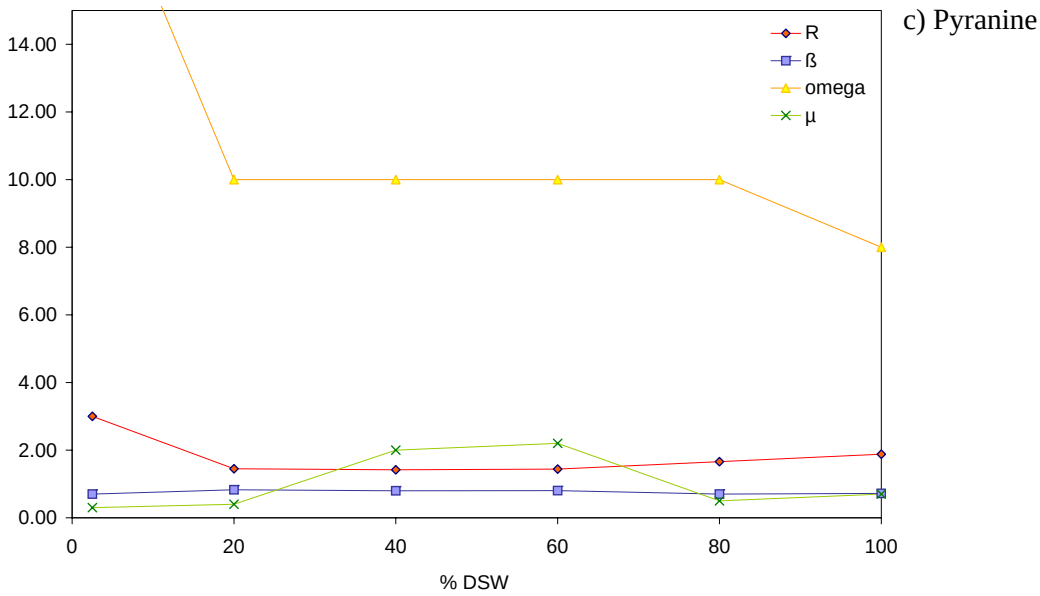

Figure 4.27 a-c: Fitting parameters determined by the CXTFIT-code:
a) Uranine, b) Naphtionate, c) Pyranine.

were conducted in the same column as multi-tracer experiments, elevated levels within the overall trend of these two parameters can be observed here, too. Therefore, it can be assumed that, as these elevated values were most probably attained through technical problems, rather than the characteristics of the tracer itself, for the Naphtionate ω is close zero and only picks up towards salinities of the saline end-member, while μ should remain zero throughout all salinities, meaning that there is no degradation of Naphtionate in all salinities.

Summing up the characteristics of Naphtionate as a tracer in varying salinities in laboratory experiments, it may be said that there is hardly any interaction between Naphtionate and the matrix, and yield should be usually around 100 % when the contact time between thetracer and the matrix are fairly short.

Pyranine

From the equilibrium model an elevated R-value signals the deceleration of the 2.5 % DSW BTC, while the values remain constant throughout all other salinities. Dispersion coefficient D on the other hand has its peak at 80 % DSW, where the effect of dispersion can be actually seen in the BTC, but puts a low D-value for the attenuated curve of 2.5 % DSW, and accentuates no features of the other BTCs.

The parameters attained from the Pyranine BTC-fittings with the non-equilibrium model offer a relatively clear picture. Retardation R is intermediate with values ranging from 1.4 to 1.9, with a peak of 3 for the strongly decelerated BTC at 2.5 % DSW. The values are constant from 20 to 60 % DSW edging upwards from there. The partitioning variable β has a negative trend, with an outlier at 2.5 % DSW, reaching values as small as 0.7 at 80 % DSW. This indicates increasing affinity of the tracer to the matrix with increasing salt content of the water. Transfer coefficient ω remains constant at a value of 10, dropping off to 8 at 100 % DSW, again with the exception of the low salinity end-member, peaking at 20. A loss of tracer or degradation is clearly marked by a peak of μ at 40 and 60 % DSW, otherwise this parameter shows a slight positive trend with increasing salinity.

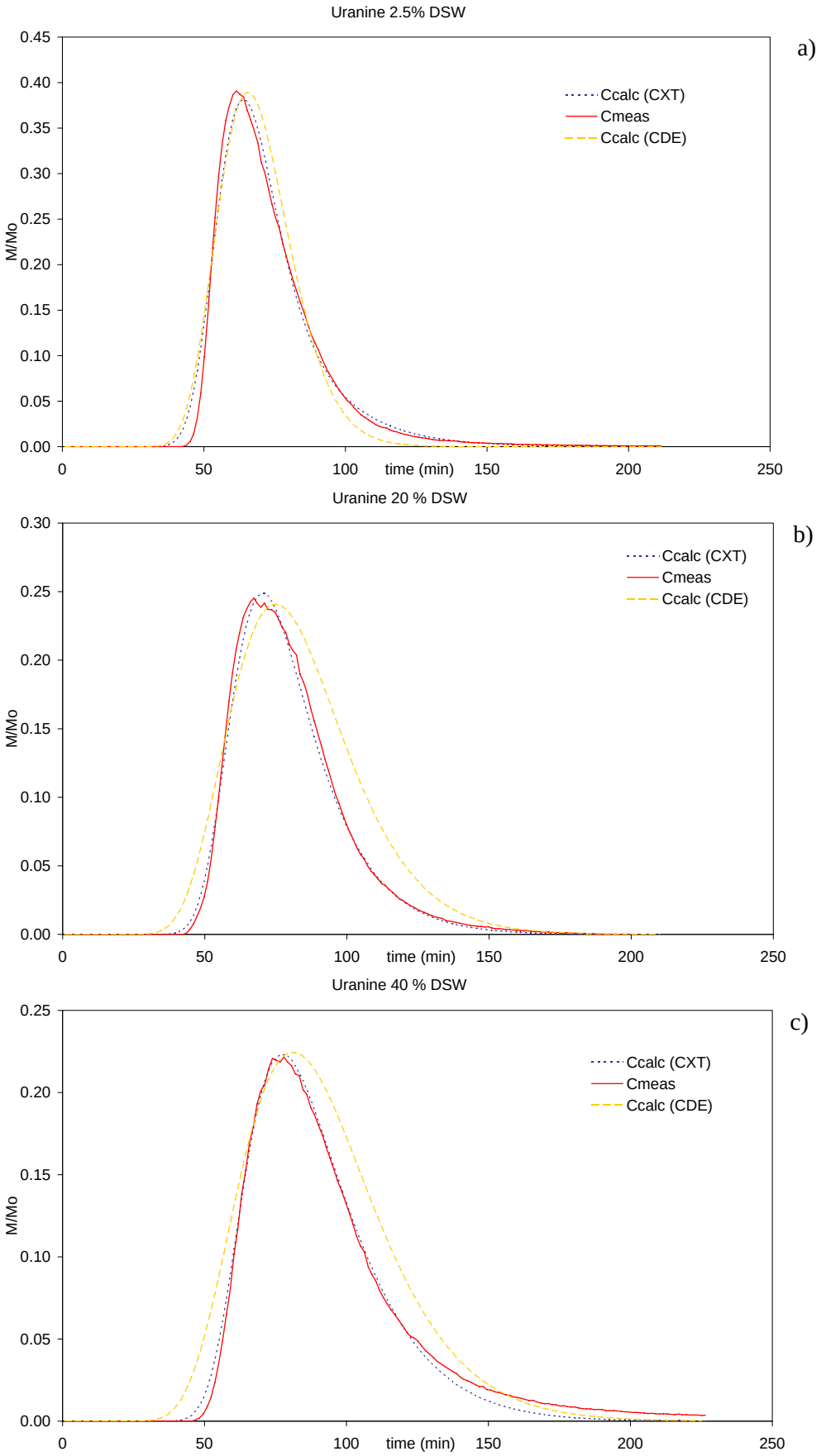

Figure 4.28 a-c: Modelled curves of the equilibrium CDE and the non-equilibrium CXTFIT-code fitted to Uranine BTCs: a) 2.5 % DSW, b) 20 % DSW and c) 40 % DSW.

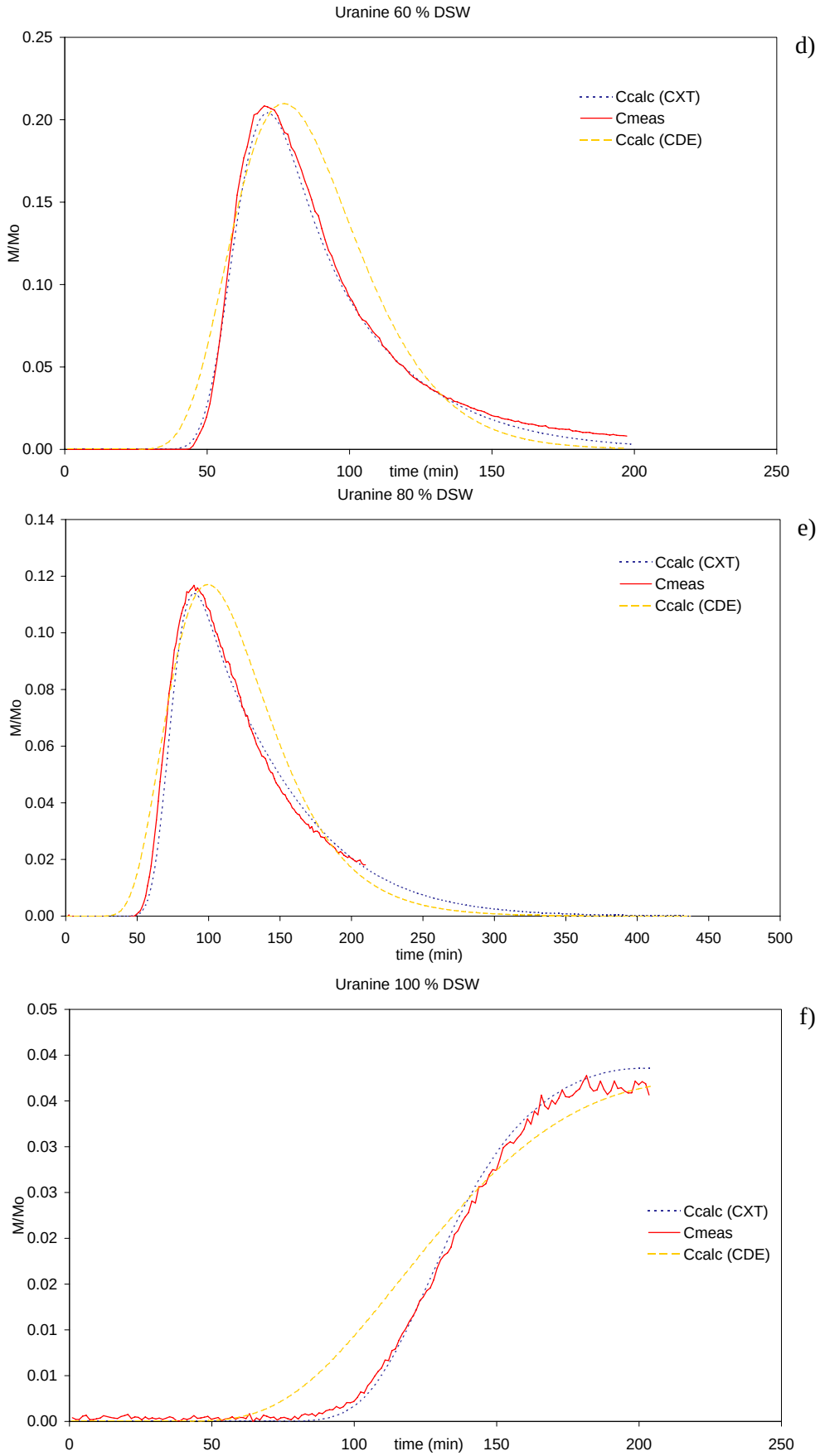

Figure 4.28 d-f: Modelled curves of the equilibrium CDE and the non-equilibrium CXTFIT-code fitted to Uranine BTCs: d) 60 % DSW, e) 80 % DSW and f) 100 % DSW.

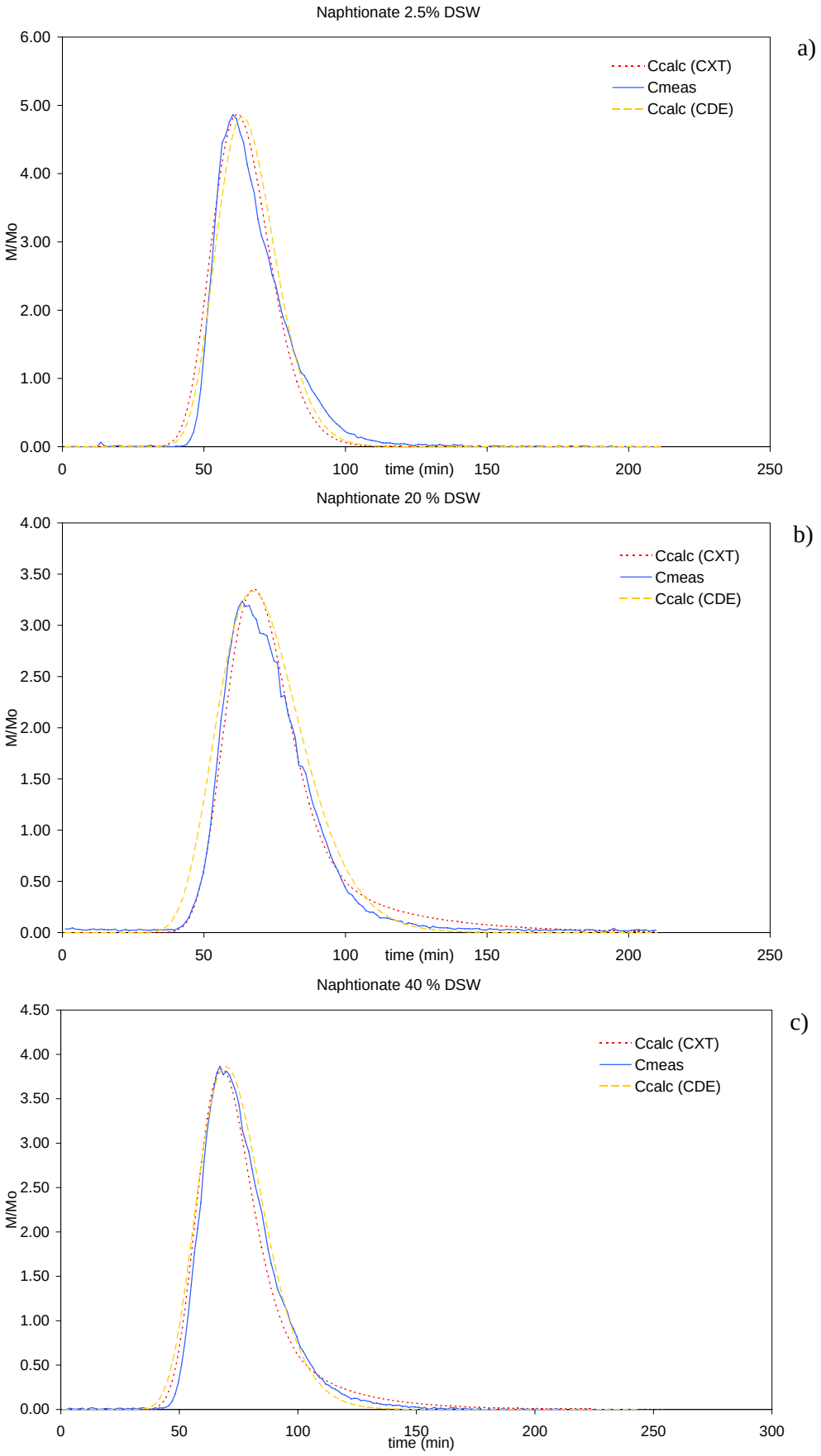

Figure 4.29 a-c: Modelled curves of the equilibrium CDE and the non-equilibrium CXTFIT-code fitted to Naphtionate BTCs: a) 2.5 % DSW, b) 20 % DSW and c) 40 % DSW.

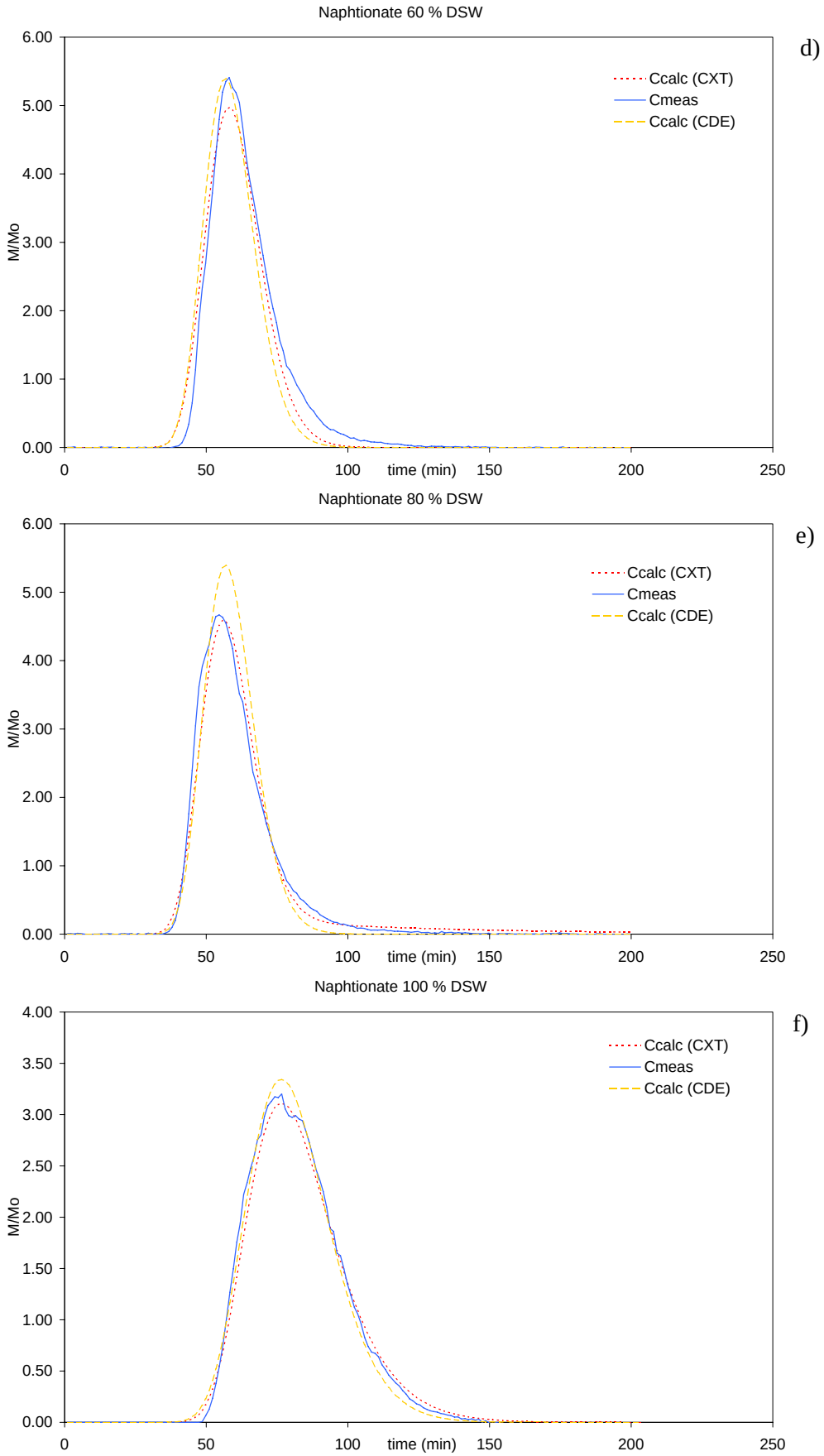

Figure 4.29 d-f: Modelled curves of the equilibrium CDE and the non-equilibrium CXTFIT-code fitted to Naphtionate BTCs: d) 60 % DSW, e) 80 % DSW and f) 100 % DSW.

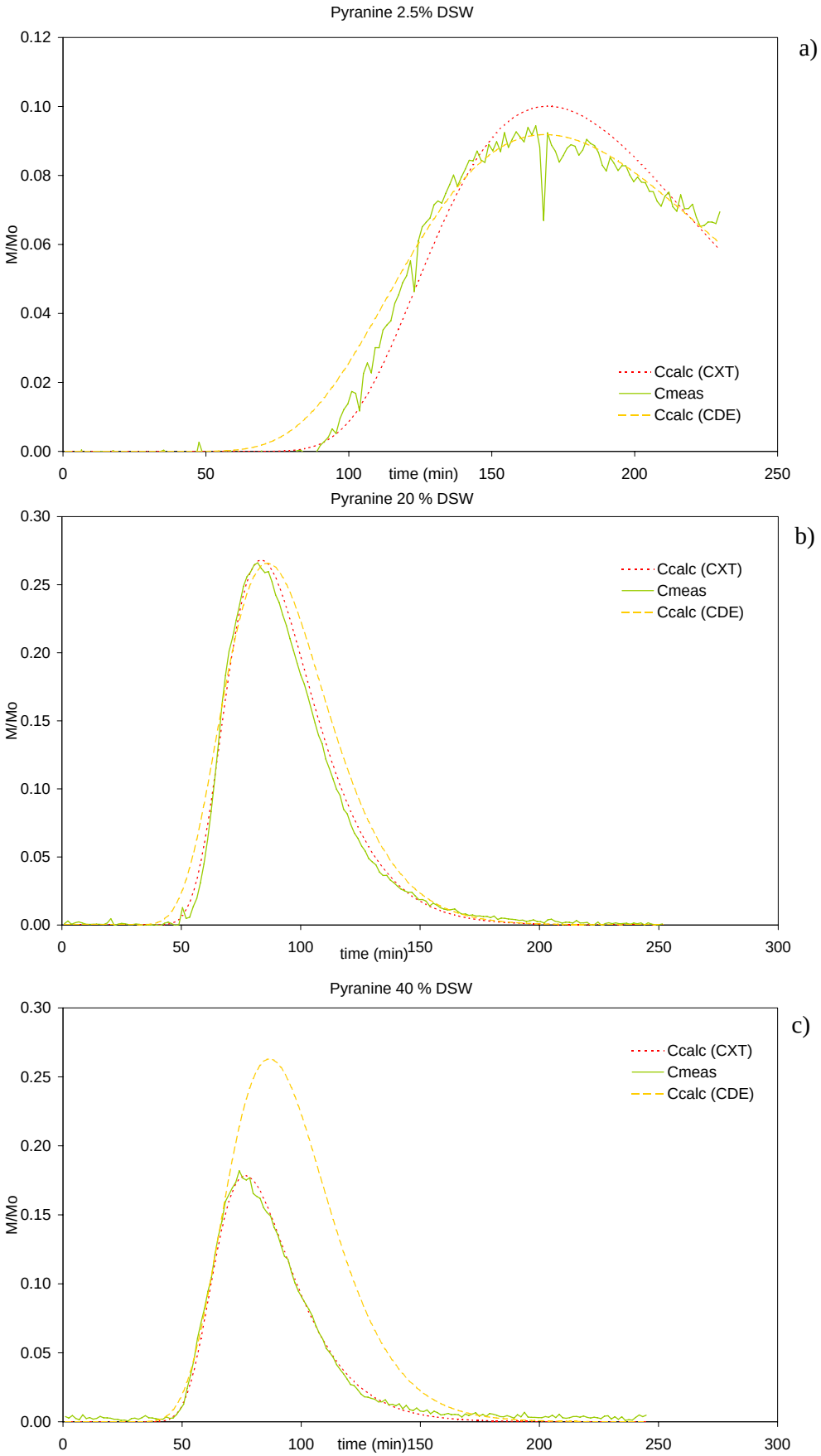

Figure 4.30 a-c: Modelled curves of the equilibrium CDE and the non-equilibrium CXTFIT-code fitted to Pyranine BTCs: a) 2.5 % DSW, b) 20 % DSW and c) 40 % DSW.

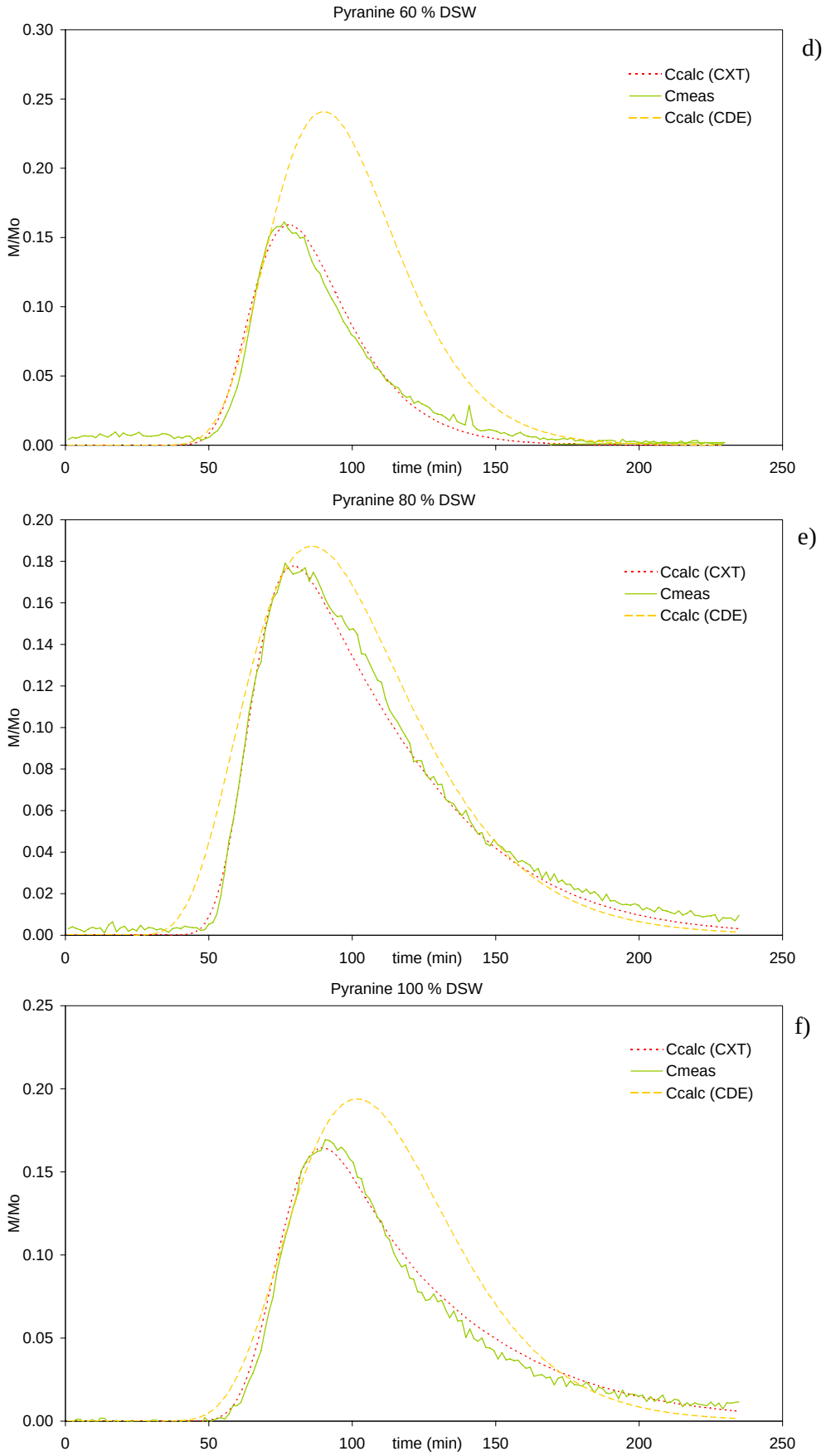

Figure 4.30 d-f: Modelled curves of the equilibrium CDE and the non-equilibrium CXTFIT-code fitted to Pyranine BTCs: d) 60 % DSW, e) 80 % DSW and f) 100 % DSW.

4.2.6 Conclusions

4.2.6.1 Response of Fluorescence to Varied Salinity

In saline solutions the fluorescence of Uranine, Pyranine and Naphtionate retains a relatively large intensity up to salinities of 60 % DSW (corresponding to a TDS concentration of approximately 200 g/l), yielding 94 % of fluorescence at this salinity for Uranine, and close to 100 % for Pyranine and Naphtionate. At 100 % DSW Uranine loses 40 % of its fluorescence intensity, Pyranine has a loss of 26 % and Naphtionate has a loss of 15 % of its fluorescence. Eosin drops out as a suitable water tracer in saline solutions, as it loses large amounts of its fluorescence even in low salinities (57 % fluorescence yield at 40 % DSW).

4.2.6.2 Response of Fluorescence in Batch Experiments

In batch experiments the response of fluorescence of all tracers is dependent on salinity, as well as on the grain size of the sediment. Uranine and Pyranine show a clearly negative trend with increasing salinity and decreasing grain size.

At 100 % DSW Uranine yields 33 % of fluorescence as compared to fluorescence at 2.5 % in the coarse grain batch experiment. This value is increased to 49 % in pH-neutralised solution. In contact with the fine sediments fluorescence yield drops down to 9 % at 100 % DSW, and is increased to 33 % in the pH-neutral solution. A bend in the decreasing trend of fluorescence can be observed from a salinity of 60 % DSW, making the decreasing slope even steeper, in both solution and batch experiments for Uranine.

Fluorescence intensity of Pyranine reaches a peak at 20 % DSW in batch experiments with both grain size distributions. The rise in intensity could have to do with an increase in pH from 2.5 % DSW to 20 % DSW, as Pyranine fluorescence reaches its optimum at pH-values > 8.5 (see figure 2.5). The trend of measured pH with respect to increasing salinity can be seen in figure 3.5.

From 20 % DSW fluorescence intensity drops off almost linearly, with a slightly steeper slope between 60 and 100 % DSW for the coarse grain batch experiment. Yields at 100 % DSW are 61 % for “coarse” batch experiments and 43 % for “fine” batch experiments when related to 2.5 % DSW, and 57 % and 39 % for “coarse” and “fine”, respectively, relative to the 20 % DSW – peak.

Naphtionate shows little response to increasing salinities and retains an almost constant level of fluorescence intensity in the coarse grain batch experiments with a small peak at 60 % DSW. However, the loss for all intensities is not insignificant and it is greatest at 20 and 40 % DSW reaching 28 % and smallest at 60 % amounting 15 %. Fine grain batch experiments though, show no explicable behaviour, jumping from high to low intensity from one concentration to the other.

Eosin batch experiments all result in higher fluorescence intensities than the solution before contact with the sediments up to a DSW-concentration of 80 %, and only drop below solution intensity at 100 % DSW. Despite the increase in fluorescence intensity through contact with the sediments, the drop in fluorescence intensity towards high salinities is still significant. A more or less constant intensity is yielded for the coarse grain batch experiments at salinities of 20 to 60 % DSW, while a major drop can be observed from 60 to

80 % DSW. In the “fine” batch experiments the major drop is shifted to lower salinities, occurring at salinities of more than 40 % DSW. Extinction at 80 % DSW amounts 55 % for “coarse” and 86 % for “fine”.

4.2.6.3 Response of Fluorescence in Column Experiments and Curve Fitting

Results from the column experiments conducted with Uranine, like the batch experiments, show a distinctive trend with increasing salinity, with a high amplitude BTC at 2.5 % DSW, which levels off and is delayed towards higher salinities. This behaviour is reflected by the fitting parameters of the non-equilibrium CXTFIT-model. Yields range from below 80 % (BTCs not fully registered) to 98 % of the initial input. Table 4.4 gives an overview of total yields of all column experiments.

Pyranine BTCs , while needing to be repeated for confirmation of the results, are consistent with the batch experiments in showing great effects of retardation (reversible sorption) at 2.5 % DSW and peaking at 20 % DSW (referring to the amplitude of the BTC). Apart from that the results of the column experiments are inconsistent with the batch results. While the batch experiments showed an almost linear decrease of fluorescence with increasing salinity from 20 % DSW onwards, 40 and 60 % BTCs yield minimum return flow of 57 and 54 %, respectively. 80 and 100 % DSW BTCs yield 90 and 75 %, respectively. Degradation coefficient μ from the CXTFIT-model clearly reflects the loss of tracer of the two BTCs at 40 and 60 %, and it is also indicated by a high partitioning coefficient (β) at these concentrations, but a high β-value for the 20 % DSW-BTC drops out of the picture. Retardation is slightly increased for 80 and 100 % DSW-BTCs which is mirrored in slightly increased retardation factors fitted with the CXTFIT-model.

Although the Naphtionate BTCs are slightly scattered on the time axis, their yield, amounting almost 90 to 100 %, consistently reaches the highest values of all three tracers. For the smaller tracer input of 10 μg shape and amplitude of the BTCs look quite similar for all salinities. Between BTCs for tracer a input of 100 μg greater differences in amplitude and retardation can be observed. Here, the highest amplitude at 60 % DSW coincides with the small peak at 60 % DSW in the batch experiments. The loss of tracer found in batch experiments, was not found in the column experiments. This may have two reasons: 1) the contact time of tracer and sorbing material was too short for adsorption to take place to a significant degree or, 2) adsorption of Naphtionate is reversible in saline solutions, and therefore the tracer is desorbed as the column is continuously flushed with water. The Naphtionate BTCs showed no tailings though, which makes the assumption of reversible sorption questionable and favours the short contact time as being the reason for the large yield of the tracer. Retardation of the 100 % DSW-BTC is mainly reflected by an elevated transfer coefficient ω fitted with the CXTFIT-model.

4.2.6.4 Fitting Models

Fitting the equilibrium-CDE model to the measured values resulted in somewhat unsatisfying fittings, with calculated curves resembling the measured values rather roughly. A disadvantage of this equation for fitting the model to the measured values is the lack of a degradation parameter, wherefore this model constantly yields return flows that are too high when the yield is less then 100 % for the measured curve. With the non-equilibrium model the curves could be fitted to the measured values to a satisfying degree.

4.2.6.5 Implications

Summing up the results of the laboratory experiments, Naphtionate seems to turn out being the most suitable tracer for the use in media of high and / or varying salinity, as its results retain the most constant values. This holds true for saline waters and all experiments conducted with the coarser grain fraction. When working in the field attention has to be paid to the composition of the subsurface material, as silty or clayey materials may lead to unexpected results. Possible irreversible sorption of up to 30 % needs to be taken into consideration when planning tracer tests with Naphtionate.

Uranine can be seen as a suitable tracer in salinities of up to 200 g/l, equalling 60 % DSW, although sorption to the solid phase, especially to fine material smaller 300 µm, reduces the amount of tracer in solution. Raising the pH ameliorates fluorescence yield of Uranine in saline solutions.

Pyranine can be considered an equally good tracer as Uranine for the use in saline media, as its yield in solution lies above that of Uranine, while its sensitivity to pH is a can be a drawdown for in-situ measurements. Pyranine is more suitable than Uranine for tracing saline groundwater of salinities greater 200 g/l. The behaviour of this tracer in the intermediate salinity range (40-60 % DSW) needs to be re-examined.

Eosin should be regarded as a poor tracer for studying saline waters and groundwaters, although the effect of increased fluorescence intensity after contact with solid material could be an interesting case to study.

Non-equilibrium models are to be preferred to equilibrium-models due to the capability of reflecting more complex processes occurring during interaction of tracers and solid material in saline solutions.

4.3 Field Experiment

As an application of the investigation results from the laboratory, a point dilution test was carried out in the En Gedi area from 10/09 – 13/09/2006. This field experiment was conducted in cooperation with E. Magal, who carried out all preparations, calculations and choice of tracers. My contribution to the field experiment was the application of an online-fluorimeter for the measurement of a fluorescent tracer in saline groundwater.

4.3.1 Site of the Experiment

The boreholes used for the field experiment were EG/11 and EG/16, which are described in chapter 4.1.1. EG/11 lies within about 50-60 m from the Dead Sea shore and shows a layered groundwater profile. The TDS-concentration of the upper layer, at 14.5 m b.w.h. was approximately 90 g/l, of the middle layer at 16 m b.w.h it was approximately 165 g/l, and of the deep layer at 19 m around 230 g/l.

EG/16, a borehole within 8 m from the Dead Sea shoreline, approximately 50 m north of EG/11, had total dissolved solids of 330 g/l, resembling DSW in the deep layer at 11 m b.w.h., and approximately 100 g/l TDS near the water surface at 4.5 m b.w.h.

4.3.2 Preparations for the Application of the Online-Fluorimeter

The tracers injected at the En Gedi site were Naphtionate for the deeper part of the aquifer and Pyranine for the shallower part of the aquifer. The online-fluorimeter GGUN-FL Fluorometer by Geomagnetism Group, University of Neuchâtel, Switzerland, was planned to read the Pyranine (the excitation lamp for shorter wavelengths, i.e. for Naphtionate reading, was not installed in the instrument), and therefore was calibrated with turbidity standards of 1, 10, and 100 NTU. These solutions were prepared from a standard solution of 800 NTU StablCal Standard stabilized Formazin Turbidity Standard by HACH Company, Loveland, USA. The GGUN – fluorimeter was then calibrated to water, as well as Pyranine at concentrations of 1, 10, 100 and 1000 ppb (µg/l), dissolved in borehole water.

4.3.3 Setup and Procedure

Three pipes of different lengths, 14.5, 16 and 19 m, respectively, were inserted into borehole number EG/11. They were attached to a borehole lid, holding them in place, with weights to make the pipes sink attached to the bottom ends. The suction pumps were attached to the lower ends of the pipes, and were run by battery power. Before filling the pumped water into the sampling tubes a certain amount of water from the borehole was let into a bucket, in order to make sure that the water sampled earlier was washed out of the pipe, completely.

Prior to the injection of Pyranine, which will be described below, Naphtionate and Renium (a lanthanide) were introduced into the deep layer of the same borehole, following the same procedure as for the Pyranine injection. The evaluation of the samples taken for Naphtionate and Renium were completed by E. Magal, whose work is still in progress, and will therefore not be explained as part of this study.

On 10th of September 120 ml of Pyranine at a concentration of 5.95 g/l were injected into the shallow layer of borehole number EG/11. The volume of the fresher water part of the borehole is 6.84 l, so the expected concentration after dilution with the borehole water was 0.1 g/l. The tracer was first dissolved in borehole water which was done in the laboratory. A pipe of 1 cm in diameter was let down to 14.5 m b.w.h., a funnel was placed inside the upper end of the pipe and the tracer solution was poured into the funnel. Funnel and pipe were rinsed with clear water in order make sure that the whole tracer was introduced to the borehole.

Within the first half hour samples were taken every five minutes by pumping with the electric suction pump and a pipe of 1 cm in diameter. After the first half hour the sampling period was reduced to ten minutes for another half hour, for the next hour to half an hour and from then on to every one hour during the day and every two hours during the night for the following four days.

The online-fluorimeter was introduced into the borehole at a depth of 14.5 m b.w.h. one hour after the injection of the Pyranine tracer. Initially, readings were set to a time period of 10 seconds, which was then increased to 1 minute after the first hour and to 5 minutes after 9 hours. Time of reading started on 10/09 at 13:00 h and ended on 13/09 at 12:00 h.

The injection of tracers and the sampling procedure in borehole number EG/16 was the

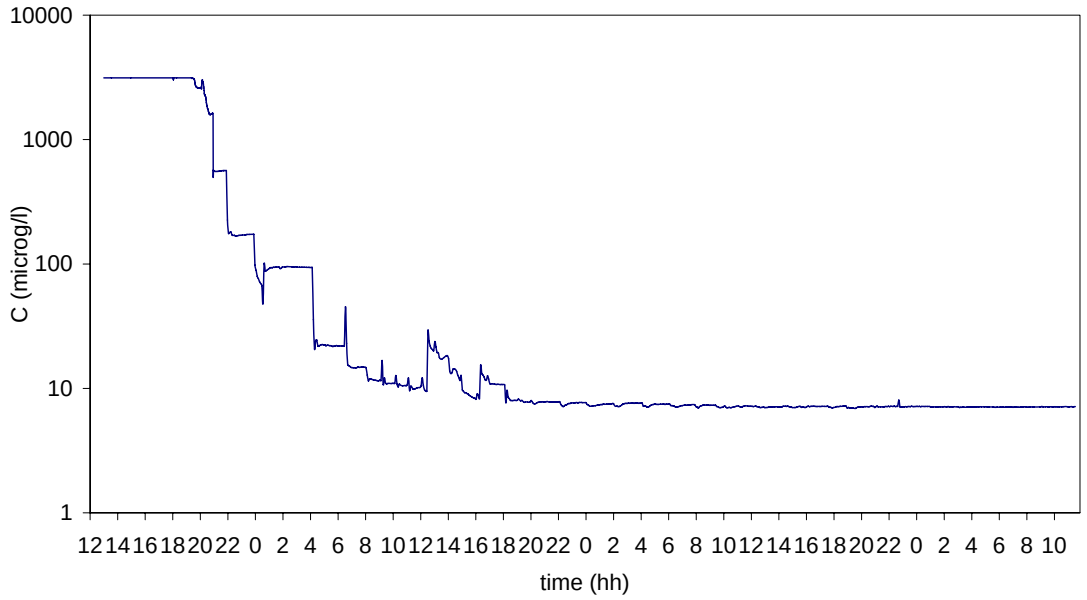

Figure 4.31: Readings of the online-fluorimeter (GGUN-FL) in borehole EG11. Injected tracer was Pyranine, depth: 14.5 m.

same as for EG/11. Injection in this borehole took place two hours after the injection of the Pyranine in EG/11. There was no reading of the online-fluorimeter in this borehole. Sampling was conducted with pipes 0.3 cm in diameter connected to a peristaltic pump. The injection of these tracers will not be explained in detail, as the evaluation of all samples was carried out by E. Magal. The work is still in progress.

4.3.4 Evaluation

The results of the online-fluorimeter readings are depicted in figure 4.31. Concentrations of the tracer during the first seven hours were too high for calculation. At 20:00 h and 21:00 h the hourly pumping for sampling is reflected in a steep decrease of tracer concentration. After 21:00 h, this period is extended to every two hours, which can be also nicely observed in the concentration curve. At 0:00 h a drop in concentration due to sampling followed by an increase in concentration can be seen. This can be explained by the observation that, because of technical problems with the pumps some of the water that had just been pumped out of the borehole got sucked back inside. No sample was collected at 2:00 h, which is reflected by the constant reading of the fluorimeter.

Clearly, from this point dilution test no concrete conclusions about the flow velocity of the groundwater can be drawn, as the flow rates were to slow in order to dilute the tracer within two samplings. Therefore most of the tracer was pumped back out of the borehole during sampling and rinsing the pipes before the sampling. In order to overcome this problem in the next field experiment, pipes of considerably smaller diameter should be used.

But the fluorimeter readings quite nicely show that this instrument is well suitable for in-situ measurements in high salinities.

In the EG/16 borehole, where smaller pipes were used for sampling, a dilution of both tracers Pyranine and Naphtionate by groundwater flow was registered. It produced a flow velocity of the groundwater of 0.2 m per day.

4.3.5 Conclusions

The outcomes of the field experiment asserted, firstly, the applicability of Pyranine and Naphtionate in brines found in the laboratory experiments, in a field tracer test.

Secondly, the clear signature of the fluorimeter readings and the endurance of the measurements over a three day period, show that the GGUN fluorimeter is suitable for the application in field tracer tests in saline environments.

And thirdly, the results of the sampling in EG/16 indicate flow velocities of 0.2 m/d (conclusions drawn in accordance with E.Magal).

Discussion

While researching the literature available on investigations into highly saline groundwater reservoirs using tracer methods, it became evident that there is a need for in-depth research, especially in the field of fluorescent tracer methods. The availability of literature on the application of natural tracers however, made it easier to interpret the data of the samples taken for these tracers, and it was therefore possible to work on specific characteristics within the area under investigation.

The results of the natural tracer analysis are clearly in keeping with the fact that the salinity in the waters sampled is the result of admixture of a fresh and a saline end-member water. This is important because another possible source of salinisation of the fresh groundwaters that approach the Dead Sea, are salt layers which would be dissolved by the intruding fresh water from the Mountain Aquifer, which triggers the shift of the fresh-saline water interface towards the lake shore as the lake level recedes.

This admixture is represented by parallel plots of cations and of anions other than SO_4^{2-} and HCO_3^-, when the ion species' concentrations are arranged relative to each other. The decrease of sulfate and bicarbonate is an indication of supersaturation of these minerals within the groundwater. With the use of the Pitzer equations for calculating the saturation indices of the various mineral phases, the presumption of supersaturation is supported by the results. Dolomite is indicated to be the most supersaturated phase followed by other carbonatic and sulfatic phases.

The analysis of the stable isotopes of H and O also seem to support the theory of a two end-member mixing process. The isotopic signature of the five samples taken, plotted in a line, connecting the average isotopic signature of the meteoric water of the surrounding area with that of Dead Sea water. However, it is doubtful that this mixing line is a definite sign of admixture. The reason for doubting this is, that if salt layers are being dissolved by approaching fresh water, located beneath the groundwater surface, they would probably not consist of dry salts, but would more likely consist of watery salt sludges. If they contained a certain amount of water they would contribute an isotopic signature in the sampled water.

However, when checking the isotopic ratios of Na/Cl, Cl/Br and Ca/SO_4 it showed that dissolution of evaporites was unlikely.

Again, these findings were supported by $^{228}Ra/^{226}Ra$ ratios of 0.3 found in the water samples. According to Moise et al. (2000) a $^{228}Ra/^{226}Ra$ ratio of approximately 0.3 is a typical value representing the local lithology, which has a carbonatic character. Salt dissolution is indicated by waters of increased salinity with $^{228}Ra/^{226}Ra$ ratios $< 0.3 – 0$. However, the samples taken for this study had radium isotopic ratios of approximately 0.3 and yet they were highly saline, which means that this ratio is set by equilibration of the groundwater with the hosting rock. This supports the theory that the salt content in the sampled waters originates from admixture of fresh with highly saline water, as the isotopic ratio is not changed by admixture of fresh and saline water.

Another detail in the groundwater system of the investigated area was found by the analysis of ^{34}S data. $\delta^{34}S$-values on the sulfate ion showed an increasing trend from the fresh towards the saline end-member. This trend did not continue in the most saline sample. The $\delta^{34}S$-values in the groundwater samples were higher relative to the value found in

Dead Sea water. Nissenbaum (1990) stated that these isotopes are almost absent in deep, anaerobic sediments from the Dead Sea. A circulation of Dead Sea water is suggested, which intrudes the near-shore sub-surface at a certain depth and then ascends and mixes with the shallower water. This water would then be a mixture of waters found upstream in borehole EG11 and Dead Sea water, re-circulated through the deep underground, which would result in the specific isotopic signature found in sample EG16/3.

For this study only one sample was taken for analysis of each of the various tracers in five different locations and only two locations were sampled for radium isotope analysis. Since such a small number is unlikely to produce a representative picture of the tracer composition in the specific locations, the reliability of the results would be questionable. However, since the results of the natural tracer analysis were embedded in the results of other authors, the outcome becomes more valuable. In fact, no doubts arose as to the validity of the results, because 1) they fitted into the results of other studies and 2) the results of the different tracers supported one another.

In addition to that the natural tracers were not analysed in order to create a picture of the processes in the Dead Sea area, but rather to test the feasibility of the respective tracers in determining of the relevant processes of the fresh-saline water interface.

The result of this feasibility test is that, each tracer brought some new information to the picture, yet a single tracer alone is not sufficient to grasp the full extent of the processes occurring in the sub-surface and to distinguish other processes from one another that may have a different root, but have a similar result, for example, as in to stable isotope composition. It is the combination of tracers that makes it possible to conclude the occurrence of a process with adequate certainty. Also, each tracer may lead to a new insight, as in the near-shore circulation found by $\delta^{34}S$.

The admixture of two water types was found to be the dominating process in the investigated study area and has been characterised with relative certainty by the various tracers. The ability to characterise this process becomes valuable when it is used to determine whether the area under investigation may be prone to subsidence or to the formation of sinkholes.

In assuming the admixture of two water types as the dominating process occurring at the study site, some deliberation took place as to what the results would be, if it was not admixture but salt-dissolution taking place. These assumptions need to be confirmed, and are suggested for further research in this field.

Further environmental tracers have been considered for the sampling in this study, they are: strontium-87, CFCs, SF_6 and noble gases. These tracers may also be valuable for the investigation of the fresh-saline water interface in hypersaline environments and CFCs and SF_6 would be valuable tools for age dating of the water. Some assumptions on the age of the local groundwater were put forward by Lewenberg (2005) using tritium and ^{14}C.

Another tracer that could be of interest is boron-11, which was used in studies on different sources of salinity in groundwater by Barth (2000) and by Kloppmann et al. (2001) and some preliminary results for the Dead Sea area were presented by Lewenberg (2005), but its distribution and possible interpretation in this location is to date not fully understood. H_2S and dissolved oxygen could also be analysed along with ^{34}S and sulfate in order to confirm the suggested theory of sulfate reduction and near-shore groundwater circulation.

For future radium sampling, it is suggested that in-situ devices be used, for example MnO_2-coated fibres, as used by Moise et al. (2000). Precipitation of radium along with $BaSO_4$ was attempted in the field, but failed possibly because of the relatively small amount of this phase compared to the high content of other ions in this water. ^{222}Rn could be a good reference for the interpretation of radium data and is suggested for sampling along with radium isotopes.

The results of the laboratory experiments present the character of the four fluorescent tracers Uranine, Pyranine, Eosin and Naphtionate in saline media. The results one might have expected based on the known characteristics of these tracers in fresh water may not be validated.

Eosin performed poorly in saline solutions and batch experiments and based on the results of this study, this tracer is judged unsuitable for the use in saline media. Uranine fluorescence showed a strongly negative trend with increasing salinity in both batch and column experiments as well as in solution and its applicability in saline water is questionable and is not advised in salinities of TDS > 200 g/l. The poor results of Pyranine fluorescence in low salinity (2.5 % DSW) is attributed to the low pH, and as Pyranine performed relatively well in all other salinity levels up to the salt concentration present in DSW, it can be recommended for use in saline media when pH > 6.5.

There was no influence on Naphtionate as salinity increased and it is therefore rated as the most suitable fluorescent tracer for the use in saline media.

The results of modelling of the breakthrough curves are unambiguous as to the fact that the effects on the tracer breakthrough triggered by high salinities are only well-represented by a non-equilibrium model as the CXTFIT-code.

The laboratory investigations of this study were of a purely empirical character and assumptions as to what the physical or chemical reason for the behaviour of the tracers (as in molecule structure of the tracer etc.) is are not attempted. Questions arise as to why there is no irreversible tracer loss of Naphtionate in the column experiments. This could possibly be answered by doing time-related controls of adsorption. In this study the fluorescence which resulted after batch experiments was measured only after a 24 hour period. It could be of interest, for instance, to measure the fluorescence every hour to see how the sorptivity of the tracer behaves over time. Only then would one know whether there was no loss in fluorescence of Naphtionate in the column experiments because of the short contact time, or whether there might have been another reason for this result. Perhaps it is also be possible to explain the non-conformist behaviour of the sorption of Naphtionate to fine grain sediments in varying salinity.

It could be of interest to research the behaviour of Pyranine in salinities > 2.5 % DSW, when the pH is increased. The tests with Uranine in pH-neutralised solutions showed improvement in tracer performance, but the effect of fluorescence extinction triggered by increased salinity could not be reversed. Would this be the same for Pyranine?

Other questions, for example as to why the decreasing slope in fluorescence of Uranine is steeper at salinities > 60 % DSW might be answered by the study of the change in physi-co-chemical character of the tracers with changes in salinity or by analysing the changing character of the water with increasing salinity.

An in-depth study of the ion-activity of Dead Sea water in different dilutions, for ex-

ample by using further options offered by the Aquachem modelling programme would be an integrated approach connecting the study of the general chemistry of the water (i.e. natural tracers) with that of the fluorescent tracers (i.e. artificial tracers). This would be a step towards the physical investigation of the behaviour of the fluorescent dye tracers in saline media. One idea which evolved while setting up the concept for this thesis, was to investigate the character of Uranine isomers in saline water. If the separation of the two isomers (perhaps one sorptive and one non-sorptive) could be simplified, it could turn out that the use of Uranine in saline media might not be so restricted.

The water of the Dead Sea has a very specific ion composition and the question arose whether a different ionic composition of a water would have the same effects on the dye tracers as does DSW. Some preliminary investigations using ’artificial‘ salt solutions of different mineral phases showed that the resulting effects, in combination with the changes in pH that the different mineral phases have on the solution, could also be an interesting field for in-depth research.

Flow conditions, as the exact direction of flow or flow velocities have until now, not been defined exactly within the study site. Now, with the evidence of the applicability of Naphtionate and Pyranine proven in a field experiment, they shall now be used in the field to investigate the conditions of flow and inter-connections of flow paths and to explore their flow behaviour through the matrix over longer distances.

References

Abraham, D. M; Charette, M. A; Allen, M. C; Rago, A; Kroeger, K. D., 2003: Radiochemical Estimates of Submarine Groundwater Discharge to Waquoit Bay, Massachusetts. Reports from the MBL General Scientific Meetings. Biology Bulletin, 205: 246-247, October 2003.

Abu-Jaber, N. S., 1998: A New Look at the Chemical and Hydrological Evolution of the Dead Sea. Geochimica et Cosmochimica Acta, 62/9: 1471-1479, 1998.

Alpert, P; Shafir, H; Issahari, D., 1997: Recent Changes in the Climate at the Dead Sea – A Preliminary Study. Climatic Change, 37: 513-537. Kluwer Academic Publishers, Netherlands, 1997.

Anati, D. A. & Shasha, S., 1989: The Stability of the Dead Sea Stratification. Israel Journal of Earth Sciences, 38: 33-35, 1989.

Appelo, C. A. J. & Postma, D., 1993: Geochemistry, Groundwater and Pollution. A.A. Balkema, Rotterdam, 1993, 3rd print 1996, 536 p.

Arkin, Y. & Gilat, A., 2000: Dead Sea Sinkholes – An Ever-developing Hazard. Environmental Geology, 39/7: 711-722, 2000.

Ayora, C; Taberner, C; Pierre, C; Pueyo, J.-J., 1995: Modeling the Sulfur and Oxygen Isotopic Composition of Sulfates Through a Halite-Potash Sequence: Implications fort he Hydrological Evolution of the Upper Eocene Southpyrenean Basin. Geochimica et Cosmochimica Acta, 59/9: 1799-1808, 1995.

Barth, S. R., 2000: Stable Isotope Geochemistry of Sediment-hosted Groundwater from a Late Paleozoic-Early Mesozoic Section in Central Europe. Journal of Hydrology, 235: 72-87, 2000.

Behrens, H., 1986: Water Tracer Chemistry – A Factor Determining Performance and Analytics of Tracers. Proceedings of 5th International Symposium on Underground Water Tracing; Morfis, A. & Paraskevopoulou, P. (edts.); International Working Group on Tracer Methods in Hydrology, Institute of Geology and Mineral Exploration (Greece), Athens, 1986.

Benischke, R. & Schmerlaib, H., 1986: Pyranin: A Fluorescent Dye for Tracer Hydrology, Review of Physico-Chemical Properties, the Toxicity and Applicability. Proceedings of 5th International Symposium on Underground Water Tracing; Morfis, A. & Paraskevopoulou, P. (edts.); International Working Group on Tracer Methods in Hydrology, Institute of Geology and Mineral Exploration (Greece), Athens, 1986.

Bennetts, D. A; Webb, J. A; Stone, D. J. M; Hill, D. M., 2005: Understanding the Salinization Process for Groundwater in an Area of South-Eastern Australia, Using Hydrochemical and Isotopic Evidence. Journal of Hydrology, 323: 178-192, 2006.

Bowman, D., 1997: Geomorphology of the Dead Sea Western Margin. In: Niemi, Ben-Avraham & Gat 1997.

Burnett, W. C; Aggarwal, P. K; Aureli, A; Bokuniewicz, H; Cable, J. E; CHarette, M. A; Kontar, E; Krupa, S; Kulkarni, K. M; Loveless, A; Moore, W. S; Oberdorfer, J. A; Ozyurt,

N; Povinec, P; Privitera, A. M. G; Rajar, R; Ramessur, R. T; Scholten, J; Stieglitz, T; Taniguchi, M; Turner, J. V., 2006: Quantifying Submarine Groundwater Discharge in the Coastal Zone Via Multiple Methods. Scienece of the Total Environment, article in press. Elsevier Sciences 2006.

Charette, M. A; Splivallo, R; Herbold, C; Bollinger, M. S; Moore, W. S., 2003: Salt Marsh Submarine Groundwater Discharge as Traced by Radium Isotopes. Marine Chemistry, 84: 113-121, July 2003.

Chung, Y. & Craig, H., 2004: Radium Redux in the Dead Sea: Profiles and Transient Ra/Ba Models. Earth and Planetary Science Letters, 218: 291-299, 2004.

Dickson, B. L., 1984: Radium Isotopes in Saline Seepages, South-western Yilgarn, Western Australia. Geochimica et Cosmochimica Acta, 49: 361-368, 1984.

Dulaiova, H., 2005: Multiple Isotopic Tracers for Study of Coastal Hydrological Processes. Dissertation submitted to the Department of Oceanography, College of Arts and Sciences, Florida State University, under supervision of Burnett, W. C. Summer Semester 2005.

Flury, M. & Wai, N.N., 2003: Dyes as Tracers in Vadose Zone Hydrology. Reviews of Geophysics, 41, 1 / 1002 2003. American Geophysical Union, April 2003.

Frumkin, A. & Elitzur, Y., 2002: Historic Dead Sea Level Fluctuations Calibrated with Geological and Archeological Evidence. Quaternary Research, 57: 334-342, 2002.

Garfunkel, Z. & Ben-Avraham, Z., 1996: The Structure of the Dead Sea Basin. Tectonophysics, 266: 155-176, 1996.

Gat, J. R., 1984: The Stable Isotope Composition of Dead Sea Waters. Earth and Planetary Science Letters, 71: 361-376. Elsevier Sciences Publishers B.V. Amsterdam, May, 1984.

Gat, J. R. & Gonfiantini, R. (edts.), 1981: Stable Isotope Hydrology, Deuterium and Oxygen-18 in the Water Cycle. IAEA Technical Reports, Series No. 21, Vienna 1981.

Gavrieli, I; Starinsky, A. & Bein, A., 1989: The Solubility of Halite as a Function of Temperature in the Highly Saline Dead Sea Brine System. Limnology and Oceanography, 34/7: 1224-1234, 1989.

Gavrieli, I; Yechieli, Y; Halicz, L; Spiro, B; Bein, A; Efron, D., 2001: The Sulfur System in Anoxic Subsurface Brines and Its Implication in Brine Evolutionary Pathways: the Ca-Chloride Brines in the Dead Sea. Earth and Planetaryn Sciences Letters, 186: 199-213, 2001.

Gertman, I. & Hecht, A., 2002: The Dead Sea Hydrography from 1992 to 2000. Journal of Marine Systems, 35: 169-181, 2002.

Ghabayen, S. M. S; McKee, M; Kemblowski, M., 2005: Ionic and Isotopic Ratios for Identification of Salinity Sources and Missing Data in the Gaza Aquifer. Journal of Hydrology, 318: 360-373, 2006.

Hall, J. K., 1997: Topography and Bathymetry of the Dead Sea Depression. In: The Dead Sea – The Lake and Its Setting. Oxford Monographs on Geology and Geophysics, No. 36. Oxford University Press:11-21, 1997.

Hammond, D. E; Zukin, J. G; Ku, T.-L., 1988: The Kinetics of Radioistope Exchange Between Brine and Rock in a Geothermal System. Journal of Geophysical Research, 93/B11: 13,175-13,186, November 1988.

Herut, B; Gavrieli, I; Halicz, L., 1998: Coprecipitation of Trace and Minor Elements in Modern Authigenic Halites from the Hypersaline Dead Sea Brine. Geochimica et Cosmochimica Acta, 62/9: 1587-1598, 1998.

Hoefs, J., 1997: Stable Isotope Geochemistry. Springer Verlag, Berlin, 4th edition, 1997.

IAEA, 2004: Isotope Hydrology Information System. The ISOHIS Database. Accessible at: http://isohis.iaea.org.

Kafri, U; Goldmann, M. & Lang, B., 1997: Detection of Subsurface Brine, Fresh Water Bodies and the Interface Configuration in Between by the TDEM Method in the Dead Sea Rift, Israel. Environmental Geology, 31: 42-29, 1997.

Kaess, W., 1998: Tracing Technique in Geohydrology. Brookfield, A. A. Balkema, 581p. 1998.

Kasnavia, T; De Vu & Sabatini, D. A., 1999: Fluorescent Dye and Media Properties Affecting Sorption and Tracer Selection. Ground Water, 37/3: 376-381, May – June 1999.

Katz, A; Starinsky, A; Taitel-Goldmann, N; Beyth, M., 1981: Solubilities of Gypsum and Halite in the Dead Sea and Its Mixtures with Seawater. Limnology and Oceanography, 26/4: 709-716, 1981.

Kelly, R. P. & Moran, S. B., 2002: Seasonal Changes in Groundwater Input to a Well-mixed Estuary Estimated Using Radium Isotopes and Implications for Coastal Nutrient Budgets. Limnology and Oceanography, 47/6, 1796-1807, 2002.

Kendall, C. & McDonnell, J. J., 1998: Isotope Tracers in Catchment Hydrology. Elsevier Science B.V. 1998, 839 p.

Kim, Y; Lee, K.-S; Koh, D.-C; Lee, D.-H; Lee, S.-G; Park, W.-B; Koh, G.-W; Woo, N.-C., 2002: Hydrogeochemical and Isotopic Evidence of Groundwater Salinization in a Coastal Aquifer: a Case Study in Jejy Volcanic Island, Korea. Journal of Hydrology, 270: 282-294, 2003.

King, P. T; Michel, J; Moore, W. S., 1982: Ground Water Geochemistry of ^{228}Ra, ^{226}Ra and ^{222}Rn. Geochimica et Cosmochimica Acta, 46: 1173-1182, 1982.

Klein-BenDavid, O; Sass, E; Katz, A., 2004: The Evolution of Marine Evaporitic Brines in Inland Basins: The Jordan – Dead Sea Rift Valley. Geochimica et Cosmochimica Acta, 68/8: 1763-1775, 2004.

Kloppmann, W; Nègrel, P; Casanova, J; Klinge, H; Schelkes, K; Guerrot, C., 2001: Halite Dissolution Derived Brines in the Vicinity of the Permian Salt Dome (N Germany). Evidence from Boron, Strontium, Oxygen, and Hydrogen Isotopes. Geochimica et Cosmochimica Acta, 65/22: 4087-4101, 2001.

Kraemer, T. F. & Genereux, D. P., 1998: Applications of Uranium- and Thorium-Series Radionuclides in Catchment Hydrology Studies. In: Kendall & McDonnell 1998.

Krest, J. M. & Harvey, J. W., 2003: Using Natural Distributions of Short-lived Radium Isotopes to Quantify Groundwater Discharge and Recharge. Limnology and Oceanography, 48/1: 290-298, 2003.

Krishnaswami, S; Bhushan, R; Baskaran, M., 1991: Radium Isotopes and 222Rn in shallow brines, Kharaghoda (India). Chemical Geology, 87: 125-136, 1991.

Kronfeld, J; Ilani, S; Strull, A., 1991: Radium Precipitation and Extreme 238U-series Disequilibrium Along the Dead Sea Coast, Israel. Applied Geochemistry, 6: 355-361, 1991.

Kronfeld, J. & Stiller, M., 1997: The Fate of Uranium in the Three Lakes of the Jordan Rift Valley. Israel Journal of Earth Sciences, 46: 13-28, 1997.

Kronfeld, J; Vogel, J. C; Rosenthal, A., 1992: Natural Isotopes and Water Stratification in the Judea Group Aquifer (Judean Desert). Israel Journal of Earth Sciences, 39: 71-71. The Weizmann Science Press of Israel, 1992.

Krumgalz, B. S., 1997: Ion Interaction Approach to Geochemical Aspects of the Dead Sea. In: The Dead Sea – The Lake and Its Setting. Oxford Monographs on Geology and Geophysics, Oxford University Press, 36: 145-160, 1997.

Lauria, D. C; Almeida, R. M. R; Sracek, O., 2004: Behaviour of Radium, Thorium and Uranium in Groundwater near the Buena Lagoon in the Coastal Zone of the State of Rio de Janeiro, Brazil. Environmental Geology, 47: 11-19, July 2004.

Leibundgut, Ch., 1974: Fluoreszierende Markierstoffe in der Hydrologie. Mitteilungen der Naturforschenden Gesellschaft in Bern, N.F. 31: 63-84, 1974.

Leibundgut, Ch., 1981: Zum Adsorptionsverhalten von Fluoreszenztracern. Festschrift J. G. Zötl, Sonderdruck: 111-129, Forschungszentrum Graz 1981.

Leibundgut, Ch. & Wernli, H. R., 1986: Naphtionate – Another Fluorescent Dye. Proceedings of 5th International Symposium on Underground Water Tracing; Morfis, A. & Paraskevopoulou, P. (edts.); International Working Group on Tracer Methods in Hydrology, Institute of Geology and Mineral Exploration (Greece), Athens, 1986.

Lewenberg, O., 2005: The Hydrogeology and Geochemistry of Groundwater in the Alluvial Fan of Wadi Arugot, En Gedi Reservation. Submitted for the degree of Master of Science to Institute of Earth Sciences, The Hebrew University of Jerusalem under the supervision of Lazar, B. and Yechieli, Y. 2005.

Maloszewski, P. & Zuber, A., 1982: Determining the Turnover Time of Groundwater Systems with the Aid of Environmental Tracers. 1. Models and Their Applicability. Journal of Hydrology, 57/3-4: 207-231, 1982.

Mazor, E., 1962: Radium and Radon content of some Israeli Water Sources and a Hypothesis on Underground Reservoirs of Brines, Oils and Gases in the Rift Valley. Geochimica et Cosmochimica Acta, 26: 765-786, 1962.

Mazor, E., 1997: Groundwaters along the Western Dead Sea Shore. In: The Dead Sea – The Lake and Its Setting. Oxford Monographs on Geology and Geophysics, Oxford University Press, 36: 265-276, 1997.

Mazor, E., 2004: Chemical and Isotopic Groundwater Hydrology. Marcel Dekker, Inc.

New York, third edition 2004, 453 p.

Moise, T., 1996: Radon and Radium Isotopes in Waters along the Jordan – Arava Rift Valley. Thesis submitted for the degree of Master of Science under supervision of Kolodny, Y. and Starinsky, A. at the Institute of Earth Sciences, The Hebrew University of Jerusalem, July 1996.

Moise, T; Starinsky, A; Katz, A; Kolodny, Y., 2000: Ra Isotopes and Rn in Brines and Ground Waters of the Jordan – Dead Sea Rift Valley: Enrichment, Retardation, and Mixing. Geochimica et Cosmochimica Acta, 64/14: 2371-2388, 2000.

Moore, W. S., 1996: Large Groundwater Inputs to Coastal Waters Revealed by ^{226}Ra Enrichments. Nature, 380: 612-614, April 1996.

Niemi, T. M; Ben-Avraham, Z; Gat, J. R. (edts.), 1997: The Dead Sea – The Lake and Its Setting. Oxford Monographs on Geology and Geophysics, No. 36. Oxford University Press 1997, 286 p.

Nissenbaum, A., 1975: The Microbiology and Biogeochemistry of the Dead Sea. Microbial Ecology, 2: 139-161, 1975.

Nissenbaum, A; Stiller, M; Nishri, A., 1990: Nutrients in Pore Waters from Dead Sea Sediments. Hydrobiologia, 197: 83-89, 1990.

Otero, N. & Soler, A., 2002: Sulfur Isotopes as Tracers of the Influence of Potash Mining in Groundwater Salinisation in the Llobregat Basin (NE Spain). Water Research, 36: 3989-4000, 2002.

Palestinian Water Authority, 2001: Boundaries of the Western Aquifer Basin and the Eocene Aquifer in the Northeastern Aquifer Basin. Working Report SUSMAQ-MOD # 6.1 V1.0, Version 1.0: Sustainable Management of the Westbank and Gaza Aquifers. Palestinian National Authority, Palestininian Water Authority, December 2001.

Purkl, S., 2002: Entwicklung und Anwendung neuer Analytischer Methoden zur schnellen Bestimmung von kurzlebigen Radiumisotopen und Radon im grundwasser-beeinflussten Milieu der Ostsee. Dissertation zur Erlangung des Doktorgrades der Mathematisch-Naturwissenschaftlichen Fakultät der Christian-Albrechts-Universität zu Kiel.

Richardson, S. D; Willson, C. S; Rusch, K. A., 2004: Use of Rhodamine Water Tracer in the Marshland Upwelling System. Ground Water, 12/5: 678-688, September-October 2004.

Shalev, W; Lyakhovsky, V; Yechieli, Y., 2006: Salt Dissolution and Sinkhole Formation along the Dead Sea Shore. Journal of Geophysical Research, 111, B03102, doi: 10.1029/2005JB004038, 2006.

Simunek, J; van Genuchten, M. Th; Sejna, M; Toride, N; Leij, F. J., 1999: The STANMOD Computer Software for Evaluating Solute Transport in Porous Media Using Analytical Solutions of Convection-Dispersion Equation, Versions 1.0 and 2.0. U.S. Salinity Laboratory, Agricultural Research Service, U.S. Department of Agriculture, Riverside, California, November 1999. Available from: http://www.ars.usda.gov/services/software

Smart, C. C. & Karunaratne, K. C., 2002: Characterization of Fluorescence Background in Dye Tracing. Environmental Geology, 42: 492-498, April 2002.

Smart, P. L. & Laidlaw, I. M. S., 1977: An Evaluation of Some Fluorescent Dyes for Water Tracing. Water Resources Research, 13/1: 15–33, February 1977.

Stiller, M. & Chung, Y. C., 1984: Radium in the Dead Sea: a Possible Tracer for the Duration of Meromixis. Limnology and Oceanography, 29/3: 574-586, 1984.

Sutton, D.J; Kabala, Z. J; Francisco, A; Vasudevan, D., 2001: Limitations and Potential of Commercially Available Rhodamine WT as a Groundwater Tracer. Water Resources Research, 37/6: 1641-1656, June 2001.

Swarzenski, P. W; Martin, J. B; Cable, J. C., 2001: Submarine Ground-Water Discharge in Upper Indian River Lagoon, Florida. In: Eve L. Kuniansky, editor, U.S. Geological Survey Karst Interest Group Proceedings, Water-Resources Investigations Report, 01-4011: 194-197, 2001.

Toride, N; Leij, F. J; van Genuchten, M. Th., 1999: The CXTFIT Code for Estimating Transport Parameters from Laboratory or Field Tracer Experiments, Version 2.1. U.S. Salinity Laboratory, Agricultural Research Service, U.S. Department of Agriculture, Riverside, California. Research Report No. 137, April 1999.

Tricca, A; Porcelli, D; Wasserburg, G. J., 2000: Factors Controlling the Groundwater Transport of U, Th, Ra and Rn. Earth and Planetary Science, 109/1: 95-108, March 2000.

Yechieli, Y., 2000: Fresh-Saline Ground Water Interface in the Western Dead Sea Area. Ground Water, 38/4: 615-623, July – August 2000.

Yechieli, Y., 2006: Response of the Groundwater System to Changes in the Dead Sea Level. In: Enzel, Y; Agnon, A; Stein, M., eds. New Frontiers in Dead Sea paleoenvironmental research: Geological Society of America, Special Paper 401: 113-126, 2006.

Yechieli, Y; Gat, J. R., 1997: Geochemical and Hydrological Processes in the Coastal Environment of the Dead Sea. In: The Dead Sea, The Lake and Its Setting. Niemi, T. M; Ben-Avraham, Z; Gat, J. R. (editors). Oxford Monographs on Geology and Geophysics, 36: 252-264, 1997.

Yechieli, Y; Kafri, U; Goldmann, M; Voss, C. I., 2001: Factors Controlling the Configuration of the Fresh-saline Water Interface in the Dead Sea Coastal Aquifers: Synthesis of TDEM Surveys and Numerical Groundwater Modeling. Hydrogeology Journal, 9: 367-377, 2001.

Yechieli, Y; Ronen, D; Berkowitz, B; Dershowitz, W. S; Hadad, A., 1995: Aquifer Characteristics Derived from the Interaction Between Water Levels of a Terminal Lake (Dead Sea) and an Adjacent Aquifer. Water Resources Research, 31/4: 893-902, 1995.

Zak, I., 1997: Evolution of the Dead Sea Brines. In: Niemi, Ben-Avraham & Gat: 122-144, 1997.

Zuber, A., 1986: On the Interpretation of Tracer Data in Variable Flow Systems. Journal of Hydrology, 86: 45-57, 1986.

URL1: http://usgs.gov/lab 20.10.2006

URL2: www.deadseaproject.org 13.07.2006

URL3: http://wwwbrr.cr.usgs.gov/projects/GWC_coupled/phreeqc/ 08.12.2006

URL4: http://water.usgs.gov/cgi-bin/man_wrdapp?phrqpitz 08.12.2006

URL5: http://www.varianc.com/cgi-bin/nav?products/ 05.12.2006

URL6: http://sofia.usgs.gov/projects 10.10.2006

Annex

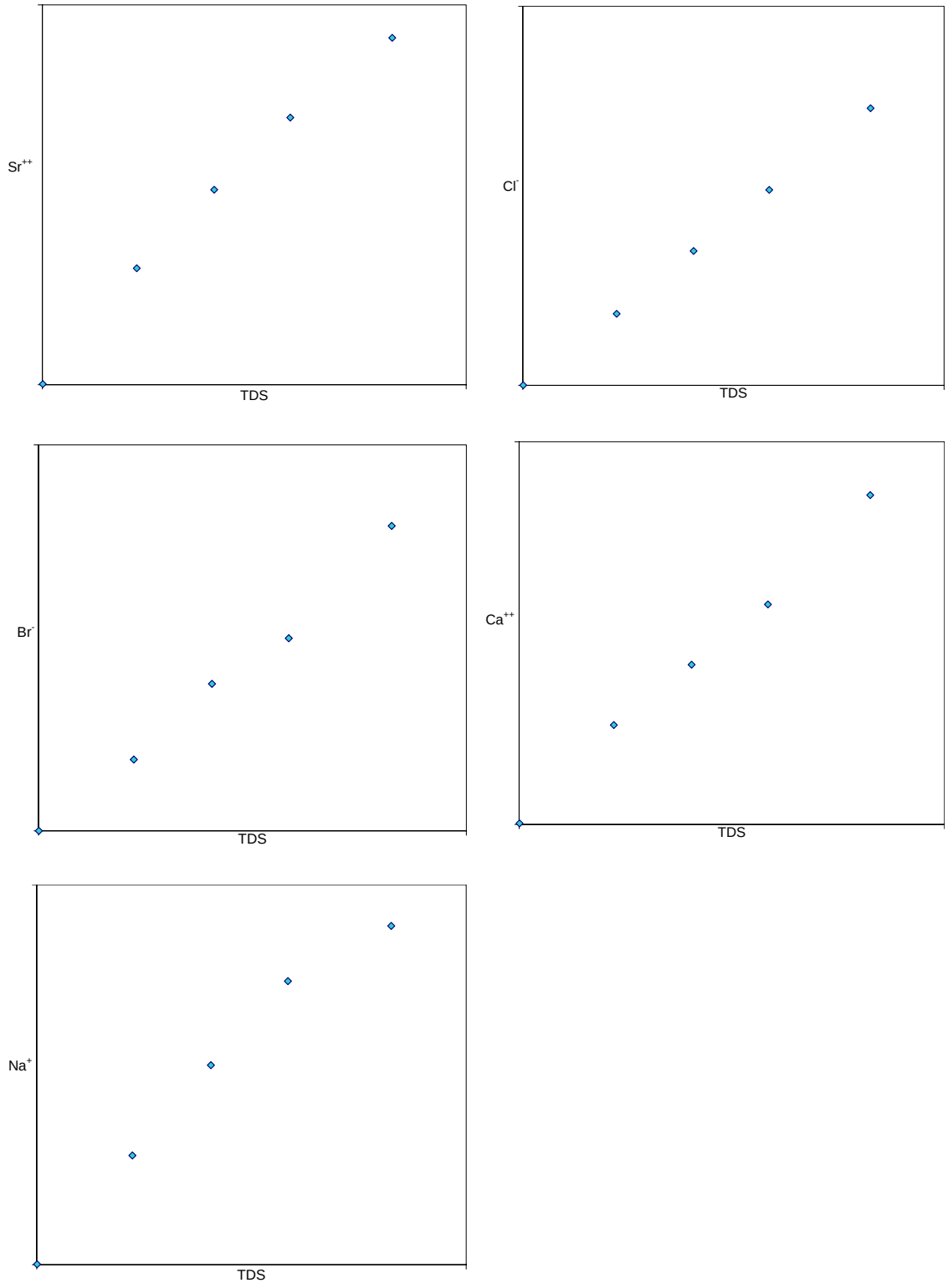

Figure A1: Composition diagrams of the samples taken in the En Gedi area. The straight lines on which the samples plot indicates mixing of two end-member waters.

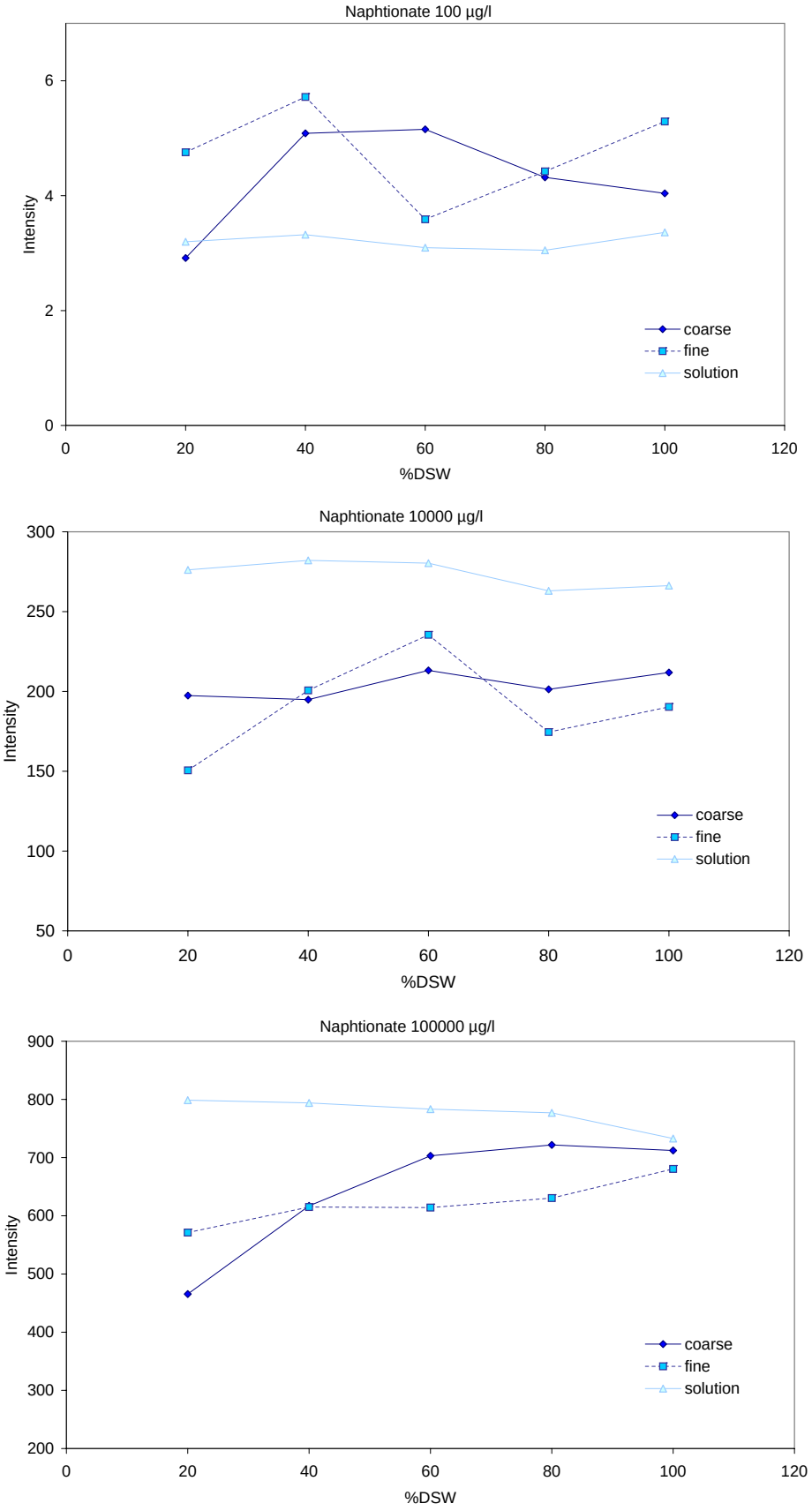

Figure A2 a-c: Results of the batch experiments of Naphtionate in different tracer concentrations.

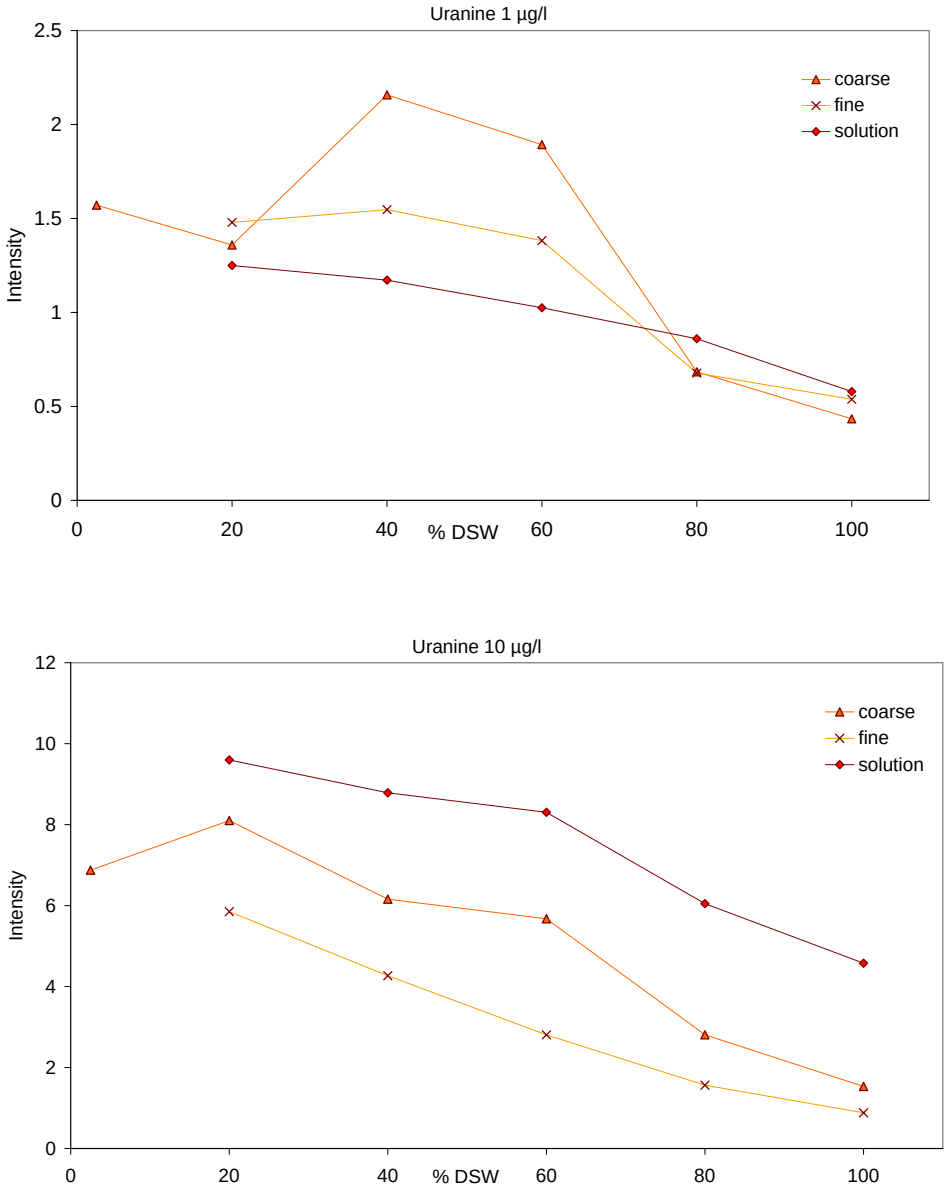

Figure A3 a-b: Results of the Uranine batch experiments at 1 and 10 µg/l tracer concentration.

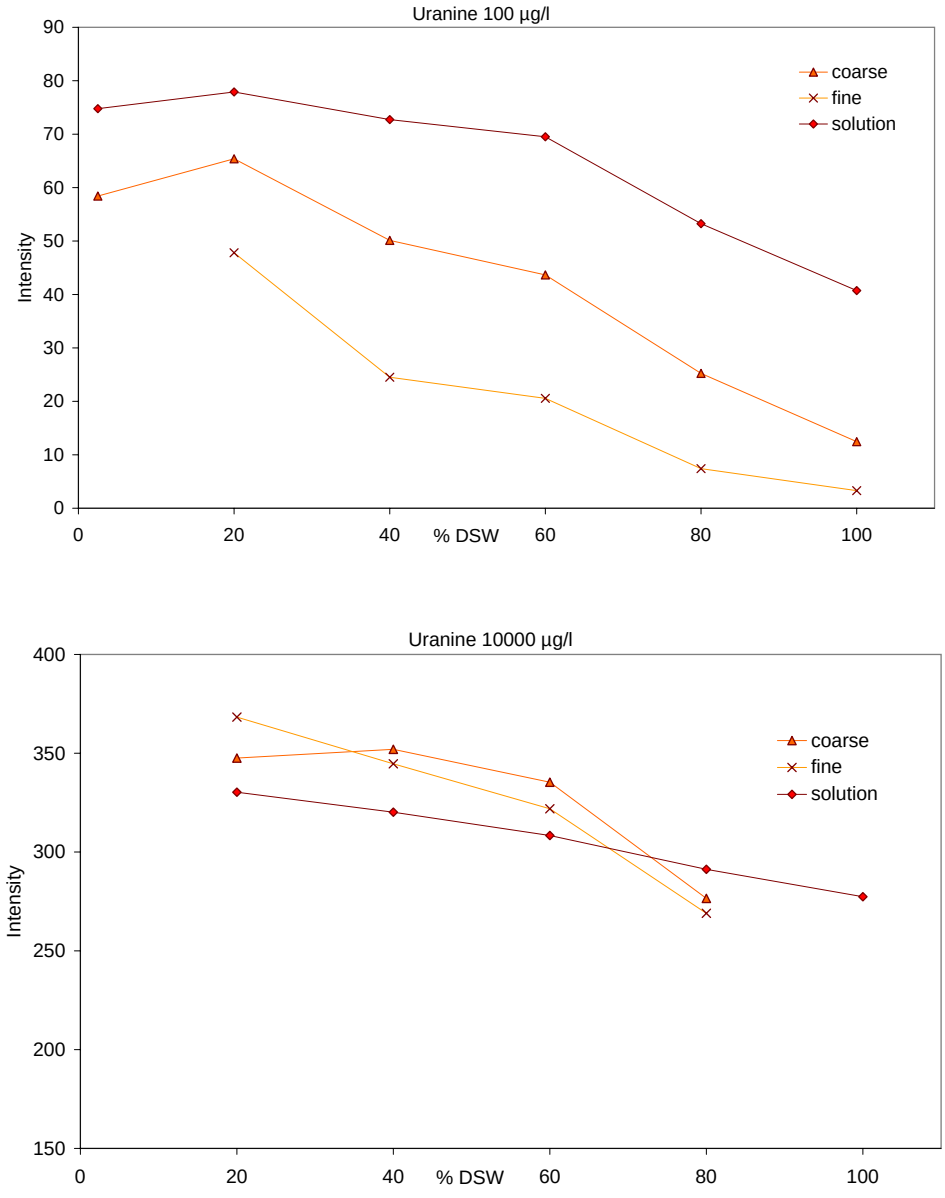

Figure A3 c-d: Results of the Uranine batch experiments in 100 and 10000 µg/l tracer concentration.

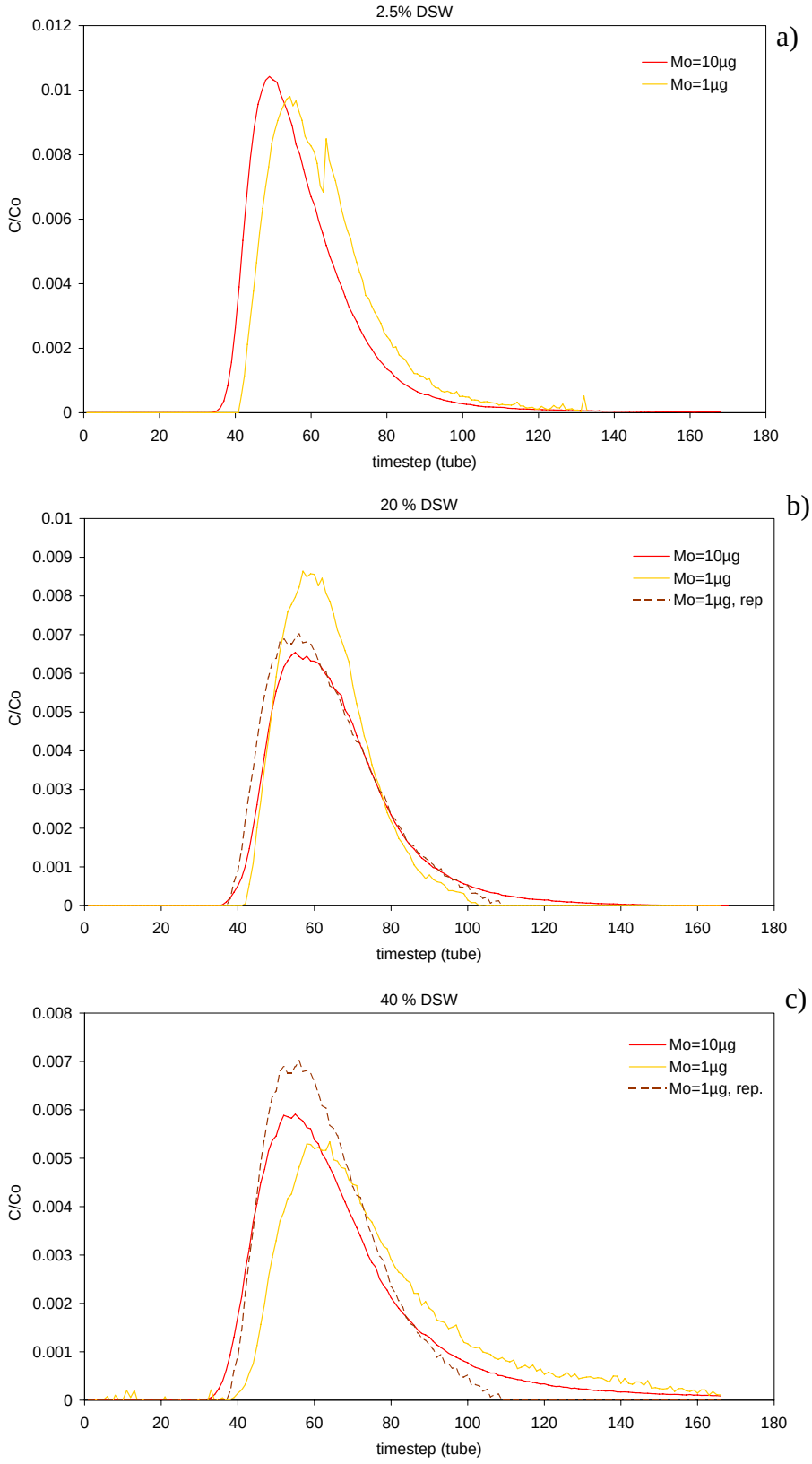

Figure A4 a-c: Comparison of Uranine BTCs in 1000µg/l and 10000µg/l concentration:
a) 2.5 % DSW, b) 20 % DSW, c) 40 % DSW.
Repetitions were carried out for M_0 = 1 µg in 20 and 40 % DSW.

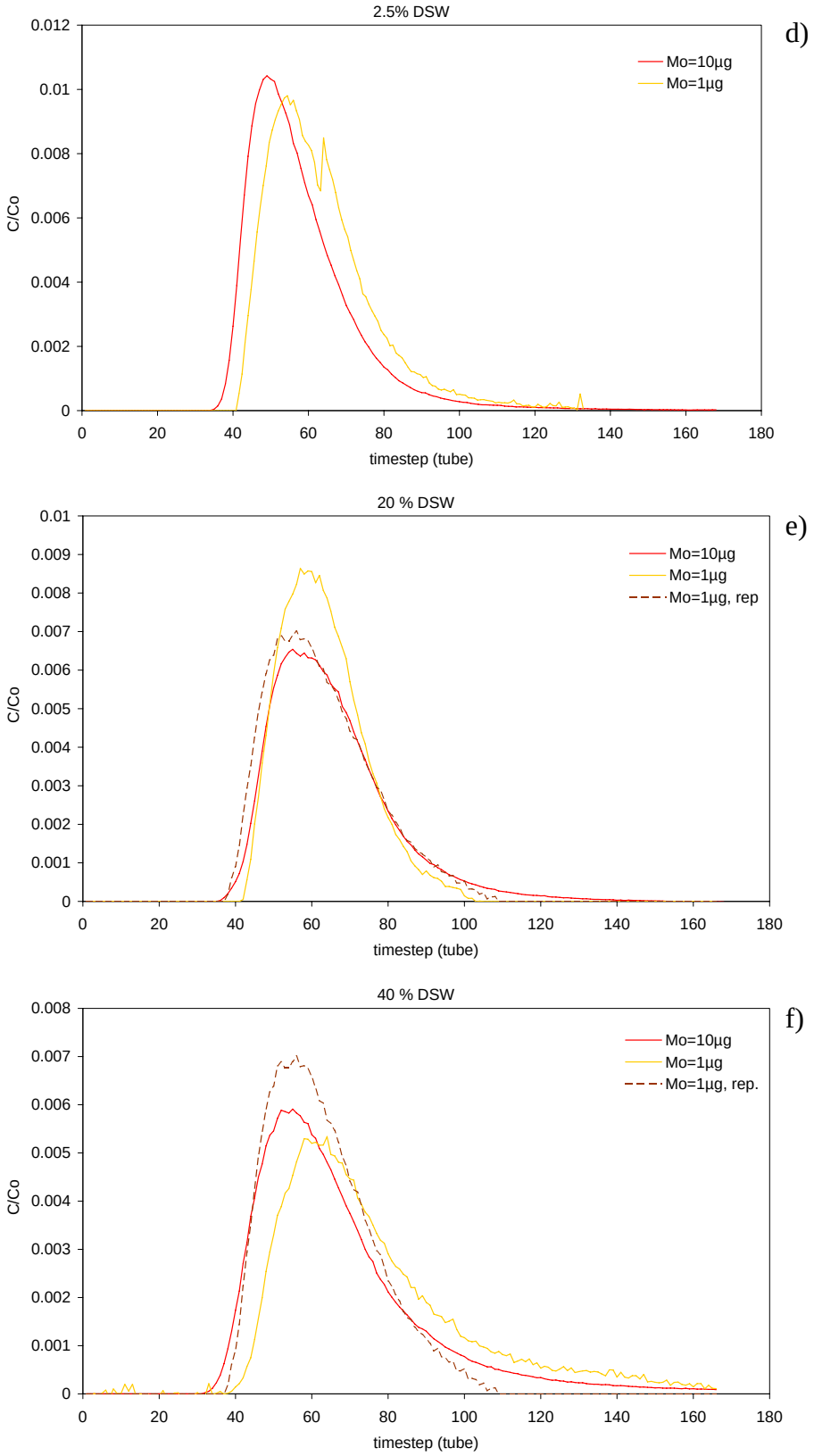

Figure A4 d-f: Comparison of Uranine BTCs in 1000µg/l and 10000µg/l concentration: d) 60 % DSW, e) 80 % DSW, f) 100 % DSW.

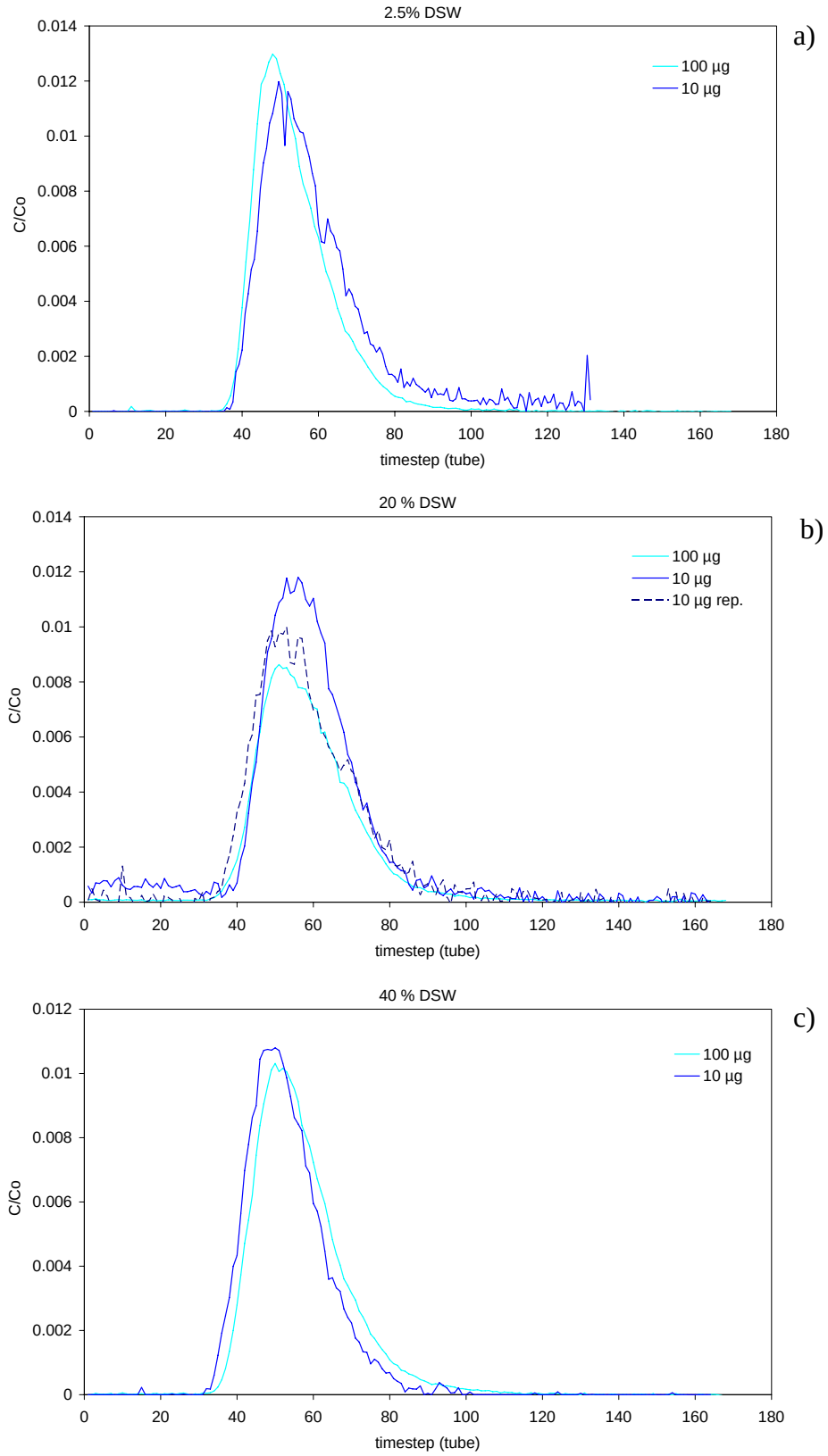

Figure A5 a-c: Comparison of Naphtionate BTCs in 10000µg/l and 100000µg/l concentration:
a) 2.5 % DSW, b) 20 % DSW, c) 40 % DSW.
A repetition was carried out for M_0 = 10 µg in 20 DSW.

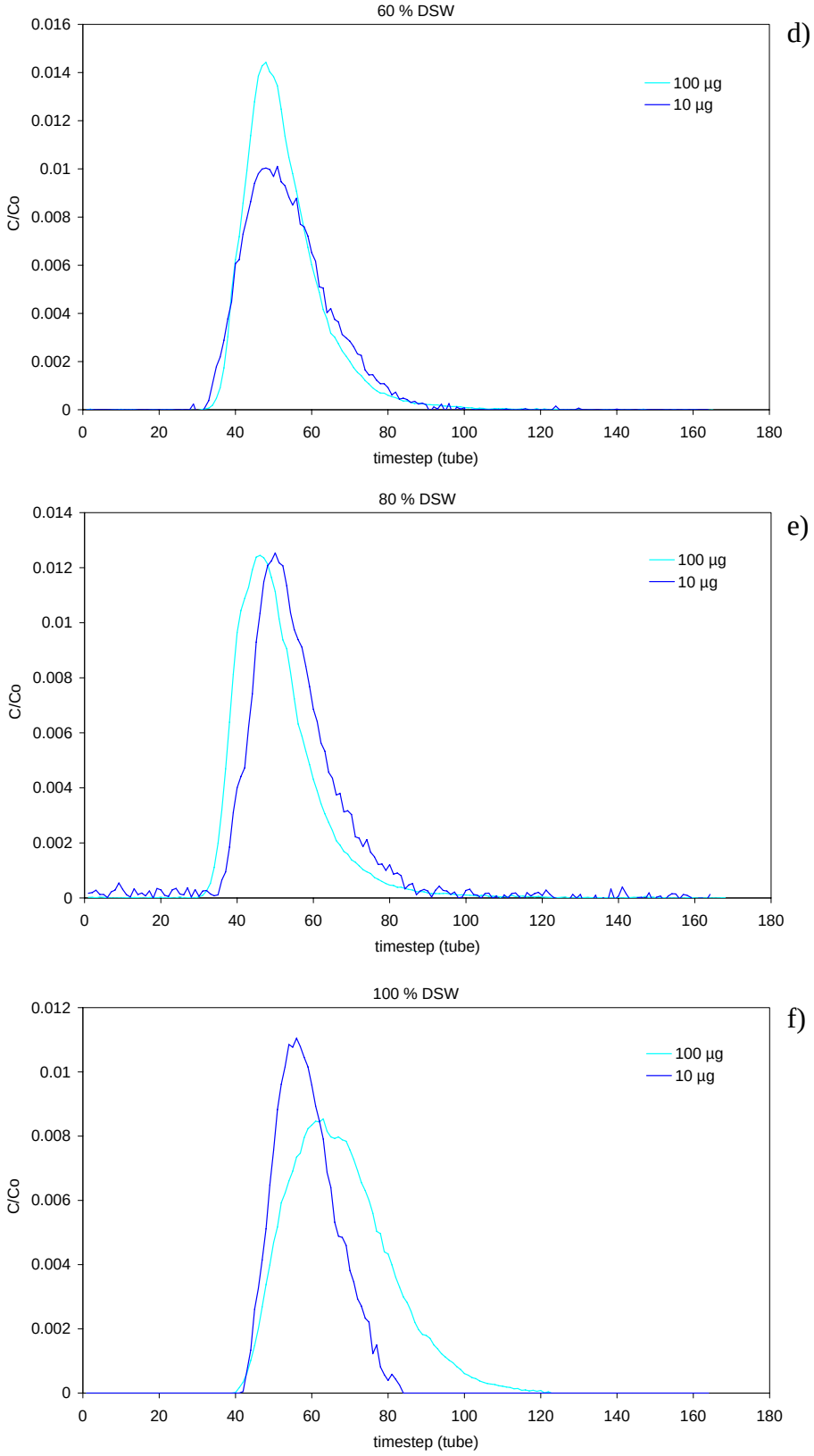

Figure A5 d-f: Comparison of Naphtionate BTCs in 10000µg/l and 100000µg/l concentration: d) 60 % DSW, e) 80 % DSW, f) 100 % DSW.

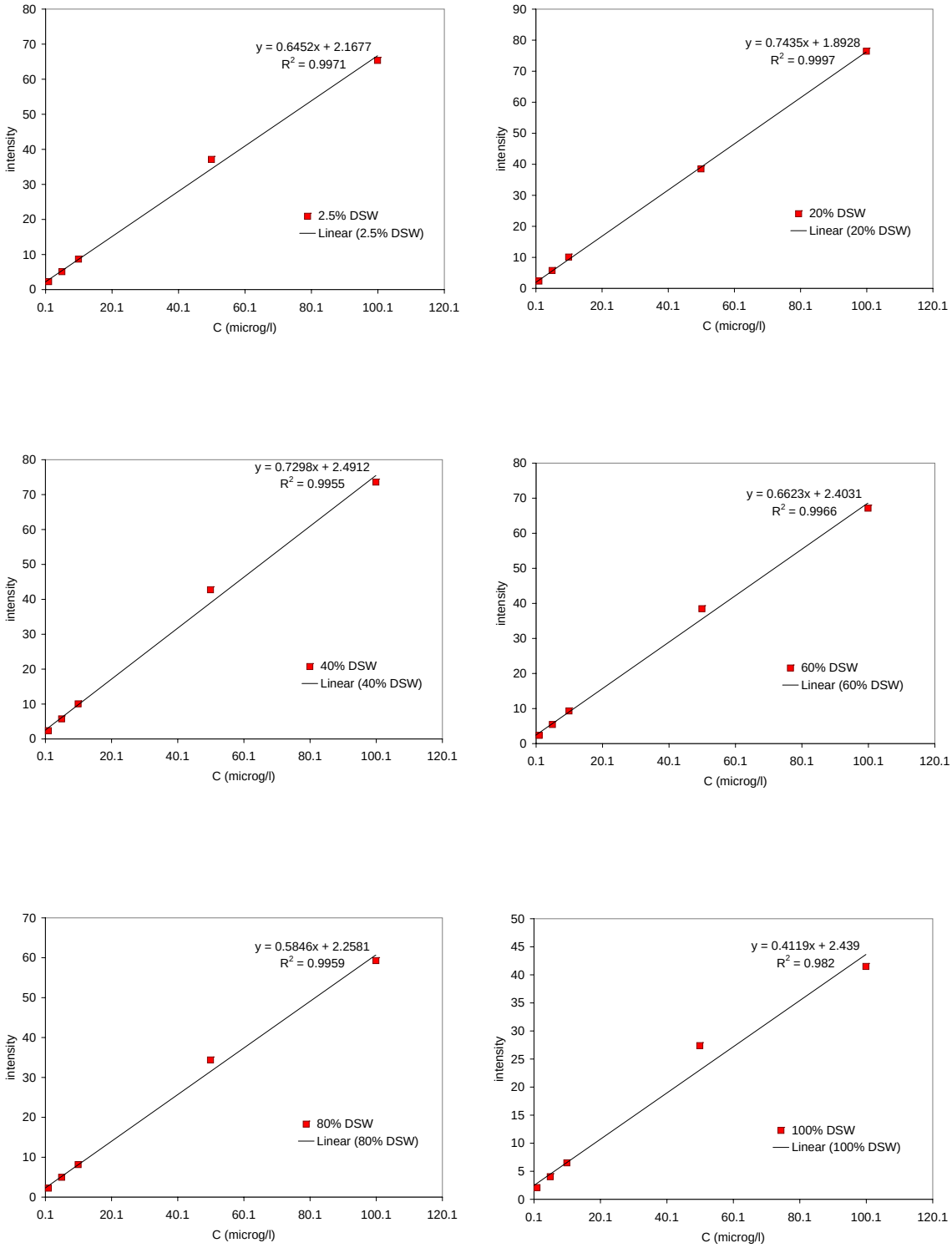

Figure A6: Calibration lines for Uranine at concentrations of 1 to 100 µg/l in varied salinities.

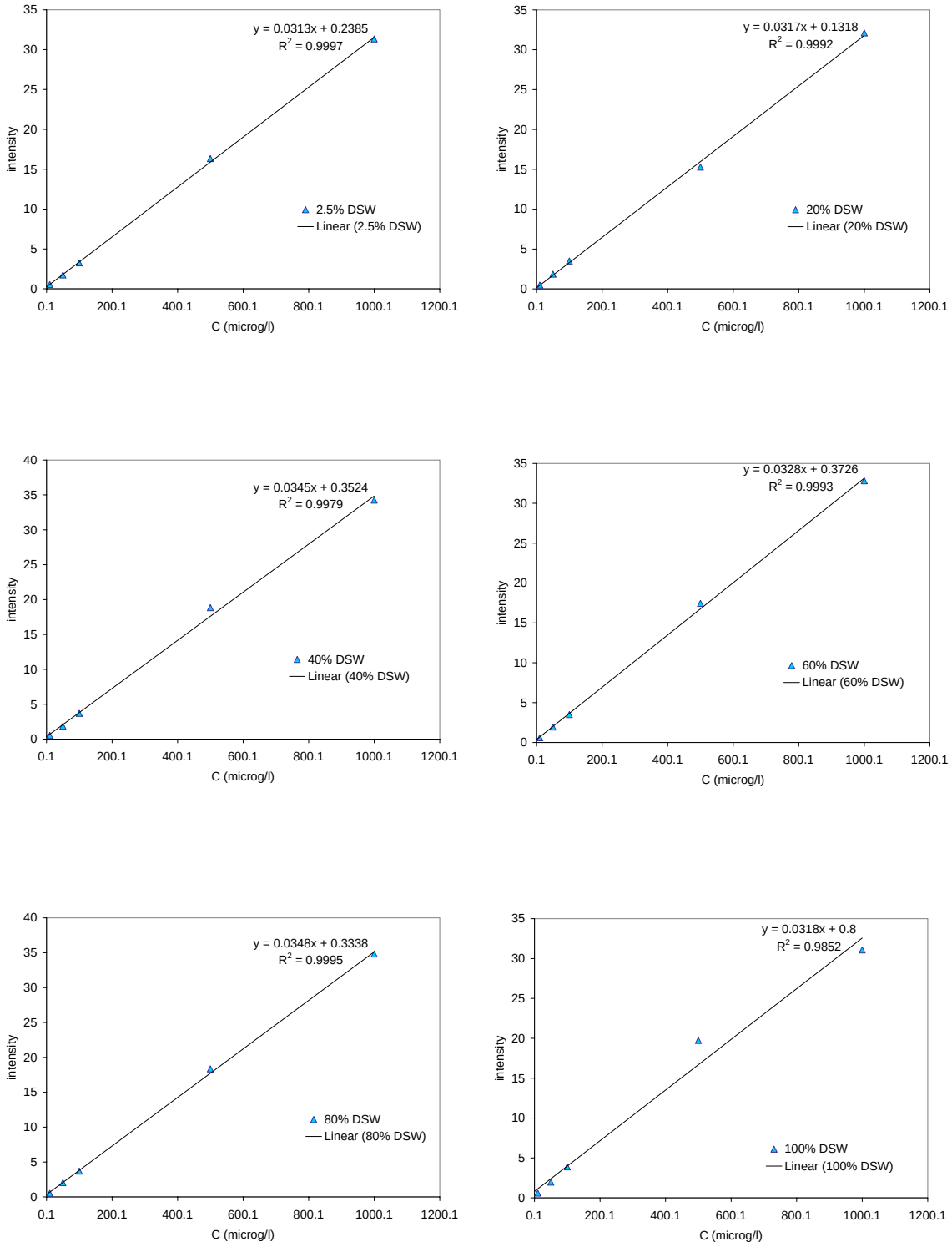

Figure A7: Calibration lines of Naphtionate at concentrations of 1 to 1000 µg/l in varied salinities

Figure A8: View from En Gedi spring down to the sampling sites of EG11 and EG16.

Figure A9: Borehole EG11 (white square in the centre).

Figure A10: Site of the En Gedi spring (above and below).

Figure A11: sampling for noble gases.

Ehrenwörtliche Erklärung

Hiermit erkläre ich, dass die Arbeit selbstständig und nur unter Verwendung der angegebenen Hilfsmittel angefertigt wurde.

Freiburg, 20. Dezember 2006

Elisabeth Helen Krüger

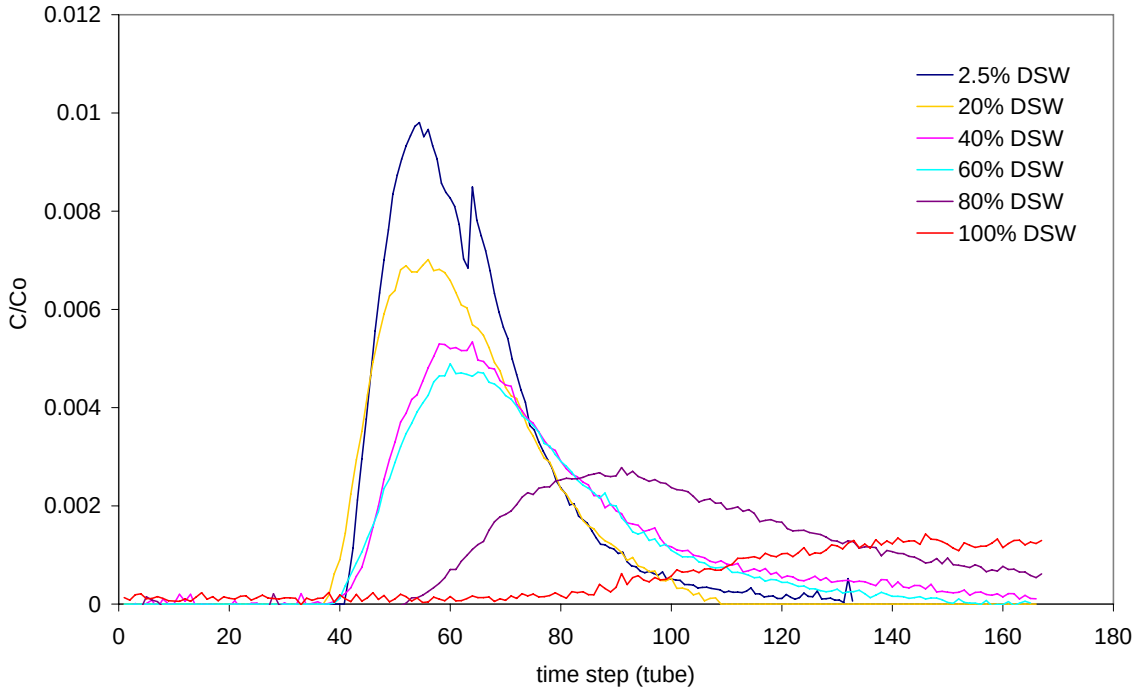

Figure 4.21a: Uranine breakthrough curves of an injected tracer mass of 1 µg.

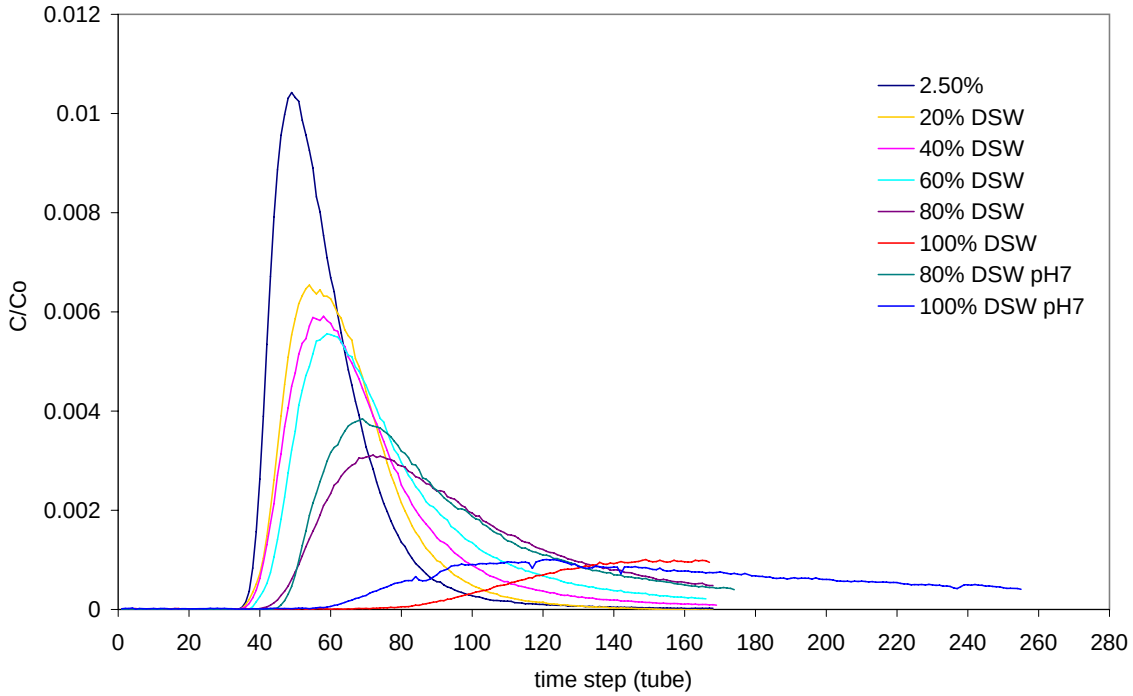

Figure 4.21b: Uranine BTCs of an injected tracer mass of 10 µg.

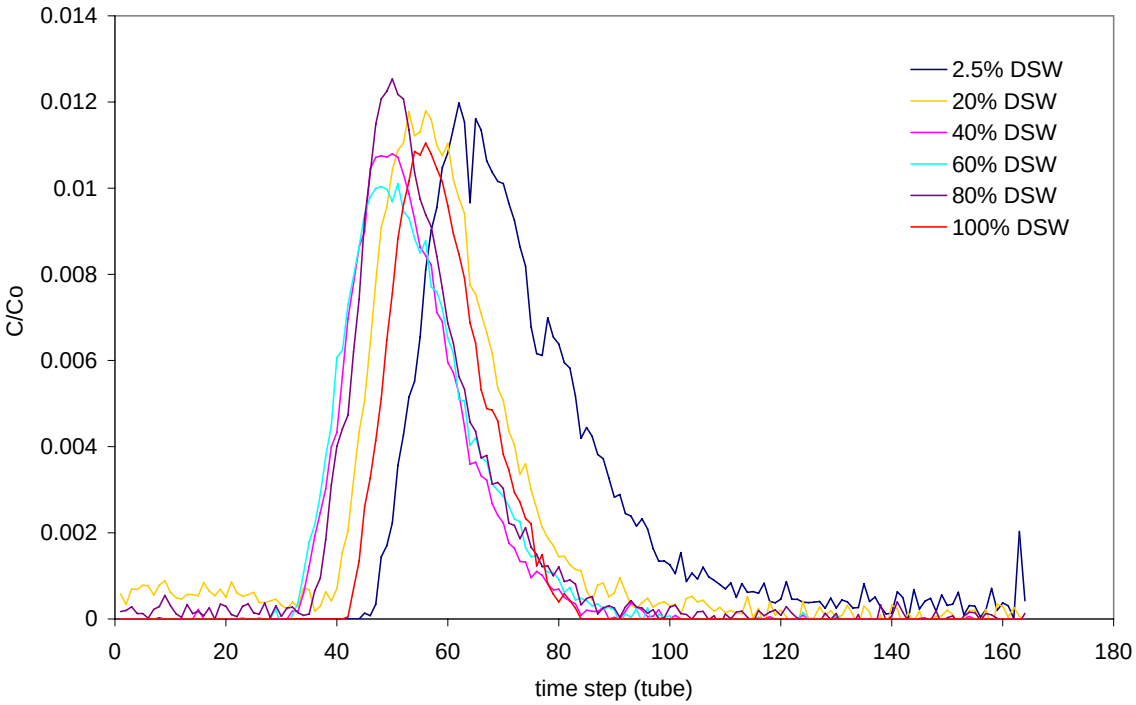

Figure 4.22a: Naphtionate breakthrough curves of an injected tracer mass of 10 µg.

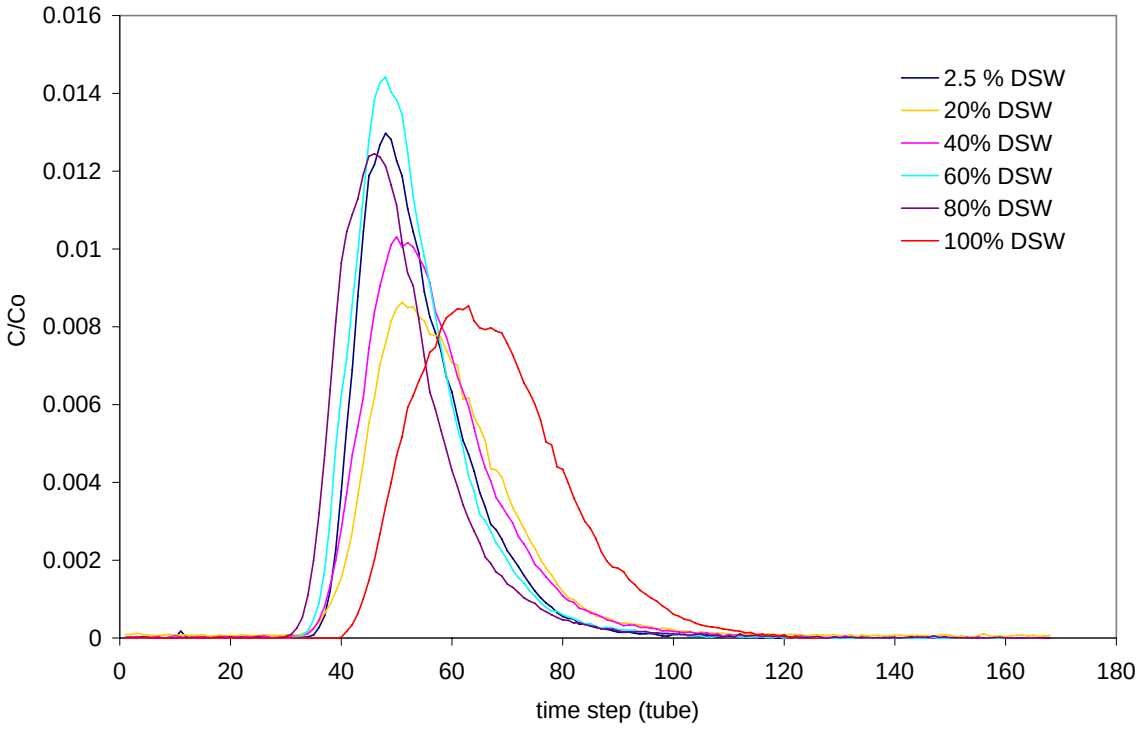

Figure 4.22b: Naphtionate breakthrough curves of an injected tracer mass of 100 µg.

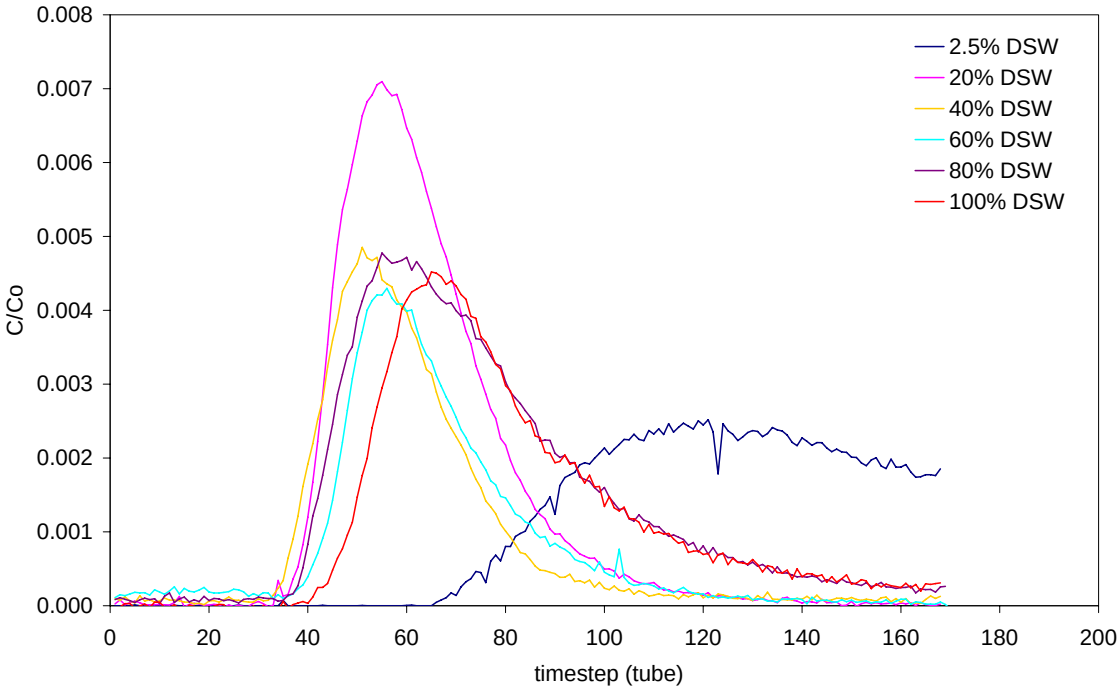

Figure 4.23: Pyranine breakthrough curves resulting from an injected tracer mass of 10 µg.

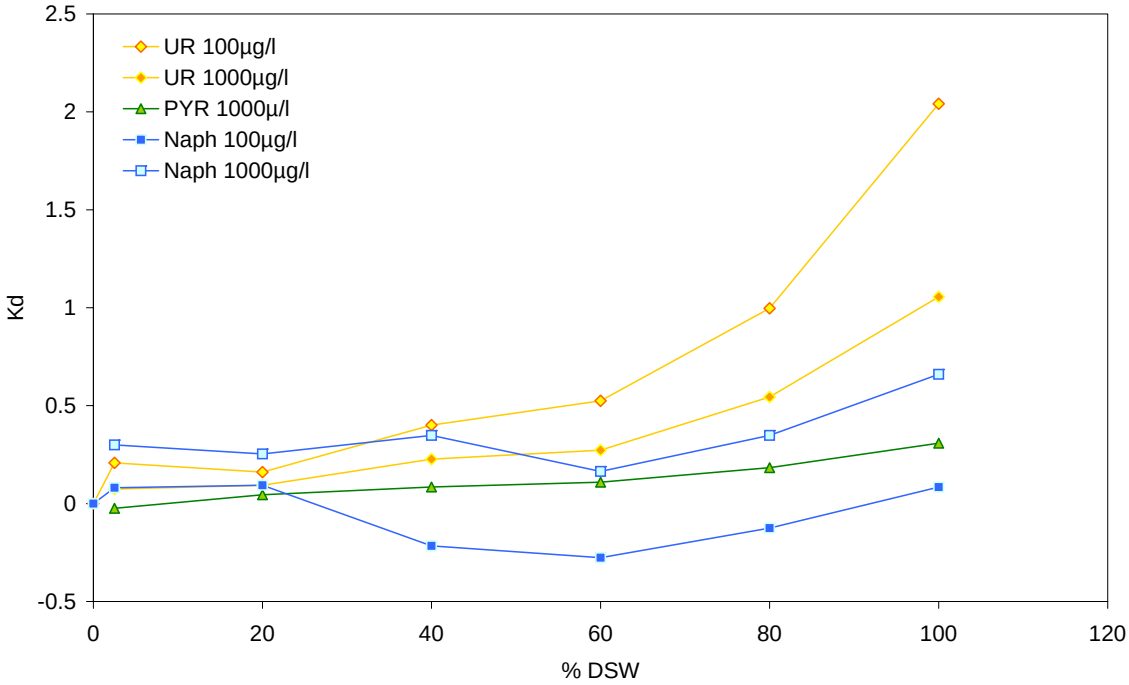

Figure 4.25: K_d-values calculated from the batch experiments.

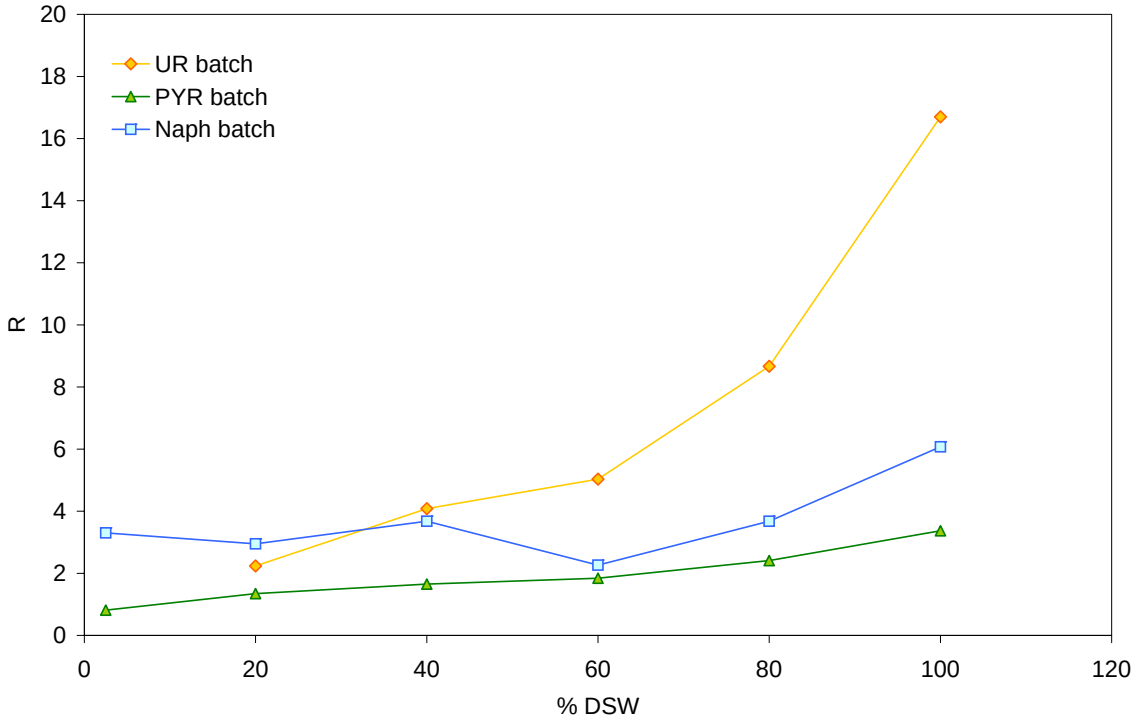

Figure 4.26: Retardation factors calculated from K_d-values (C 0 1000 µg/l)

Due to malfunctions in the printing process the following figures

4.21a, b,

4.22a, b,

4.23,

4.25,

4.26

have been included in a higher quality in the loose appendix, which can be found at the end of this document.